ISBN 978-82-326-7034-5 (printed ver.)
ISBN 978-82-326-7033-8 (electronic ver.)
ISSN 1503-8181 (printed ver.)
ISSN 2703-8084 (electronic ver.)

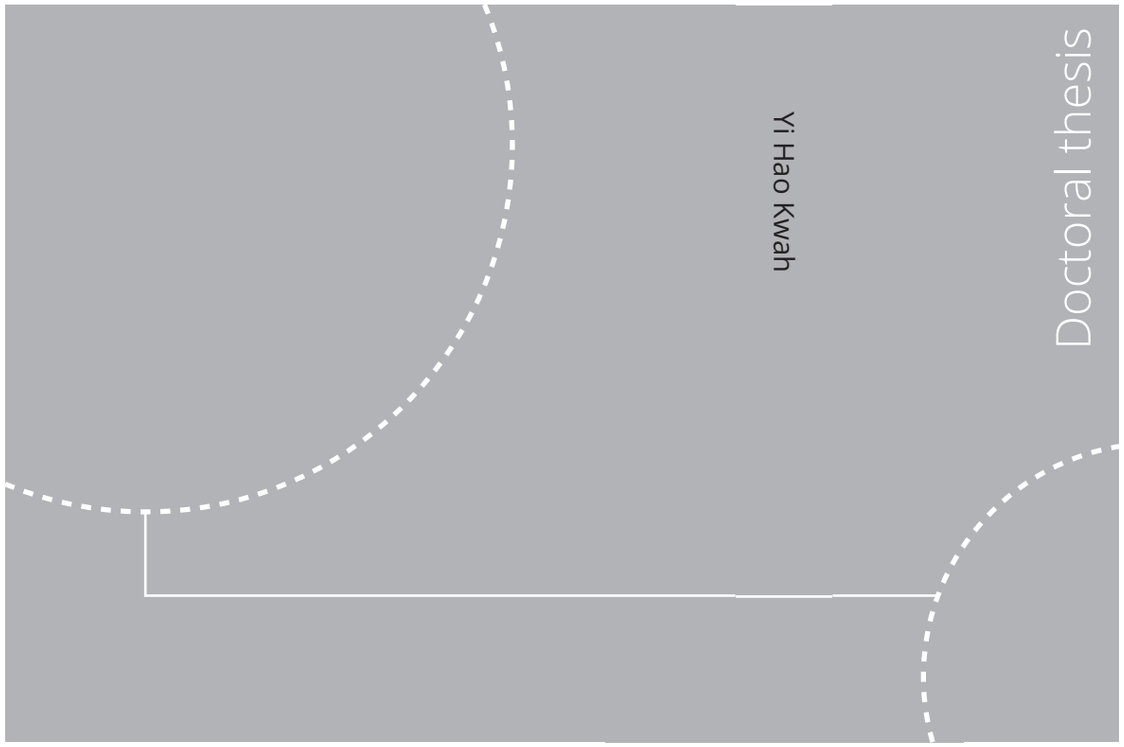

Doctoral theses at NTNU, 2023:165

Yi Hao Kwah

Ignition and lean blowoff dynamics of turbulent flames in annular combustors

Doctoral theses at NTNU, 2023:165

NTNU

Norwegian University of Science and Technology

NTNU
Norwegian University of Science and Technology
Thesis for the degree of Philosophiae Doctor
Faculty of Engineering
Department of Energy and Process Engineering

NTNU

Norwegian University of Science and Technology

Yi Hao Kwah

Ignition and lean blowoff dynamics of turbulent flames in annular combustors

Thesis for the degree of Philosophiae Doctor

Trondheim, June 2023

Norwegian University of Science and Technology
Faculty of Engineering
Department of Energy and Process Engineering

NTNU
Norwegian University of
Science and Technology

NTNU
Norwegian University of Science and Technology

Thesis for the degree of Philosophiae Doctor

Faculty of Engineering
Department of Energy and Process Engineering

ISBN 978-82-326-7034-5 (printed ver.)
ISBN 978-82-326-7033-8 (electronic ver.)
ISSN 1503-8181 (printed ver.)
ISSN 2703-8084 (electronic ver.)

Doctoral theses at NTNU, 2023:165

PRINTED IN NORWAY
NO - 1598

NORDIC SWAN ECOLABEL
Printed matter
2041 0731

Printed by Skipnes Kommunikasjon AS

Abstract

This thesis aims to provide experimental insights on the transient phenomena of *ignition light-around and lean blowoff dynamics of turbulent flames in annular combustors*. Numerous ignition experiments have been performed in single flame setups but are unable to replicate the physics of flame spreading and propagation from one injector to the next in an annular geometry. Similarly, lean blowoff studies of a single flame fail to account for any flame interaction present in multi-injector configurations which is known to affect the eventual lean blowoff limit. The present work aims to contribute to the existing limited data concerning these transient flame dynamics through various experiments conducted on three different laboratory-scale annular combustors.

The first of such designs is the Cambridge/NTNU annular combustor which has a greatly simplified geometry to facilitate fundamental studies. Ignition studies using hydrocarbons corroborated past findings that the ignition speed is positively correlated to a lumped parameter of laminar flame speed and thermal expansion (quantified using dilatation ratio). Mixture blends of hydrogen and ammonia were used to isolate effect of the dilatation ratio and the laminar flame speed. The use of these non-carbon fuel blends strongly suggests the dominant role of thermo-diffusivity in influencing flame propagation speed. Notably, a decrease in the volumetric expansion effect (lower dilatation ratio) leads to an unexpected increase in flame speed which is contrary to behaviour of hydrocarbon fuels and highlights that due consideration is needed when generalising existing findings to non-carbon fuels which often have drastically different flame properties.

In collaboration with SAFRAN Helicopter Engines and CERFACS, two new laboratory-scale combustors were conceived to replicate the design principles of a SAFRAN spinning combustion technology (SCT) engine: (i) strong azimuthal swirl, (ii) Rich-Quench-Lean (RQL) combustion mode, and (iii) azimuthal fuel staging. These setups are named SCT V1 and SCT V2. SCT V1 was used to assess effect of strong azimuthal swirl on light-around and

lean blowoff in premixed flames. SCT V2 explored these effects in a RQL configuration with and without azimuthal fuel staging.

The presence of strong azimuthal swirl in SCT V1 and V2 was shown to promote higher injector-to-injector propagation speeds, and improve ignition and lean blowoff limits. Under a RQL combustion mode in SCT V2, non-premixed flame ignition behaviour was observed in that no clear correlation could be established between propagation speed and bulk flow velocity. Careful design of azimuthal fuel staging may lead to substantial improvements in the ignition limits, increasing the operating envelope of an engine.

Lean blowoff limits of the three annular combustors and setups representative of their single flame equivalent were also mapped. It is found that in all three annular configurations, multiple interacting flames may extend the global extinction limits. Notably, in the case of SCT V1 and V2, there are indications that under the influence of strong azimuthal swirl, flames from an injector often have a piloting (and stabilising) effect on adjacent injectors. This finding is substantiated with Large Eddy Simulation work performed by CERFACS.

Efforts are currently underway to further characterise and elucidate the various findings reported in this dissertation which have sought to (i) explore the ignition dynamics of ammonia and hydrogen in anticipation of the transition to a carbon-free future, and (ii) evaluate the ignition and lean blowoff physics of various combustor designs closely mimicking that of a Spinning Combustion Technology (SCT) engine.

Preface

This thesis is submitted to the Norwegian University of Science and Technology (NTNU) for partial fulfilment of the requirements for the degree of philosophiae doctor. The doctoral work has been performed at the Department of Energy and Process Engineering (EPT) from August 2018 to April 2023. The work has been supervised by Professor James R. Dawson and co-supervised by Associate Professor Jonas P. Moeck.

The research was funded by the European Union's Horizon 2020 research and innovation programme under Grant Agreement No. 765998 (ANNULIGhT).

The thesis consists of 5 chapters and 4 scientific papers.

Article I

Numerical and experimental flame stabilization analysis in the new spinning combustion technology framework
Pasquale Walter Agostinelli, Yi Hao Kwah, Stephane Richard, Gorka Exilard, James R. Dawson, Laurent Gicquel, Thierry Poinsot
ASME Turbo Expo 2020: Turbomachinery Conference and Exposition, Volume 4A: Combustion, Fuels, and Emissions, Page V04At04A058

Author's contributions: All authors conceived the idea of the setup. YHK and JRD designed and commissioned the setup. PWA performed the numerical simulation and analysed the relevant numerical results with guidance from LG. YHK performed the experiment and analysed the relevant experimental results with guidance from JRD. PWA took the lead in writing the manuscript. All authors discussed the results and commented on the manuscript.

Article II

Effect of strong azimuthal swirl on ignition and light-around in an annular combustor
Yi Hao Kwah, Pasquale Walter Agostinelli, Stephane Richard, Gorka Exilard, Stephane Pascaud, Laurent Gicquel, James R. Dawson
Journal of Engineering for Gas Turbines and Power, Volume 144, Issue 11, Pages 11010

Author's contributions: All authors conceived the idea of the setup. YHK, PWA, SR, GE and JRD designed and commissioned the setup. YHK and PWA also carried out the experiment. YHK analysed the results and wrote the draft manuscript. JRD edited the paper with input from all authors.

Article III

The effect of methane-ammonia and methane-hydrogen blends on ignition and light-around in an annular combustor
Yi Hao Kwah, Samuel Wiseman, James R. Dawson
Accepted to: Turbomachinery Technical Conference and Exposition 2023
Recommended for publication in: Journal of Engineering for Gas Turbines and Power

Author's contributions: YHK and SW planned and carried out the experiment. YHK took the lead in writing the manuscript with guidance from SW and JRD.

Draft article IV

The impact of azimuthal swirl on the lean blow-out dynamics in an annular combustor
Pasquale Walter Agostinelli, Yi Hao Kwah, Stephane Richard, Gorka Exilard, James R. Dawson, Laurent Gicquel
Submitted to: Combustion and Flame

Author's contributions: All authors conceived the idea of the setup. YHK and JRD designed and commissioned the setup. PWA performed the numerical simulation and analysed the relevant numerical results with guidance from LG. YHK performed the experiment and prepared the relevant experimental results with guidance from JRD. PWA took the lead in writing the

manuscript. JRD and LG read and reviewed the manuscript and provided technical and editorial guidance.

Additional article not formally included in this thesis:

Self-excited longitudinal and azimuthal modes in a pressurised annular combustor
Marek Mazur, Yi Hao Kwah, Thomas Indlekofer, James R. Dawson, Nicholas A. Worth
Proceedings of the Combustion Institute, Volume 38, Issue 4, Page 5997-6004

Author's contributions: MM designed and commissioned the setup. MM, YHK, and TI performed the experiments. MM and NW analysed the results and wrote the draft manuscript. JRD and NW read and reviewed the manuscript and provided technical and editorial guidance.

15th April 2023

Yi Hao Kwah

Dedication

To dad, mum, sister, and my twin brother,

thank you for the boundless love and support.

Acknowledgements

"I didn't think it would end this way."

It was August 2018 that I started on my PhD. In a blink, this journey is coming to an end, and I would like to express my gratitude to the many people who have helped me along the way.

To James and Nick, thank you for seeing me through this entire PhD with much patience and guidance. It is certainly not easy to be coaching someone like me who neither has any prior practical skills nor theoretical combustion knowledge. I certainly would not have come that far without you guys.

To Epaminondas Mastorakos and Ronan Vicquelin, thank you for agreeing to be my opponents and spending time assessing my thesis. Special thanks to Ronan for introducing me to the world of fluid dynamics and combustion back in École Centrale Paris.

To the technicians, a big thank you goes out to you all the unsung heroes. The numerous experiments would not have been possible without your expertise. Thank you Eugen and your apprentices for the IT support. Thank you Bård for your help in helping me get my first combustor setup fabricated. Special shout-out to Stein. Even when you were out in a cabin, you still took the effort in fixing the ventilation fans. Also thanks to Bjørn, Martin, Morten, Paul, and Per for helping us out in one way or another.

To the admin personnel, particularly Debbie, Ingrid, Marianne, Trond, Wenche, thank you for facilitating all the administrative matters. I will miss the interesting chats we had.

To Gorka, Laurent, Stéphane, and Walter, it has been a pleasure working with you all under the ANNULIGhT framework. I have certainly gained much from our interaction, and learnt to better appreciate the field of combustion from a numerical and industrial point of view.

To Samuel Wiseman, I could not have completed the PhD without you.

Everyone needs a Samwise Gamgee in their lives, and I am grateful that I met mine during my time in Norway. Your nifty lab tricks and insightful comments have always been invaluable. Outside of work, your encouraging statements have always kept me going on in spite of whatever setbacks I have faced for:

> *"In the end, it's only a passing thing this shadow, even darkness must pass. A new day will come, and when the sun shines, it'll shine out the clearer."*

To José, I really appreciate the countless northern light hunting, cross-country skis, and fun times we had. I will always keep in mind of your academic and life advice. Your "hosing" tactics such as swapping the 'm' and 'n' on my keyboard, inverting my screen, and unintentionally but deliberately introducing bugs to my codes shall always remain as unrivalled legacy.

Thank you Marek for orientating me around the lab when I was still a newbie who had no clue in experimental work. And not forgetting your set of special engineering skills, on top of the outdoor trips we have been through which are always of second degree fun! C'était mieux avant! :P

To the IPA colleagues: Marek, Luk, Sam, and Thomas. No matter how brief a stint it was for me on the IPA combustor, it has been a pleasure to be working with you all. To Dirren and Loïc, thanks for always volunteering to help me out in the lab even when it is the late evenings or the dreadful weekends.

To my "batchmates": Eirik, Håkon, Magnus, and Olav, thank you for the engaging discussions we have. I have certainly learned a lot from you guys sharing your rich experiences both in the lab and beyond the work life.

To the past and present office and lab colleagues, Aksel, Andreas (Andy), Bala, Farid, Ingrid, Julian, Leon, Martin, Melissa, Pawel, Ramgopal, Sutong, Viktor, Zhaoyu (Jackie), Zibo, it has been a pleasure knowing you all. I appreciate the social interaction we had.

To Srikar, thanks for the thoughtful scarf and social initiatives.

To Ben, thanks for granting me a roof over my head during some challenging times.

To Pim and Shuyana, thanks for the car rides and motivational support. I am happy to have met two empathetic souls who never fail to inject that

dose of positivity into my life.

To Vipin, thanks for looking out for me. Always enjoyed the time with you, no matter how brief it may have been.

To my deskmate Johannes, you have been the most wonderful and understanding deskmate. Happy to share a quicklunsj with you anytime!

To Belma, we probably share a bit more in common than we thought. Thanks for all the meaningful exchanges we had, and I wish you and your family the best.

To Elena, Maddy, and Rafael, thank you for all the times we have spent together. I really appreciate the deep conversations we had which have emotionally supported me through these years in Norway.

To the ever-friendly neighbour Au, thanks for always looking out for me. Hope to always see you around in Trondheim.

To my fellow Southeast Asian colleague Yi Hui who happens to share the same initials as me, thanks for alleviating my homesickness in one way or another, especially with your hand-delivered, life-saving pineapple tarts.

To my morning swimmate Frida, you never fail to cheer me up and motivate me. I look forward to doing more swims and skis with you whenever the opportunities arise. Cross-country, fjellski, downhill, you name it, and I am up for it!

To Harish, your keen kanelbolle observations have helped stretched my kroner a bit during these tough times of rapid price inflation. Thank you for your motivation and encouragement, and I wish you all the best in your future academic endeavours.

To Philip, my onetime flatmate but longtime friend, thanks for the motivation and encouragement. Your oatmeal recipes (yes, I do remember that you demanded an acknowledgement for this), ski and bouldering tips, countless funny memes, and more recently cool lofi music picks are lively additions to my everyday life.

To Kevin, thanks for making the trip to Norway, and for emphasising the importance of mental health. Continue having fun in Cambridge!

Merci à tous mes potes francais et aussi ma petite famille francaise de m'avoir soutenu: Mirelle et René, Sylvie, Berlot. Je pense toujours à vous.

也感谢甘薯、大厨、汉卿菜和mingo 一直以来的友谊与支持。

To Clara and Yannick, thanks for all the memorable times we had and always being there for me. I appreciate and am grateful for that. Keen for more ski, hikes, swims, and COUUUP!!! But let's try to be speedy gonzales only when on the ski tracks (proceeds to imitate Yannick's signature wink).

To the Bakklandet bois, Dirren and Loïc, you guys will always have a special place in my heart. Nothing I say is sufficient to express my deepest, heartfelt gratitude. I hope that our adventures never end, and I will still see you guys around at every corner of my life.

> *I have found that it is the small everyday deed of ordinary folks that keep the darkness at bay. Small acts of kindness and love.*

Thank you everyone for the small (and big) acts of kindness and empathy in seeing me through this PhD. It has not been the easiest stage of my life, but I am grateful that you all have been there for me. I hope to continue our friendship for the many years to come.

"No, the journey doesn't end here."

15th April 2023

Yi Hao Kwah

Contents

List of Tables

List of Figures

Nomenclature

The nomenclature in the attached publications at the end of the thesis may differ from the one given here and may include items that are not listed here. This list is not exhaustive.

Abbreviations

C_2H_4	ethylene
C_3H_8	propane
CH_4	methane
CO	carbon monoxide
H_2	hydrogen
NH_3	ammonia
NOx	mono-nitrogen oxides, which includes nitric oxide, NO and nitrogen dioxide, NO_2
PMT	photomultiplier tubes
ACW	anti-clockwise
AFR	air-fuel ratio
CHAIRLIFT	Compact Helical Arranged combustoRs with lean LIFTed flames
CRZ	central recirculation zone
CTA	Constant Temperature Anemometry
CW	clockwise
EASA	European Union Aviation Safety Agency

EM2C	Laboratoire Énergetique Moleculaire et Macroscopique, Combustion
EU	European Union
FAA	Federal Aviation Administration (of the United States of America)
FOV	field of view
FSD	flame surface density
FWHM	full width at half maximum
HRR	heat release rate
ITN	Innovative Training Network
LBO	lean blowoff
LOS	line of sight
MFC	mass flow controller
MICCA	Multiple-Injector Combustor for Combustion dynamics Analysis
NTNU	Norwegian University of Science and Technology
OH*	OH radical
ORZ	outer recirculation zone
PCX	plano-convex
PIV	Particle Image Velocimetry
PLIF	Planar Laser-Induced Fluorescence
SCT	spinning combustion technology
SHC	short helical combustor
TRL	technology readiness level
UHC	unburned hydrocarbons
UV	ultraviolet

Greek symbols

α	pitch angle
β	yaw angle
χ	species mole fraction
$\dot{\omega}$	consumption rate
ε	emissivity
ν	kinematic viscosity
ϕ	equivalence ratio
ρ	density
τ	characteristic time
θ	(azimuthal) angle

Latin symbols

$\dot{m}$	mass flow rate
$\mathcal{A}$	mixture strength
$\mathcal{L}$	integral length scale
$\mathcal{P}_{\mathrm{th}}$	thermal power
$\mathcal{R}$	universal gas constant
$\mathcal{S}$	Swirl number
$\vec{\mathbf{u}}$	flow velocity
$\vec{\mathbf{w}}$	flame front velocity
A	flame surface element
c_{p}	specific heat capacity of substance at constant pressure
d	diameter
D_{th}	thermal diffusivity
D_i	molecular (mass) diffusivity of gas species i

E	voltage
h	height
$I_{j=1,2,3,...}$	j=1$^{\text{st}}$, 2$^{\text{nd}}$, 3$^{\text{rd}}$, ... injector sector
l	length
q	specific heat of reaction
q^*	(non-dimensional) heat release
r	radius
S	flame speed
T	temperature
t	time coordinate
U	bulk velocity
u	local velocity
x	axial direction
Y	species mass fraction
Ze	Zel'dovich number
Da	Damköhler number
Le	Lewis number
Re	Reynolds number

Modifiers

$(\cdot)^0$	unstretched. S^0 represents unstretched flame speed.
$(\cdot)'$	fluctuating quantity
$(\cdot)_{\text{ad}}$	adiabatic
$(\cdot)_{\text{air}}$	air
$(\cdot)_{\text{atm}}$	atmospheric
$(\cdot)_{\text{a}}$	absolute. S_{a} represents absolute flame speed.

$(\cdot)_{\mathrm{bb}}$	bluff body
$(\cdot)_{\mathrm{bo}}$	blowoff
$(\cdot)_{\mathrm{b}}$	burned mixture
$(\cdot)_{\mathrm{cool}}$	cooling (duct/plate)
$(\cdot)_{\mathrm{dil}}$	dilution
$(\cdot)_{\mathrm{D}}$	deficient reactant
$(\cdot)_{\mathrm{d}}$	displacement. S_{d} represents flame displacement speed.
$(\cdot)_{\mathrm{E}}$	excess reactant
$(\cdot)_{\mathrm{f}}$	fuel
$(\cdot)_{\mathrm{g}}$	geometric
$(\cdot)_{\mathrm{hub}}$	(swirler) hub
$(\cdot)_{\mathrm{inj}}$	injector
$(\cdot)_{\mathrm{i}}$	inner
$(\cdot)_{\mathrm{L}}$	laminar. S_{L} represents laminar flame speed.
$(\cdot)_{\mathrm{ox}}$	oxidiser
$(\cdot)_{\mathrm{o}}$	outer
$(\cdot)_{\mathrm{pyro}}$	pyrometer
$(\cdot)_{\mathrm{ref}}$	reference
$(\cdot)_{\mathrm{s}}$	sector
$(\cdot)_{\mathrm{u}}$	unburned mixture
$(\cdot)_{\mathrm{w}}$	wire
$(\cdot)_{\theta}$	azimuthal component
$(\cdot)_{x}$	axial component
$(\cdot)_{\mathrm{t}}$	tangential components

1 Introduction

1.1 Motivation

Air travel is one of the safest modes of transportation with consistently low accident rates (Barnett 2020). The good safety track record can be attributed to the stringent tests that an aircraft has to undergo before being certified as airworthy by the relevant aviation authority. For instance, the U.S. Federal Aviation Administration (FAA) and the European Union Aviation Safety Agency (EASA) regularly update guidelines detailing the aircraft's safety test requirements. Particular emphasis is placed on the relight capabilities of an aircraft engine: both the FAA (Federal Aviation Adminstation 2020) and the EASA (European Union Aviation Safety Agency 2015) have specific memoranda stipulating the relight scenarios which an engine must fulfil. Specifically, an engine must demonstrate its ability to:

- restart immediately ($t < 5\,\mathrm{s}$) after a flameout[1] with typical temperature $T \geq 1000\,\mathrm{K}$ (Lefebvre and Ballal 2010, Soares 2015),

[1] Defined by EASA as the global extinction of flame within the engine's combustion chamber. Distinction between various terminology (blowoff, blowout etc.) will be refined later in the chapter.

- re-ignite after extended periods ($t \geq 15\,\text{min}$) of engine shutdown or when the fuel has cooled to its cold soak value[2] with ambient temperature $T \leq 200\,\text{K}$ for a cruising altitude of 30,000 feet (Soares 2015).

These criteria must be fulfilled across a reasonable range of altitude and aircraft speed[3], known as the relight envelope (Klinger et al. 2011). Depending on the regime of the relight envelope, the permissible ignition methods differ. Figure 1.1 provides an overview of the permissible relighting methods based on the prevailing airspeed and altitude of the aircraft.

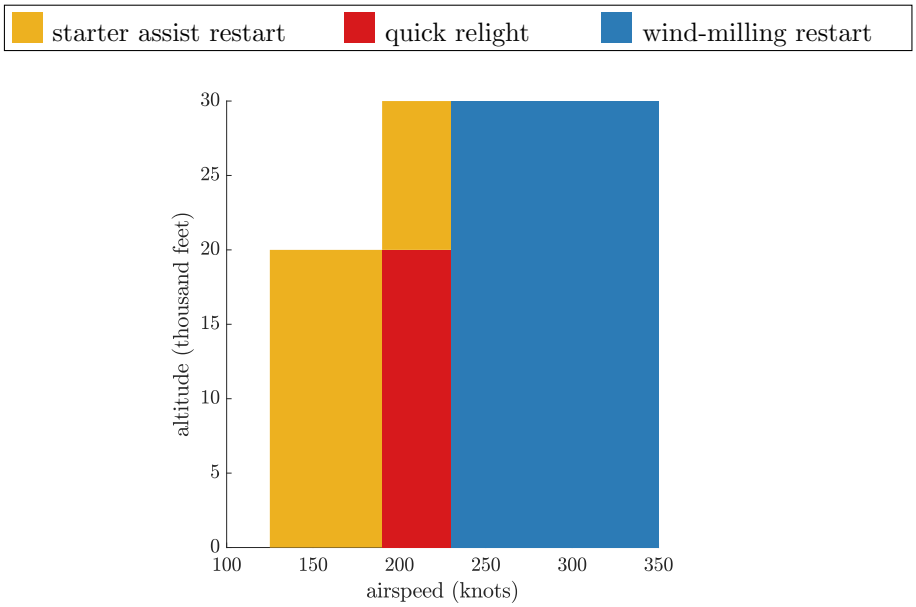

Figure 1.1: Aircraft engine in-flight relight requirements laid out by EASA. Starter assist restart refers to reigniting engine with starter assistance within a set time, quick relight means to immediately relight engine after a flame out, and wind-milling restart requires engines to be restarted within a specified time. Adapted from Klinger et al. (2011). 1 knot $\approx 0.514\,\text{m/s}$. See footnote 3.

In addition to having an acceptable relight envelope (or ignition limit) under vastly different thermal scenarios as described above, the engine must also remain continually operational upon a successful relight. The range of operating conditions in which a stable, sustained combustion may be achieved is

[2] This refers to exposing the fuel to sufficiently low temperatures for long periods of time, to the point that it has cooled to the ambient temperature.

[3] Aircraft speeds are often reported in knots since one knot is the time taken to travel a minute of latitude in an hour (International Civil Aviation Organization 2010).

known as the stability limit (Lefebvre and Ballal 2010). Ideally, the engine should be able to operate over a wide range of air-fuel ratio (AFR) for a given temperature and pressure so that any fluctuations in the AFR will have minimal impact on aircraft safety (Mellor 1990).

A typical range of the operational AFR limit, known as the combustor stability loop, is shown in Figure 1.2. This shows that as the air mass flow increases, the range of AFR which maintains stability narrows.

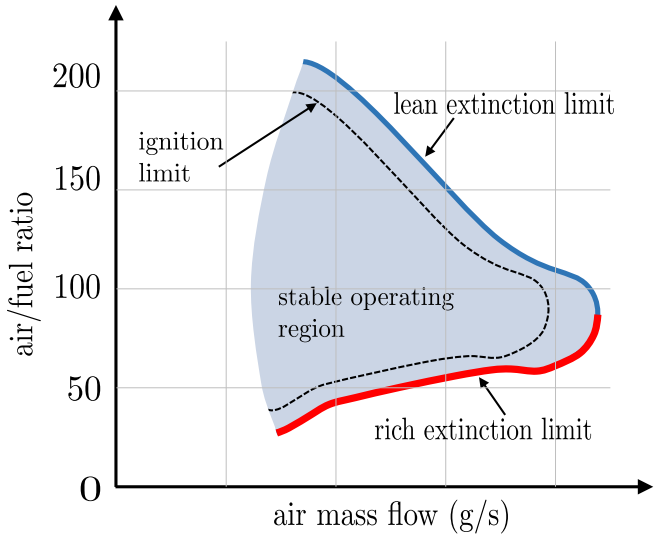

Figure 1.2: A typical combustor stability loop. Adapted from Soares (2015).

Fluctuations in the AFR can pose a threat to stability and may be due to various reasons (European Union Aviation Safety Agency 2020) such as:

- ingestion of rain or hail, reducing the effective fuel mass burned,
- mechanical failure leading to involuntary throttle, or
- over/undershooting of fuel intake rate due to imperfect response system of aircraft control.

In extreme cases, rich extinction may occur. The rich extinction limit is defined as the critical fuel mass flow rate in which any further increase in the fuel flow rate will result in an engine flameout. On the other end of this spectrum, is the lean extinction limit. The lean extinction limit, or the lean blowoff (LBO) limit, occurs when excess air leads to global flame extinction in the combustion chamber (Lefebvre and Ballal 2010).

Aside from safety considerations, understanding LBO dynamics and its associated limits is of critical importance to the design of lean burn engines that minimise emissions. Ambitious goals have been laid out by the EU to achieve a 75% reduction in CO_2 emissions and 90% reduction in NOx emissions for all EU flights by 2050 (European Commission 2012), As such, the lean burn mode has emerged as the main solutions to reducing the environmental footprint of the aviation industry. For each specific aircraft engine, there is a need to determine the ideal lean operating conditions since at high AFR values, the flame temperature is lower which reduces thermal NOx formation (Dunn-Rankin et al. 2008). Too high an AFR however leads to an increase in CO emissions with an associated risk of lean blowoff (Lieuwen and Yang 2013).

To better design engines with good relight characteristics that are capable of reliable operations across a wide range of conditions, experiments investigating ignition and lean blowoff dynamics have been conducted on laboratory-scale combustor setups. In the following sections, studies on ignition and lean blow-off are presented. The objectives of the thesis are then stated, indicating how experimental work performed within this thesis aims to contribute to a better understanding of ignition and lean blowoff dynamics in an effort to help contribute to an even safer and better aircraft engine.

1.2 Ignition dynamics

The successful formation of a flame kernel may occur either via:

- auto ignition in which inflammable reactants spontaneously combust without any external source, or
- forced ignition whereby an external trigger, such as an electrical discharge (in the form of a spark), heated surface, or pilot flame, is required to initiate the combustion process (Glassman 1997).

Forced ignition via spark is by far the most common design in combustion engines and as such, has been the focus of many studies (Lefebvre and Ballal 2010, Lieuwen 2012). Performing ignition studies in aeronautical engines however, is challenging due to the following:

- ignition is a complex phenomenon by itself (Mastorakos 2009): transient chemical and thermal processes are interacting in a turbulent flow field (Glassman 1997, Jürgen Warnatz et al. 2006). This is further complicated by flame-flame interaction which arises from injectors tightly positioned in an annular configuration for compactness (Mellor 1990).

- it is difficult and expensive to design an optically transparent combustion chamber for pressurised conditions of more than 10 atm with temperature T between 200 K to upwards of 1000 K (Lefebvre and Ballal 2010, Soares 2015). Optical access is unavailable for the visualisation of ignition dynamics in annular systems.
- for efficient combustion, air and fuel are usually introduced into the combustion chamber in stages via different injection mechanisms and is non-premixed: spray nozzles, dilution holes, etc., as shown in Figure 1.3. The complex flow field arising from multiple inlets may be challenging for performing experimental diagnostics and/or numerical simulation.

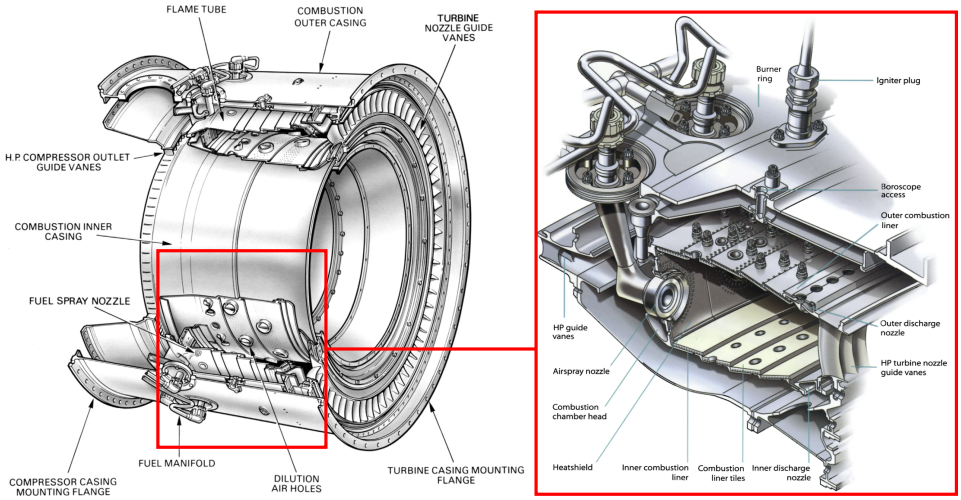

Figure 1.3: Parts of an aircraft engine. (a) Schematics showing the annular reaction zone enclosed within the combustor inner casing and outer casing. (b) An annulus sector view of the combustion chamber. Adapted from Soares (2015).

Laboratory-scale combustors have therefore been conceived to allow detailed experimental study on mechanisms governing the ignition process. These setups have been simplified, by necessity, to allow high-speed diagnostics with full optical access of the combustion chamber. Some ways in which the complexity is reduced include:

- single-sector instead of multi-injector flames,
- atmospheric combustor outlet compared to a pressurised combustor chamber,

- fuel injected as a single premix inlet and flames stabilised on simple geometry flame holders as an alternative to the engine's complicated injection mechanism(s).

These setups aim to replicate the essential physics of a real engine, and have since deepened our understanding on various aspects of ignition. Some examples include spark conditions influencing (forced) ignition (Ballal and Lefebvre 1975a,b, 1977, 1981, Blanc et al. 1947, 1948, Swett 1957), the impact of spray dynamics (Aggarwal 1998, Mastorakos 2017, Neophytou et al. 2012), and the stochastic nature of ignition (Ahmed and Mastorakos 2006, Ahmed et al. 2007, Cordier et al. 2013, Neophytou et al. 2012). These systems enable us to study flame kernel formation and propagation, and flame stabilisation but cannot capture flame propagation from one burner to another. This process of circular flame spreading (in an annular geometry) is known as light-around, and is critical to complete ignition of an annular combustion chamber (Boileau et al. 2008). Yet as recently as about a decade ago, Mastorakos (2009) pointed out the absence of experimental data concerning ignition in annular combustors, except for a single Large Eddy Simulation (LES) study in a full 18-injector annular helicopter combustor (Boileau et al. 2008). This is due to the fact that at that time, most (if not all) laboratory-scale combustors had only single-sector flames and flame propagation from one fuel injector to the next could therefore not be replicated (Vignat et al. 2020). Full engine demonstrators on the other hand, are fully capable of recreating the relight phenomenon (Klinger et al. 2011) but are very expensive to run and too complicated to have sufficient optical access for light-around visualisation or allow fundamental studies into the relevant physics involved.

Since then, annular combustors well-suited for the study of light-around in a laboratory setting have been built. At present, these annular setups are primarily based on two designs: (i) the Cambridge/NTNU annular combustor, and (ii) the MICCA combustor which are shown in Figure 1.4(a) and Figure 1.4(b) respectively.

The Cambridge/NTNU atmospheric combustor was first conceived by Worth and Dawson (2013a,b). As the name befits, the setup has been built in both Cambridge University, UK and later at NTNU, Norway. With a chamber diameter of 170 mm, it allows either a 12-, 15-, or 18-injector configuration. Flames are stabilised by means of conical bluff bodies and/or axial swirlers. Details of the combustor are presented in Chapter 3.

(a) (b)

Figure 1.4: 2 main designs of laboratory-scale atmospheric annular combustors: (a) that of Cambridge/NTNU, and (b) the MICCA (EM2C), reproduced from Bourgouin et al. (2013).

The MICCA (short for Multiple-Injector Combustor for Combustion dynamics Analysis) was developed in EM2C, France. With a diameter of 350 mm, it is about twice the size of the Cambridge/NTNU combustor. A radial swirler is used to aerodynamically stabilise each of the 16 flames. A MICCA variant sharing similar geometric features as the one in EM2C has also been built in Zhejiang University (Xia et al. 2019).

In both annular designs, geometric variation may be easily implemented, facilitating relevant parametric studies. For instance, injector spacing may be adjusted (Ciardiello et al. 2020a,b, Machover and Mastorakos 2016, 2017a). The gaseous fuel injectors may also be modified to introduce liquid spray fuel (Lancien et al. 2018, 2019, Prieur et al. 2017, 2018), conical laminar flames (Bourgouin et al. 2014, 2015), or azimuthally directed flames (Wang et al. 2021, Ye et al. 2018).

Full optical access is also present in both designs. High-speed imaging could then be used to track flame fronts from above the chamber by means of an overhead mirror (Bach et al. 2013) or from the side (Bourgouin et al. 2013). Time instants of flame fronts propagating past each injector may also be recorded at a much higher temporal resolution by means of photomultiplier tube(s) or PMT(s), installed at each injector sector (Lancien et al. 2019). The measured ignition delay between successive injectors is known as the light-around time and its significance is discussed in the following paragraphs.

1.2.1 Light-around time (and speed)

The light-around time is taken to be the duration between the onset of an ignition sequence to the eventual ignition of all injectors in the annular chamber. To identify the start and end ignition events, it is relevant to understand the five phases of light-around proposed by Philip et al. (2014b, 2015):

(I) A hot gas kernel is formed from the high-energy deposit generated by the spark.
There is a rapid increase in the heat release rate (HRR). Blue shaded region in Figure 1.5.

(II) The kernel expands and grows into a flame arch with two flame fronts: one on the left side of the annulus, and the other on the right side.
The increase in HRR is constant. Yellow shaded region in Figure 1.5.

(III) The flame fronts propagate along the annulus in both directions: anti-clockwise (ACW) for the left flame front, and clockwise (CW) for the right flame front. The flame branches sequentially ignites injectors along their circumferential paths until they meet and merge.
There is considerable fluctuations in the HRR during this phase before reaching maximum value. Red shaded region in Figure 1.5.

(IV) Any fresh reactants still residing in the combustion chamber is progressively burnt off.
The HRR tapers.

(V) Flames of all injectors are fully stabilised.
A steady HRR is attained.

Figure 1.5 shows the time evolution of HRR segmented into phases (I) - (V) for a typical light-around sequence. The normalised HRR is estimated from integrated OH* chemiluminescence images. This is a reasonable assumption since OH* chemiluminescence is a reliable HRR marker for premixed turbulent flames (Balachandran et al. 2005, Higgins et al. 2001). Figure 1.5 also shows the instantaneous images of each light-around phase.

The start of a light-around is typically defined to be at some time instant during phase (I) when the flame kernel has exceeded a certain critical size. This is inferred using an intensity threshold of the measured OH* emissions (Bourgouin et al. 2013) and is therefore an arbitrary choice. For example, Ciardiello et al. (2020a) considered 3% of the maximum measured OH* from high-speed imaging as the start of light-around, as shown in Figure 1.6.

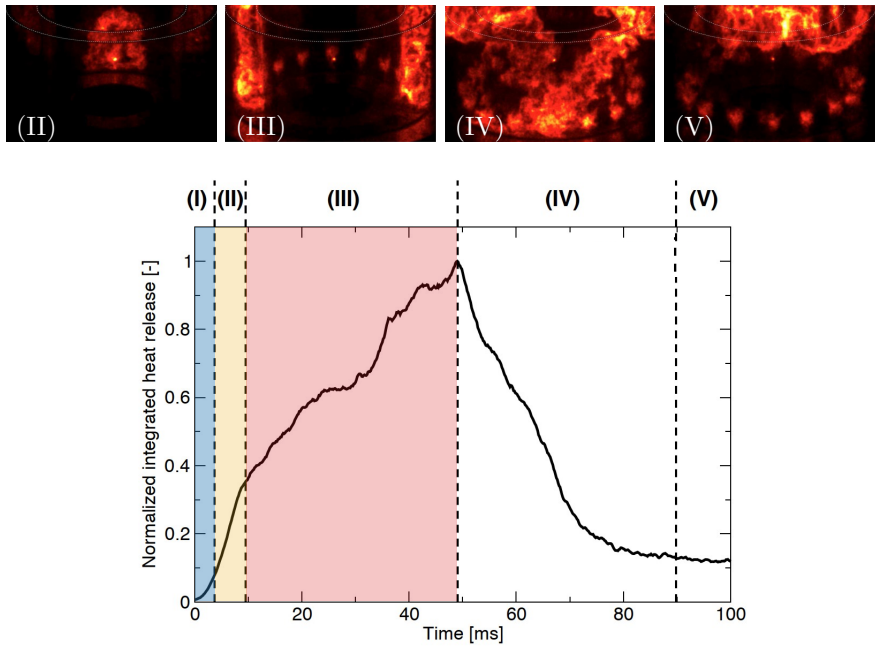

Figure 1.5: The normalised integrated heat release (rate) is plotted against time. Adapted from Philip (2016), Philip et al. (2014b).

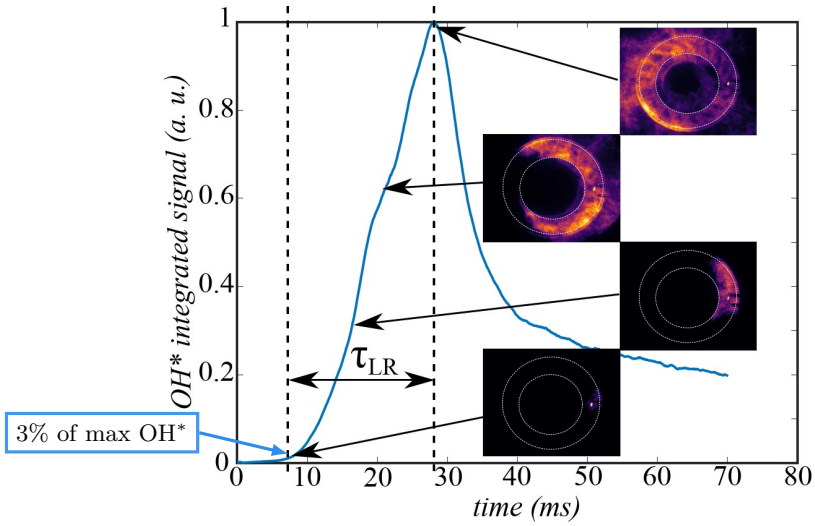

Figure 1.6: Light-around time defined using a threshold value (3% of maximum OH*) for the start and a maximum intensity value for the end. Adapted from Ciardiello et al. (2020a).

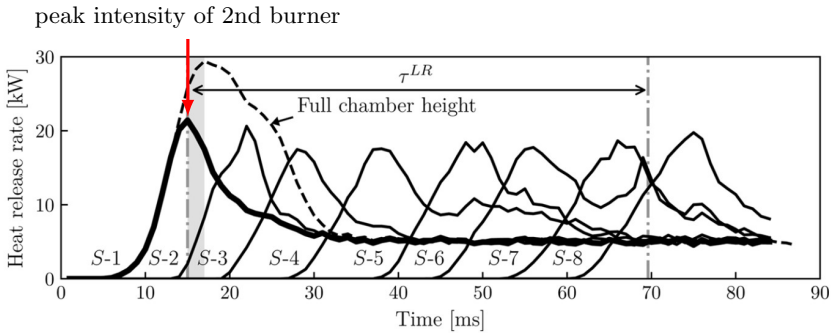

Figure 1.7: The start of the sequence is chosen to be upon the successful ignition of injector sector 2 (labelled S-1)[†], which is marked by the HRR intensity peak. It is considered complete when the two flame fronts are merged (determined through visual inspection of high-speed images). Adapted from Töpperwien et al. (2022).
[†] Injector sector 1 is designated as S-0.

Ignition and kernel formation during phase (I) is characterised by high temporal variability, owing to the stochastic nature of initial flame growth (Lancien et al. 2019). This is supported by past works studying spark ignition probability in single flames (Ahmed and Mastorakos 2006, Ahmed et al. 2007). Recent studies by Lancien et al. (2019) and Töpperwien et al. (2022) consider the onset of a light-around to be only upon the successful ignition of the first (or second) injector to reduce variability between experimental runs. This corresponds to the linear HRR growth in phase (II) which is shaded in yellow (see Figure 1.5). The peak intensity values measured by the PMTs at each individual injector sector are used to identify the characteristic times. Figure 1.7 is an example: in this case, the second injector sector (denoted by S-1) is chosen to be the reference point to increase data reproducibility.

For the end ignition event, a convenient choice is the peak integrated OH* intensity measured at the end of phase (III) as shown in Figure 1.5 and Figure 1.6. It reasonably estimates the flame merging instant compared to the more accurate method (barring human error) of manually inspecting images to determine the exact moment when the two flame fronts merge (Bourgouin et al. 2013, Töpperwien et al. 2022).

A more representative quantity for characterising ignition delay is the (absolute) propagation speed S_a, since the light-around process of a larger combustion chamber evidently takes longer than a smaller one. It may be computed as: $S_a = (\pi D/2)\,/\tau_{ign}$ where D is the mean diameter of the combustor and τ_{ign} is the light-around time. The factor of $1/2$ assumes that

the CW and ACW flame fronts each travel approximately half of the annulus circumference, which is generally valid (Ciardiello et al. 2020a). If a more accurate measurement of the distance travelled by the flame branch is possible, S_a may be computed using that (Lancien et al. 2019). For ease of reading, all existing studies presented shall be described in terms of propagation speed, whenever possible. A distinction between various concepts of flame speeds is discussed in Section 2.1. For now, it suffices to state that the (absolute) propagation speed, light-around speed, or ignition propagation speed all refer to the same quantity S_a, which is the distance travelled by the flame branch divided by the ignition delay or time lapsed between the start and end ignition event, as is discussed earlier.

1.2.2 Factors influencing light-around speed

Existing studies are primarily focused on investigating parameters which affect ignition propagation speed S_a since a quick and predictable light-around are desirable characteristics of an engine. At present, the identified factors can generally be divided into: (i) flow field effects, (ii) flame properties, and (iii) thermal effects.

Bach et al. (2013) performed the earliest known light-around study on an 18-injector Cambridge/NTNU rig and showed that S_a decreased significantly when injector bulk flow velocity U is increased from 10 to 18 m/s ($Re = 12000$ to 22000). Later studies have shown the contrary: using the same combustor, Machover and Mastorakos (2017a) showed a positive correlation between S_a and U when considering identical operating conditions. The same conclusion was also made for the MICCA combustor operating at $Re = 7800$ to 15600 (Bourgouin et al. 2013, Philip et al. 2014b) or when spray flames are considered (Lancien et al. 2018, Prieur et al. 2017). This is attributed to increased turbulence fluctuation u' and enhanced convection effects from larger U values. A power law of the form: $S_a \propto U^{0.38}$ has been proposed by Bourgouin et al. (2013) to characterise the flame-turbulence interaction. This relationship predicts a diminishing effect of U on S_a and this has been observed in a recent study by Ciardiello et al. (2020a): for $Re \gtrapprox 24500$, S_a remains approximately constant despite an increase in U. Several propositions have been put forth to explain the plateauing trend, such as unfavourable flow conditions near injector exit (Machover and Mastorakos 2017a) or higher probability of local flame extinction (Ciardiello et al. 2020a), but these have not been verified in detail. Ciardiello et al. (2020a) has also drawn parallel between the diminishing effect of U on S_a with the "bending effect" of flame speed at increased levels of turbulence fluctuation u' (Poinsot and Veynante 2001).

The effect of U may also be influenced by the operation mode of the combustor. Under partially premixed and non-premixed conditions, the influence of U diminishes (Gao et al. 2021a,b, Machover and Mastorakos 2016). The order of spark and fuel injection also matters. In all of the above-mentioned studies, the chamber is prefilled with air-fuel before spark is initiated, a procedure described as Fuel First Spark Later (FFSL) by Xia et al. (2019). If the ignition procedure is reversed to have Spark First Fuel Later (SFFL), which is often the case for a starter assist restart (see Figure 1.1), the effect of U on S_a is much greater. Finally, combustors with non-negligible azimuthal velocity components have a propagation speed which is more correlated with U. The presence of azimuthal velocity may be due to:

- reactants being injected into the chamber at an oblique angle[4], or
- the addition of swirlers as a flame stabilisation mechanism.

For the former, the strong circumferential velocity component resulting from the oblique fuel injection makes S_a almost solely dependent on U (Wang et al. 2021, Ye et al. 2018). In the latter case, Machover and Mastorakos (2017a) conducted light-around studies on both swirling and non-swirling flames. They concluded that in the presence of a swirling flow field, S_a is higher for the same operating condition. An increase in U also leads to a proportionally larger increase in S_a for swirling flames compared to non-swirling ones.

However, azimuthal velocity enhancing burner-to-burner propagation is likely only applicable at sufficiently small injector spacing based on experimental studies performed on a linear array injector setup. Barré et al. (2014) systematically varied the distance between adjacent injectors to evaluate its impact on flame propagation. Consider l_s the distance from the axial centreline of one burner to the next, and d_{inj} the diameter of the injector outlet. At $l_s/d_{inj} \leq 7.5$, high S_a values are reported due to the strong tangential velocity component of the swirling flames promoting a spanwise propagation mode. For $l_s/d_{inj} \geq 10$, flames are observed to propagate along a longer axial trajectory at a much slower speed and higher variability. In an annular configuration, the effect of injector spacing on S_a has so far only been investigated in the Cambridge/NTNU combustor. l_s/d_{inj} is varied between 2.34 to 1.56, corresponding to the 12-injector and 18-injector configuration. Results have not been conclusive. For non-premixed flames, the 18-injector combustor has a higher S_a value compared to the 12-injector (Machover and Mastorakos 2016). Under premixed conditions, the reverse is true with

[4] Oblique fuel injection is a geometric feature characteristic of certain combustor designs and will be elaborated in Section 2.3.

the 12-injector generally having a shorter ignition delay (Machover and Mastorakos 2017a). However, a recent study by Ciardiello et al. (2020a) suggests that there is little or no influence.

Aside from flow field effects, flame properties play a major role in influencing the ignition propagation speed. Laminar flame speed S_L^0 has been identified by Bourgouin et al. (2013) as a critical parameter. Machover and Mastorakos (2017a), Prieur et al. (2017), Xia et al. (2019) have since corroborated this key finding via ignition studies of gaseous and spray flames under premixed conditions. The strongest evidence correlating S_L^0 to S_a is provided in a recent investigation by Ciardiello et al. (2020a): two different hydrocarbon mixtures, specifically that of CH_4-air and C_2H_4-air, produce very similar light-around times (and hence speed) for the same S_L^0 value. Similar to flow velocity U, the effect of S_L^0 under partially or non-premixed conditions is much less clear (Gao et al. 2021a,b). It is important to mention that when using pure hydrocarbon as fuel, S_L^0 is varied by changing the equivalence ratio ϕ. For $\phi \lessapprox 1$, an increase in ϕ leads to an increase in both S_L^0 and dilatation ratio, which is the ratio of the density of unburned reactants (ρ_u) to that of the hot burnt products (ρ_b) which is also known to influence the ignition light-around speed. The effect of ρ_u/ρ_b is discussed later in the section.

The dependence of ignition propagation speed on the bulk velocity U and laminar flame speed S_L^0 logically leads to the choice of expressing S_a in terms of the turbulent flame speed S_T, a flame speed concept which encapsulates both turbulent flow field effects and the flame property S_L^0. Review papers by Driscoll (2008), Lipatnikov and Chomiak (2005, 2002) provide a detailed summary on the extensive research concerning S_T correlations. Notably, Bourgouin et al. (2013) modelled the flame ignition behaviour using $S_T = \left(S_L^0\right)^{0.6} U^{0.4}$ with reasonable success. Xia et al. (2019), Zhong et al. (2021) have also used S_T correlation of the form: $S_T = S_L^0 + C\left(u'\right)^{0.5}\left(S_L^0\right)^{0.5} Re_{\mathcal{L}}$ (Lipatnikov and Chomiak 2002, Zimont 1979) to characterise the propagation speed of the flame front's leading points. In the above S_T expression, $Re_{\mathcal{L}} = u'\mathcal{L}/\nu$ is the integral-scale Reynolds number, u' is the velocity fluctuation, $\mathcal{L}$ is the integral length scale within the combustor, ν is the fluid's kinematic viscosity and C is a constant.

Some studies have also chosen to represent the light-around propagation speed in the form: $S_a = (\rho_u/\rho_b)\, S_T$ (Bourgouin et al. 2013, Prieur et al. 2017). The term ρ_u/ρ_b reflects the effect of the volumetric expansion of hot gases during ignition. It is also a key parameter affecting S_a and is discussed

in the following paragraph.

Across a flame reaction zone, there is a significant density change between the downstream hot burned combustion products ρ_b and the upstream cold unburned reactants ρ_u. During ignition, this difference in density enhances flame propagation since the newly formed burned gas expands and drives the fresh reactants further downstream. This phenomenon has since been aptly known as the thrust (Barré et al. 2014) or the piston effect (Prieur et al. 2018). The concept of a density-weighted flame displacement speed given by $S_d = S_a/(\rho_u/\rho_b)$ is used to quantify this combustion-induced density variation (Poinsot and Veynante 2001, Ruetsch and Broadwell 1995), and may be computed by considering the ratio of the adiabatic flame temperature to the temperature of the unburned fresh reactants (Prieur et al. 2017). This expression has been extensively adopted in numerous flame research (Echekki and Chen 1998, Im and Chen 1999) and more recently, in light-around studies (Bourgouin et al. 2013, Ciardiello et al. 2020a, Prieur et al. 2017, Xia et al. 2019). Notably, the effect of the dilatation ratio ρ_u/ρ_b was evaluated by Töpperwien et al. (2022) in a recent LES study on the MICCA combustor. It was found that the volumetric expansion of hot burned gases during the early phase of light-around may result in an increase of the azimuthal velocity component by up to 400%, greatly enhancing the ignition speed. However, Ciardiello et al. (2020a) suggests that the influence of ρ_u/ρ_b is much more limited compared to that of S_L^0. It is also widely believed that the effect of ρ_u/ρ_b is highly dependent on the thermal operating conditions, in comparison to S_L^0. For instance, if the combustor is preheated prior to ignition, there is minimal or no heat loss from the hot expanding gases to the combustor walls since they are (almost) in thermal equilibrium. ρ_b and thus ρ_u/ρ_b remains largely constant. This adiabatic scenario is akin to an immediate relight upon engine shutdown, and is known to exhibit speeds up to 60% faster than in a (cold) non-preheated case (Philip et al. 2014b). In contrast, for a non-preheated case, the combustion chamber is ignited with combustor walls at ambient room temperature to approximately mimic relight after an extended period of engine shutdown. Considerable heat loss is expected from the huge temperature gradient as hot flame fronts impinge upon the cold combustor walls. The increase in burned gas density ρ_b weakens the thrust effect, with a reduced azimuthal velocity U_θ, leading to an eventual decrease in S_a (Puggelli et al. 2020).

Two recent LES studies by the EM2C group however, has shed light on the complexity of the interaction between dilatation ratio and thermal conditions in liquid fuel spray combustion: (i) A higher ρ_u/ρ_b value due to little

or no heat loss does not lead to a proportionate increase in S_a. This is attributed to a corresponding increase in the outflux of burned gases from the combustion chamber outlet, which partially negates the increase in propagation speed due to a volumetric expansion of hot gases (Töpperwien et al. 2022). (ii) The effect of dilatation ratio may be much more diminished than previously thought. Despite considerable heat loss throughout the light-around sequence in the ambient temperature case, the value of ρ_u/ρ_b at any instant is still much larger that of the preheated, adiabatic case since ρ_u is larger for preheated reactants (Töpperwien and Vicquelin 2022). Therefore, the lower ignition speed for the non-preheated case as compared to the preheated case cannot in any way, be explained by the dilatation ratio effect. Instead, it was found that unburned reactants at elevated temperatures have higher S_L^0 which leads to larger S_a values. Compared to density variation across a flame front, laminar flame speed is shown to be much more susceptible to changes in thermal conditions. The role of laminar flame speed may be much more dominant and that of dilatation much more limited than previously thought.

1.2.3 Findings and knowledge gaps of existing light-around studies

Table 1.1: Summary of past ignition light-around studies in annular combustors. Unless otherwise stated, experiments are taken to be conducted on premixed gaseous flames.

2008	First LES performed by Boileau et al. (2008).
2013	First experiments by Bach et al. (2013) on the Cambridge combustor, and Bourgouin et al. (2013) on the MICCA. Investigation of bulk velocity U and turbulence effects.
2014	Experimental and LES investigation on ignition phases by Philip et al. (2014a,b, 2015). Thermal effects identified.
2016	First non-premixed flames study by Machover and Mastorakos (2016). Investigation on bulk velocity U, injector spacing l_s/d and equivalence ratio ϕ.
2017	First liquid spray ignition experiment by Prieur et al. (2017). Study on thermal effects, dilatation ratio ρ_u/ρ_b, and laminar flame speed S_L^0.
	Study on the effect of injector spacing l_s/d, bulk velocity U, equivalence ratio ϕ, and swirl by Machover and Mastorakos (2017a).
	Numerical study on non-premixed flames by Machover and Mastorakos (2017b). Investigation on stochasticity.
2018	Ignition dynamics of liquid spray flames by Prieur et al. (2018).
2018	Two-phase reactive flow LES on spray flames by Lancien et al. (2018).
2018	First study on the effect of strong azimuthal swirl by Ye et al. (2018).
2019	Effect of volumetric expansion (dilatation ratio) on leading point dynamics in liquid spray flames by Lancien et al. (2019).
	Study of ignition modes (Fuel First, Spark Later or Spark First, Fuel Later) by Xia et al. (2019).

2020
- LES on wall temperature for liquid spray flames by Puggelli et al. (2020).
- LES study on ignition dynamics by Zhao et al. (2020).

2021
- Spark location, lean ignition probability and laminar flame speed S_L^0 by Ciardiello et al. (2020a,b).
- Study of ignition modes (Fuel First, Spark Later or Spark First, Fuel Later) and effect of bulk velocity U and equivalence ratio ϕ under strong azimuthal swirl by Wang et al. (2021).
- Propagation dynamics and effect of bulk velocity U and equivalence ratio ϕ in staged partially premixed flames by Gao et al. (2021a,b).
- Flame subgrid-scale wrinkling modelling of liquid spray flames by Puggelli et al. (2021).
- Experimental study on the flow field dynamics during light-around by Zhong et al. (2021).

2022
- Low-order modelling of light-around by Ciardiello et al. (2022a).
- LES study on the impact of two-phase flow and wall heat transfer on the propagation mechanism of liquid spray flames by Töpperwien and Vicquelin (2022), Töpperwien et al. (2022).
- Leading point dynamics in staged partially premixed flames by Wang et al. (2022).

Existing studies have mainly focused on the investigation of light-around propagation speed S_a in annular combustors using premixed hydrocarbon-air. A list of past works is listed in Table 1.1, and the experimental findings could be summarised as follows.

- An increase in bulk velocity U generally leads to faster light-around propagation speed S_a likely due to increased turbulence and convection effects. The effect plateaus with increasing values of U.

- The presence of azimuthal velocity component favours spanwise over axial flame propagation. This mode of propagation is faster, and leads to increased S_a values.
- The effect of flame interaction (through variation of injector spacing) is inconclusive but seems to have little or no impact on S_a.
- Laminar flame speed S_L^0 is identified as a dominant factor influencing ignition propagation speed which is further enhanced with increased temperature T.
- The volumetric expansion of hot burnt gases (quantified using dilatation ratio ρ_u/ρ_b) has been shown to have a much more diminished impact on S_a.

In light of these past works, the relevant knowledge gaps may be formulated into questions which are grouped into sub-topics:

On flame properties

Q1. *Are current light-around findings based on hydrocarbon fuels applicable to non-carbon fuel types such as NH_3 and H_2?*
It is unknown if existing findings based on hydrocarbon fuels are equally valid for carbon-free fuels that have different flame properties. For instance, NH_3 has a much lower laminar flame speed (Valera-Medina et al. 2018) while H_2 has a much faster molecular diffusion (Rieth et al. 2022) with Lewis number Le much less than one. Given that flame properties may heavily influence ignition propagation speed S_a as seen in previous studies which have established a strong correlation between laminar flame speed S_L^0 and S_a (Ciardiello et al. 2020a, Prieur et al. 2017, Xia et al. 2019) or that the dilatation ratio ρ_u/ρ_b, has been suggested to be a key mechanism of flame propagation (Bourgouin et al. 2013, Töpperwien et al. 2022), it is imperative to gain a better understanding on how these flame properties affect ignition dynamics. This is particularly relevant when there is increased interest in using non-conventional fuels such as NH_3 and H_2 to reduce carbon emissions yet little is currently known about the effect of these fuel types on ignition dynamics.

Q2. *What is the isolated effect of laminar flame speed and dilatation ratio on ignition light-around?*
Related to the previous objective on the effect of flame properties on ignition dynamics, the effects of dilatation ratio ρ_u/ρ_b and laminar flame speed S_L^0 have not been independently investigated due to the limitation of using a single hydrocarbon species as fuel: increasing equivalence ratio ϕ leads to

larger S_L^0 values and invariably, increases ρ_u/ρ_b as well. As such, identifying the individual contribution of ρ_u/ρ_b and S_L^0 in light-around propagation of lean premixed hydrocarbon fuel-air mixtures is not easily achieved.

On combustion modes

Q3. *Do more realistic combustion modes like Rich-Quench-Lean (RQL) share similar ignition behaviour to the conventional laboratory combustor?*
Light-around ignition studies are usually conducted in greatly simplified annular combustors operating in a non-staged, premixed mode. This is done by necessity due to limitations in a laboratory setting. Limited studies performed under non-premixed or partially premixed conditions, which are more realistic to engines presently in operation, indicate that ignition under non-premixed conditions is very different from that of premixed flames. More complicated multi-stage burning modes, such as azimuthal staging or Rich-Quench-Lean (RQL) staging[5] have so far not been investigated for its effect on ignition dynamics as well.

On statistical convergence

Q4. *Are conclusions drawn upon limited number of light-around runs (which is a transient and stochastic process) valid?*
Finally, current findings are concluded based on limited runs, usually between three to five repetitions for a given operating condition. It is not exactly clear if findings deduced from such small sample sizes are necessarily conclusive given that ignition light-around is a transient phenomenon occurring under turbulent flow conditions to which we end off this introductory section on ignition dynamics by quoting Mastorakos (2017) in his recent review paper:

> *Since ignition is a transient process and the flows we are interested in are turbulent, the average behaviour must be understood as an ensemble over many ignition realisations.*"

There is evidently a need to provide more experimental data related to light-around and Section 1.4 provides an overview of how various experiments are conceived to address the relevant research questions.

[5]The different staging methods are discussed in Chapter 2.

1.3 Lean blowoff dynamics

Similar to challenges in conducting ignition studies, the investigation of lean blowoff (LBO) dynamics in actual engines is difficult due to: (i) the inherent complexity of the transient phenomenon, (ii) lack of optical access, and (iii) the complicated geometry of a typical engine as discussed earlier in Section 1.2. Numerous LBO studies have since been performed in single flames, and are summarised in the review papers of Longwell (1953), Mellor (1980), Penner and Williams (1957), Radhakrishnan et al. (1981) and more recently that of Shanbhogue et al. (2009). Compared to ignition light-around studies however, investigation of LBO in annular configurations is even more limited. To the best of knowledge, studies have so far only been performed on the atmospheric annular combustor in Cambridge, UK (Allison and Mastorakos 2017, Ciardiello et al. 2020c), as well as a preliminary LBO study of a 4-injector annular combustor in Jadavpur University, India (Bhattacharya et al. 2019). Before discussing existing LBO studies performed on turbulent premixed flames which is the focus of this thesis, some definitions are first briefly discussed.

First, a distinction between the terms blowoff and blowout is often made. As described by Mansour (2003), blow-off (blowoff) refers to the extinction of attached flame while blow-out (or blowout) is specific to the extinction of a lifted flame. In the current work, no such distinction is made. The choice is motivated by existing studies which show that a series of local flame liftoff and subsequent reattachment/reignition events usually occurs prior to the eventual global extinction of flames. Discerning whether it is a blowoff or blowout event at each injector sector is complicated in an annular combustor and generally not of practical interest. (Lean) blowoff or blowout will be used interchangeably to refer to the global extinction of fuel-lean flames independent of the status of the flame (lifted or attached) prior to extinction, similar to the approach adopted in Cavaliere (2013) and Ciardiello (2021). Blowoff however, is not synonymous with local extinction as emphasised by Shanbhogue et al. (2009). In fact, local extinction should be regarded as part of the blowoff process which is described below.

1.3.1 Lean blowoff process

The lean blowoff process can be regarded as a two-stage process (Lieuwen 2012) and is shown in Figure 1.8.

(I) *Local extinction of flames.* This is the instant where holes start forming in the flame sheets, generally in regions with high stretch rate.

With increasingly lean fuel mixtures or higher flow velocities[6], the occurrence and duration of these local extinction events increase.

(II) *Change in wake dynamics leading to global extinction of flames.* As the blowoff process progresses, the flow field becomes more unsteady and is usually characterised by large velocity fluctuations (Hertzberg et al. 1991) and strong flame flapping (Chaudhuri and Cetegen 2008, Nair and Lieuwen 2005, 2007). Flames can no longer stabilise well at the shear layers and all flames are eventually extinguished.

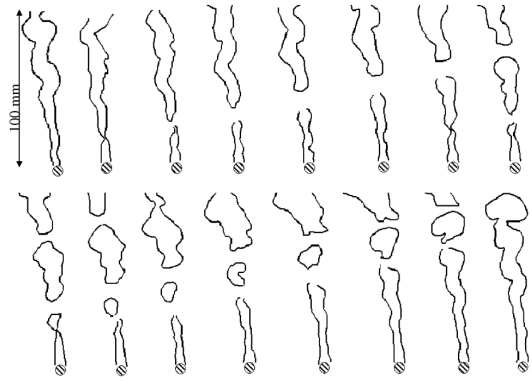

Stage (I): occurrence of flame holes which indicate local flame extinction.

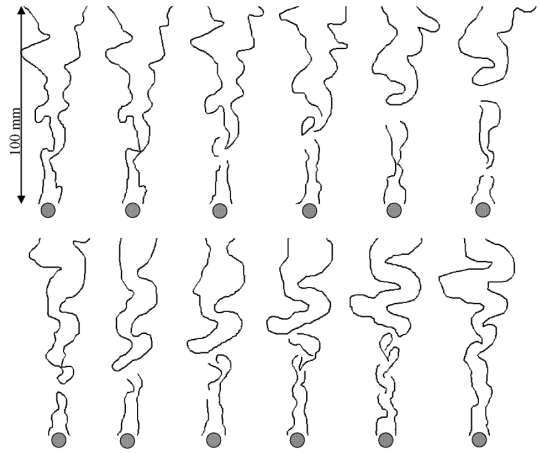

Stage (II): flapping of flame fronts which are also observed to be more wrinkled.

Figure 1.8: Sequence of flame images showing stages (I) and (II) of the lean blowoff process. Reproduced from Nair and Lieuwen (2007).

[6]The experimental procedure for lean blowoff studies is discussed in detail under Section 3.7.

It is worth mentioning that in stage (I) of the blowoff process, the unstable flame undergoes cycles of local extinction and recovery, but is able to persist in this state perpetually according to Nair and Lieuwen (2007). It is only at some point in stage (II) that flame recovery is impossible, resulting in the inevitable consequence of global flame extinction. Recent advances in high-speed optical diagnostics have provided insights on the instants leading to the final blowoff event.

1.3.2 Lean blowoff mechanism

Planar light scattering from seeded oil droplets and OH* chemiluminescence performed by Muruganandam and Seitzman (2005) suggested that highly strained lean flames have holes which allow continual penetration of cold reactants into the recirculation zone. The hot gas recirculation is disrupted and the heat release rate decreases to a point whereby successful reignition along the shear layer is no longer possible, leading to the eventual global flame extinction. Simultaneous measurements of OH*-Planar Laser-Induced Fluorescence (PLIF) and Particle Image Velocimetry (PIV) by Chaudhuri et al. (2010, 2011) support this finding. However, it was emphasised that the findings do not exclude other possible blowoff mechanisms, particularly for combustors with different geometries and operating conditions. LBO experiments conducted in Cambridge University suggested that it is also the entrainment of cold reactants, but from the downstream end of the recirculation zone that leads to the eventual blowoff (Dawson et al. 2011, Kariuki et al. 2012a,b). A later study by Kariuki et al. (2013) showed that geometric factors such as injector spacing and the presence of swirl alter the flow field and influence whether the entrainment of reactants is along the sides or at the downstream end of the recirculation zone. An experimental and numerical study by Zhang et al. (2021) suggested that aside from geometric factors, the blowoff behaviour is also affected by the fuel type. For a swirling CH_4 flame, a decrease in heat release rate (from decreased fuel consumption) results in local extinction near the flame root, causing the flame to lift off and eventually lead to a final blowoff. In the case of a NH_3 flame, excessive strain rate was identified as the reason which causes local extinction at the downstream end of the recirculation zone that progressively leads to the flames being fully extinguished. Wiseman et al. (2020) also considered different fuel types, and it was reported that for a given strain rate, CH_4 flames have a much lower heat release rate compared to NH_3-H_2-N_2 blends, and therefore have worse blowoff limits. PIV and OH* chemiluminescence by Morales et al. (2019) provided insights on how interaction between the flames and flow field vorticity along the shear layer

induces high strain rates, leading to flame extinction.

Simultaneous OH and CH_2O PLIF has also been recently employed by Kumar et al. (2020) to quantify reactant pockets (or flame holes) of a premixed swirl-stabilised flame. The reactant pockets were found to be small in volume and with short lifetimes. They do not entrain far into the wake, and simply react and/or mix quickly with the hot gases. The average wake composition of a lean, unsteady flame approaching blowoff is thus, surprisingly not very different from that of a stable flame. The large-scale flow disruptions observed during stage (II) of the blowoff process therefore cannot be explained solely by the presence of reactant pockets.

In all existing studies, identification and generalisation of a unifying physical mechanism(s) governing the final blowoff event in stage (II) of the LBO process remains an unresolved key issue (Lieuwen 2012, Shanbhogue et al. 2009).

Geometric factors influencing lean blowoff limits

Aside from fundamental investigations on the LBO mechanism, various geometric influences on the eventual lean blowoff limits of premixed flames have also been studied. The presence of a confinement chamber improves the LBO limits in both bluff body stabilised (Dawson et al. 2011) and swirling flames (Ji et al. 2022), and is likely attributed to the different stabilisation mechanisms involved. In addition, Ji et al. (2022) concluded that a larger confinement area leads to flames which are more resilient to lean extinction, similar to previous findings by Tong et al. (2017). The chamber height was also investigated by Kariuki et al. (2013) but the results were inconclusive. Interestingly, it was found that a square enclosure better stabilises a flame compared to a circular one.

In the same study by Kariuki et al. (2013), the presence of a swirling flow field in a twin-flame configuration was found to have minimal impact on the eventual blowoff limits. However, it is suggested that a higher swirl intensity, measured in terms of swirl number $\mathcal{S}$, does lead to an improvement in LBO limits for a single flame (Jerzak and Kuźnia 2016, Syred et al. 2014).

Injector spacing in a multi-injector combustor is another key geometric paramter which has also been considerably studied in various works (Ciardiello et al. 2020c, Jella and Bergthorson 2022, Kariuki et al. 2013, Kwong and Steinberg 2019a,b, Yamaguchi et al. 1985). This is discussed later in the chapter under Section 1.3.4.

1.3.3 Lean blowoff correlation

Despite the difficulty in determining the actual LBO mechanism as discussed earlier, there has been some considerable success in formulating lean blowoff correlations based on existing single flame studies.

Early works suggested the blowoff limit equivalence ratio ϕ to be a function of injector diameter d_{inj}, temperature T, pressure P, and bulk flow velocity U, as summarised by Longwell et al. (1953). To better relate the blowoff phenomenon to fluid and chemical fundamentals, Zukoski and Marble (1956) proposed the use of Damköhler number Da which is the ratio of the characteristic fluid time scale τ_{flow} to the characteristic chemical time scale τ_{chem} as shown in Equation 1.1:

$$Da = \frac{\tau_{\text{flow}}}{\tau_{\text{chem}}} \tag{1.1}$$

Karlovitz number Ka may also be used, and is usually regarded as the inverse of Damköhler number Da. A critical value of Da or Ka exists such that the relevant chemical process needs to occur at a faster rate than that of the characteristic fluid time for the successful stabilisation of flame. This critical value is dependent on the choice of the characteristic times τ_{flow} and τ_{chem}. For the fluid mechanic time scale τ_{flow}, it is given as $\tau_{\text{flow}} = \frac{l}{U}$ where l is the characteristic length scale which may be the wake length behind a flameholder or diameter of the flameholder. U is the characteristic velocity at the blowoff limit which may be chosen as the average burned gas velocity or the injector exit velocity. For the chemical time scale τ_{chem}, there is a lack of consensus on the definition, reflecting the limited understanding of the underlying reaction and blowoff mechanism as discussed earlier. In the most recent review paper by Shanbhogue et al. (2009), different τ_{chem} were considered:

- the "blowoff residence time" of a perfectly stirred reactor τ_{psr}, or
- the inverse of extinction strain rate of a laminar premixed flame (flamelet) $\tau_{\text{ext}} = 1/\kappa_{\text{ext}}$.
- the unstretched laminar premixed flame time $\tau_{\text{pf}} = \delta_{\text{L}}/S_{\text{L}}^0$ where δ_{L} is the laminar flame thickness and S_{L}^0 is the laminar flame speed.

The computation of these characteristic chemical times is usually obtained from CHEMKIN (Morales et al. 2019, Shanbhogue et al. 2009). In the case of τ_{psr}, it is assumed that there is rapid mixing of cold reactants and hot burnt gases within the combustor, similar to a well-stirred reactor. Within this homogeneous reaction zone, extinction occurs if the entrainment rate of cold

reactants into the recirculation zone exceeds the consumption rate at which these reactants are being burned (Law 2006, Longwell et al. 1953, Penner and Williams 1957). However, there is little or no evidence to support the assumption of a well stirred reactor (with infinitely quick mixing) as pointed out by Driscoll (2008). On the other hand, existing studies suggest that the concept of flamelets is applicable to a wide range of flow conditions and is more appropriate (Driscoll 2008). In this case, the flame front is assumed to consist of numerous small laminar flames (flamelets). When these flamelets are subjected to sufficiently high strain rates[7] and/or heat losses, extinction occurs (Law 2006, Poinsot and Veynante 2001). It is interesting to note that despite limited understanding of the final flame extinction mechanism in stage (II) of the blowoff process, Da values reported from various datasets using different choices of τ_{chem} all give a reasonable collapse with respect to the Reynolds number of the flow. This is likely attributed to current approaches being capable of capturing at least part of the physics involved in stage (I) of the blowoff process (Shanbhogue et al. 2009).

Another possible expression of the fluid and chemical time scale is proposed by Radhakrishnan et al. (1981) and expressed as in Equation 1.2.

$$\frac{1}{Da} = \left[C \underbrace{\left(\frac{U}{l} \right)}_{\frac{1}{\tau_{\text{flow}}}} \underbrace{\left(\frac{\nu}{\left(S_{\text{L}}^{0} \right)^{2}} \right)}_{\tau_{\text{chem}}} \right]^{1/2} \tag{1.2}$$

It is derived based on consideration of coherent structures in turbulent flows, assuming that the time needed for laminar flame propagation through turbulent small eddies, taken as τ_{chem}, needs to occur faster than the characteristic fluid mechanic time τ_{flow} for successful flame stabilisation. It has been used to scale the blowoff limits of not just single flames (Cavaliere et al. 2013, Kariuki et al. 2012a) but also two adjacent flames (Kariuki et al. 2013) in one of the first attempts to describe the lean blowoff limits of a multi-injector setup by means of a Damköhler number Da. Reasonable collapse was achieved for the twin-flame configuration at different injector spacing for both swirling and non-swirling cases. At present, there are limited lean blowoff studies in multi-injector configuration to conclusively validate the

[7] This is also known as the flame stretch rate κ, which is the rate of change of a flame surface element A, given by $\kappa = (1/A)\, \mathrm{d}A/\mathrm{d}t$. See Chapter 2 for details.

generality of Equation 1.2, especially given the much more complex flame interaction taking place in an annular geometry. This is illustrated in the following section whereby key findings of lean blowoff investigations in linear array and annular combustors are summarised.

1.3.4 Blowoff dynamics in multi-injector combustor

Studies on correlations and governing mechanism of the lean blowoff (LBO) have been mainly restricted to only single flames by necessity to reduce the associated complexity and cost, but with a clear limitation of being incapable of replicating the complex flame interaction present in adjacent injectors as highlighted earlier in Section 1.2 when discussing ignition dynamics. An early study by Yamaguchi et al. (1985) using multiple cylindrical rod bluff bodies suggested that with decreased injector spacing, the lean stability limit is reduced. A twin-flame study by Kariuki et al. (2013) arrived at similar conclusions in which the single flame cases always have a leaner fuel limit for a given injector bulk velocity. Consideration of the Damköhler number Da in Equation 1.2 did however, result in a reasonable collapse of the blowoff limits for both single and twin flames.

The first LBO study in an annular configuration was performed only as recent as 2017 by Allison and Mastorakos (2017) on the 18-injector Cambridge combustor. The annular combustor was noticed to have an asymmetric blowoff behaviour in which individual injectors blowoff at different instants. Two distinct stages of LBO were identified: (I) local flame extinction on individual injector sectors, followed by (II) the eventual global extinction, There was a 20% reduction in equivalence ratio ϕ from the first instant of local flame extinction to the eventual global extinction, an indication of the prolonged transient process of lean blowoff. This is similar to stages (I) and (II) of the LBO process described by Shanbhogue et al. (2009) for single premixed flames. The preliminary study was followed up with a detailed investigation by Ciardiello et al. (2020c) in which the lean operational limit of a 12- and 18-sector combustor was mapped. These geometric configurations correspond to an injector spacing of $l_s/d_{inj} = 2.34$ and 1.56 respectively where l_s is the distance from the axial centreline of one burner to the next, and d_{inj} is the diameter of the injector outlet. The 12-injector setup was able to better withstand blowoff when compared against the 18-injector. Equation 1.2 was again used to correlate the LBO limits. The Da values corresponding to the 12-injector combustor agrees well with the single flame results previously measured by Kariuki et al. (2012b) if the blowoff limit is taken to be at the onset of stage (I) which is the time instant when local flame extinction first occurs. This follows a similar hypothesis

by Shanbhogue et al. (2009) in which he reasoned that Da correlations work well in correlating stage (I) of the LBO process (see Section 1.3.3). However, no satisfactory scaling was possible for the 18-injector configuration which has a greater extent of flame interaction due to the tighter injector spacing.

The flow field and flame interaction between adjacent injectors, a characteristic noticeably absent in single flame setups, also amplifies any local flame extinction and/or lift-off as reported by Ciardiello et al. (2022b). Whenever flames at an annular sector is lifted or extinguished, the sector(s) in proximity also undergo subsequent local extinction and when the flame reattaches back to the injector bluff body, the adjacent (lifted) flames are also likely to reattach in successive instants. The dependence behaviour of adjacent flames has also been previously observed in multiple injectors arranged in a linear array as evidenced by the experimental works of Kwong and Steinberg (2019a,b). Simultaneous OH*-PLIF and stereoscopic-PIV were performed, and local extinction and reattachment events occurring at a single injector site were observed to drastically change the flow fields in the immediate vicinity. In a two-injector configuration, it enhances and extends the lean operational limit compared to a single flame while the reduced injector spacing in a 5-burner case increases flame strain rate κ and weakens the recirculation zone, resulting in a poorer LBO limit. A subsequent Large Eddy Simulation (LES) study was also conducted to replicate the flame stabilisation observed experimentally (Jella and Bergthorson 2022, Jella et al. 2021). Interestingly, the reactant residence time, which is closely related to the perfectly stirred reactor model, was able to account for the observed non-monotonic LBO trend with decreased injector spacing. Flame strain rate however, was unable to explain the LBO behaviour.

A recent LBO study was also performed by Ciardiello et al. (2022b) in a linear arrangement of five injectors and exhibited very similar LBO behaviour to that of the 12-injector annular combustor. The reported $1/Da$ values computed using Equation 1.2 for the case of the linear array of injectors lie in the same range as that of the annular combustor. It was concluded that the linear arrangement can reliably replicate the lean blowoff limits of an annular combustor.

1.3.5 Findings and knowledge gaps of existing blowoff studies

Existing studies have established that lean blowoff is a two-stage process for which:

- the onset of stage (I) local extinction may be reasonably predicted by the Damköhler number Da for the case of single flame and to some

extent, multi-injector flames.

- Flame interaction in a multi-injector setup (be it in an annular or linear arrangement) amplifies any local flame extinction or local flame reattachment, and may either worsen or improve the LBO limits.

Various pertinent questions concerning lean blowoff dynamics remain unaddressed and are attributed to the lack of understanding in the underlying mechanism particularly in the case of multi-flame combustors. This is due to the lack of experimental studies as shown by the limited past investigation in Table 1.2.

From single flame studies, it is clear flames are able to withstand some form of extinction, given that they may exist perpetually in stage (I) of the blowoff process. However, current studies have not been able to exactly pinpoint the mechanism triggering the global extinction event which could either be the entrainment of cold reactants quenching the reaction or overly stretched flames rendering flame stabilisation impossible, to name a few. There is also no agreement on the appropriate measure of quantity which determines the critical limit at which flame recovery is impossible, resulting in the inevitable global flame extinction. For instance, strain rate κ and heat release rate (indicative of the reaction rate) have been used to define relevant thresholds for different stages of the blowoff process. However, flames have been observed to survive even when κ exceeds the supposed extinction strain rate or when the heat release rate (indicative of the reaction rate) is well below the extinction value. As discussed earlier in Section 1.3.2, the analysis of the blowoff process requires advanced imaging diagnostics which may not always be available.

Table 1.2: Summary of past lean blowoff studies in annular combustors. Relevant studies on linear array combustors are also included. Unless otherwise stated, experiments are taken to be conducted on premixed gaseous flames.

2013	Visualisation of twin-flame lean blowoff by Kariuki et al. (2013).
2017	First LBO study in an annular configuration by Allison and Mastorakos (2017).
2019	Detection of LBO in an annular combustor by Bhattacharya et al. (2019).
2019	LBO dynamics in a linear combustor by Jella et al. (2021), Kwong and Steinberg (2019a,b). Investigation on injector spacing l_s/d and reattachment dynamics.
2020	LBO study on single sector and annular configurations by Ciardiello et al. (2020c). Investigation on the use of Damköhler number Da to characterise LBO limits.
2022	Comparison of LBO dynamics under premixed and non-premixed mode for both linear array and annular combustors by Ciardiello et al. (2022b).
	Numerical study on the influence of injector spacing in a linear array combustor by Jella and Bergthorson (2022).

In view of the inherent complexity of LBO mechanism(s) and the possible limitations in our laboratory, the thesis mainly focuses on the characterisation of lean blowoff behaviour in an annular configuration. The following questions are considered:

On combustion modes

Q5. *Is it possible to modify laboratory-scale combustors to more closely replicate the lean blowoff physics of real engines? If so, does it still share similar lean blowoff characteristics to the conventional laboratory combustor?*
Similar to ignition studies, experimental work on lean blowoff are usually performed in simplified non-staged laboratory-scale combustors. It is not unknown whether the physics of lean blowoff process replicated in these model combustors are drastically different from actual engines which typ-

ically have quench cooling or in some cases, have unique geometric design inducing strong azimuthal swirl for instance.

On multi-flame interaction

Q6. *How does the lean blowoff dynamics of annular combustors compare to that of a single flame?*
Compared to light-around ignition which is unique to annular combustors, the lean blowoff phenomenon can be found in both single and multiple flames arranged either in a linear or annular configuration. Despite the large amount of literature on the lean blowoff dynamics on single flames, current data concerning annular combustors is too limited however to arrive at any conclusive findings, such as whether the Damköhler number Da can always be used to describe multiple-flame extinction as in the case of single sector flames, or determining the effect of flame interaction on LBO which current studies have only just begun to investigate.

As the first step to better understanding LBO in annular combustors, there is a pertinent need to gather more experimental data concerning the lean blowoff dynamics in such a geometry which constitutes part of the research objectives discussed in the following section.

1.4 Objectives

The past decade of research has increased our understanding of the relevant physics governing the light-around process but also highlighted various knowledge gaps. Likewise, advances in high-speed diagnostics have painted a better picture of lean blowoff dynamics yet fundamental questions remain unaddressed. This section outlines how experimental work performed in the framework of this thesis attempts to address the various research questions for *ignition and lean blowoff dynamics of turbulent flames in annular combustors* listed in Section 1.2.3 and Section 1.3.5 respectively.

First, to address Q4, multiple runs are performed for each experiment to ensure at least some form of statistical convergence In the case of ignition light-around, each operating point is repeated 10-15 times for the data presented in Article II, and at least 30-50 times for Article III. For lean blowoff, each operating point of interest is also repeated multiple times on separate occasions to check for repeatability.

The remaining research questions could be classified into three main research objectives as shown in Figure 1.9 which are elaborated in the following paragraphs.

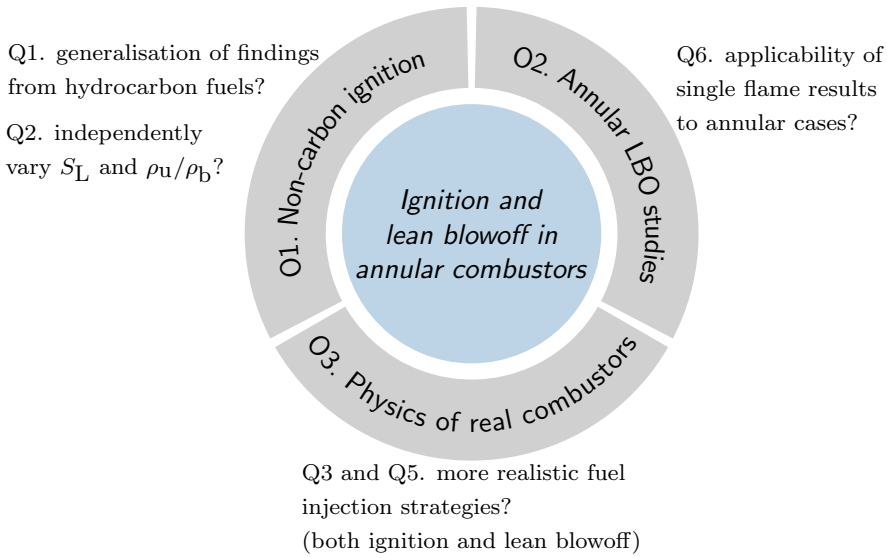

Figure 1.9: Chart summarising the research objectives.

O1. Ignition studies using non-carbon fuels

Fuel blends of NH_3 and H_2 are investigated in the NTNU annular combustor for their effect on ignition dynamics. To the best of understanding, this is the first such attempt to consider the use of non-carbon fuels in light-around studies. This helps to answer Q1 and verify if current findings are applicable to non-carbon fuels which have vastly different flame properties. The use of NH_3 and H_2 blends also helps to address Q2 since a mix of different fuel types allows independent variation of the laminar flame speed S_L^0 and dilatation ratio ρ_u/ρ_b, something which is not achievable when using only a single hydrocarbon fuel. Details of these are discussed in Article III.

O2. Lean blowoff studies using different annular injector configurations

To the best of knowledge, there has been only one detailed lean blowoff (LBO) study performed on the Cambridge annular combustor (Ciardiello et al. 2020c). LBO experiments are thus conducted on annular combustors as well as their single flame equivalents, details of which is covered in Chapter 3, to provide more experimental insights to address Q6. The lean extinction limits are mapped for different geometries of the annular combustor, and high speed diagnostics are employed in the form of OH* chemiluminescence imaging and planar laser-induced fluorescence (PLIF) and PIV will be used to characterize flame-to-flame interactions, which has

been identified as a key factor influencing LBO in multi-flame configurations. Preliminary data is presented in Chapter 4.

O3. Studies more closely replicating physics of real combustors

In response to Q3 and Q5, two new laboratory-scale combustors are conceived to mimic key design features found in the SAFRAN spinning combustor, in collaboration with SAFRAN Helicopter Engines under the innovative Training Network of ANNULIGhT, an EU funded project under the Marie Skłodowska-Curie Actions. The simplified laboratory-scale models are designed to include:

- a strong mean azimuthal swirl around the annular chamber,
- a Rich-Quench-Lean (RQL) staging mode, and
- azimuthal fuel staging.

Section 2.3 describes these features in detail. Though these two combustors are still simplistic in nature, they serve as more realistic replications of actual engines compared to current laboratory models which may have been grossly simplified in some instances. A preliminary characterisation followed by ignition and lean blowoff experiments are performed to identify the relevant physics which are replicated from high to low technology readiness level (TRL). The characterisation data serves to validate the fidelity of Large-eddy Simulation (LES) performed by CERFACS, France and SAFRAN Helicopter Engines, France in simulating flames present in a spinning combustor, and is documented in Article I. Results pertaining to ignition dynamics under the effect of strong azimuthal swirl in a RQL staged combustor is presented in Article II. Azimuthal fuel staging is also evaluated for its impact on ignition limits in the second part of the paper. The effect of strong mean azimuthal swirl on lean blowoff is discussed in Article IV.

1.5 Thesis outline

This current chapter gives an introduction to *ignition and lean blowoff dynamics of turbulent flames in annular combustors*, providing the relevant research context and motivations. Relevant concepts are next discussed in Chapter 2 before a presentation of the relevant experimental setup and diagnostics in Chapter 3. Chapter 4 briefly covers some unpublished data, mainly pertaining to that of lean blowoff dynamics. The relevant research articles are summarised in Section 5.1 before concluding with a future outlook. Appendix A contains the technical drawings of experimental setups which have been specifically conceived for the purpose of this thesis.

2

Fundamentals

In this chapter, various definitions and concepts used in the current work are briefly outlined as follows.

(2.1) The properties of a canonical flame is briefly presented,
(2.2) followed by characteristics of a swirling flow before finally introducing,
(2.3) the design concepts of the SAFRAN Spinning Combustion Technology.

2.1 Flame properties

Different non-carbon fuel blends are used to independently vary combustion properties, specifically the laminar flame speed S_{L}^{0} and dilatation ratio $\rho_{\mathrm{u}}/\rho_{\mathrm{b}}$, to study their effects on the absolute flame speed S_{a} during the ignition light-around process. It serves to evaluate whether existing findings based upon hydrocarbon fuels are equally valid for non-carbon fuels. As seen in Article III, it is revealed that the thermo-diffusivity properties of a fuel mixture, which may be quantified by the effective Lewis number Le_{eff}, may also influence the ignition propagation speed. These key flame properties are thus briefly presented in the following sections to provide readers with the relevant context. The content is based on Cant and Mastorakos (2007), Law (2006), Poinsot and Veynante (2001) and readers may wish to refer to them for details.

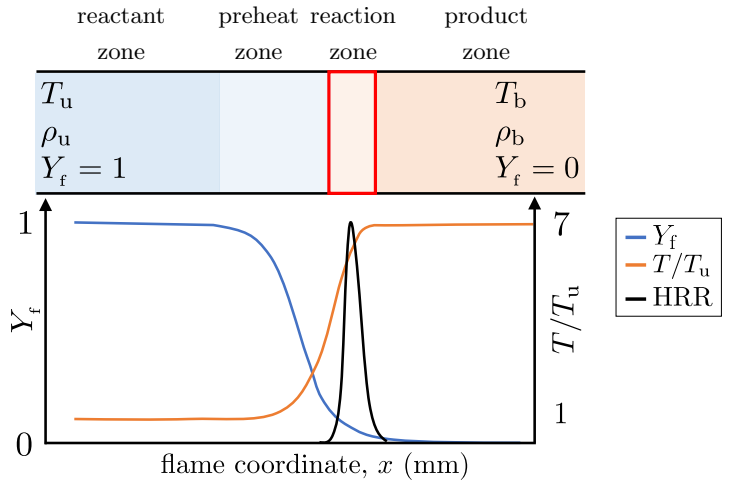

Figure 2.1: Simple illustration showing the relevant flame quantities of a 1-D laminar flame propagating in a premixed gas under adiabatic conditions.

Consider a one-dimensional (1-D) stationary, planar, unstretched laminar flame freely propagating in a premixed gas under adiabatic conditions as illustrated in Figure 2.1. Quantities denoted with $(\cdot)_u$ are that of the unburned fresh reactants upstream of the flame, and $(\cdot)_b$ refer to that of the burned products downstream of the flame. Upstream of the flame, the reactant mixture has temperature T_u, density ρ_u, and fuel mass fraction $Y_f = 1$. Reaction only takes place within a very narrow spatial zone as denoted by the red box. The flame surface, usually defined by an isocontour of a scalar quantity[8], lies within this region. It is characterised by a spike in heat release rate (HRR) with a fuel consumption rate of $\dot{\omega}_f$ that eventually depletes the fuel (assuming the oxidiser is in excess), such that $Y_f \to 0$. The formation of hot combustion products from the exothermic reaction leads to a rapid rise in temperature from T_u to T_b. In the simple case where we assume no heat loss and no work done (constant volume), the temperature of the burned mixture T_b is known as the adiabatic flame temperature T_{ad}. The density of the cold fresh reactants ρ_u also decreases to ρ_b which is the density of the hot combustion gas. The ratio ρ_u/ρ_b is known as the dilatation ratio. The speed at which this laminar planar flame freely propagates into the premixed gas is known as the laminar flame speed or the laminar

[8]The scalar quantity may be for instance, temperature T or the mass fraction of a species i, Y_i.

burning velocity S_L^0. The superscript $(\cdot)^0$ is used to denote that the laminar flame speed is that of an unstretched flame (see Section 2.1.1 for stretch effects).

Typical values of the flame properties are listed in Table 2.1. Depending on the fuel type, the values of the quantities, in particular that of S_L^0, may vary by up to an order of magnitude for a given equivalence ratio ϕ. For instance, at stoichiometric, NH_3 has S_L^0 which is 5 times slower than that of CH_4, while that of H_2 exceeds 2 m/s. The vast differences may be attributed to the following properties of the fuel species: (i) the adiabatic flame temperature T_{ad}, (ii) the thermo-diffusive effects quantified by *Le* (See Section 2.1.2), and (iii) the molecular structure of the fuel. A detailed discussion on the influence of these factors on S_L^0 may be found in Law (2006). The speed at which the flame propagates, denoted as S_L, is also affected by the rate of change of flame surface A, otherwise known as the stretch κ which is discussed in Section 2.1.1. In this case, the superscript $(\cdot)^0$ is dropped since the assumption of an unstretched flame is no longer valid.

Table 2.1: Table summarising typical values of flame properties at equivalence ratio $\phi = \{0.7, 1.0\}$ for a 1-D freely-propagating planar, unstretched premixed laminar flame. Values corresponding to $\phi = 0.7$ is in blue. Properties computed using Cantera (Goodwin et al. 2018).

Fuel	S_L^0 (m/s)	ρ_u/ρ_b (-)	$T_{ad}(K)$
hydrocarbon fuels			
CH_4	{0.19, 0.35}	{6.27, 7.66}	{1838, 2227}
C_2H_4	{0.34, 0.64}	{6.84, 8.22}	{2003, 2373}
C_3H_8	{0.19, 0.39}	{6.62, 8.14}	{1885, 2270}
non-carbon fuels			
NH_3	{0.02, 0.07}	{6.12, 7.43}	{1723, 2059}
H_2	{1.33, 2.28}	{6.06, 6.98}	{2002, 2378}

Flame speeds

Three types of flame speeds are often defined and they are: (i) consumption speed S_c, (ii) displacement speed S_d, and (iii) absolute speed S_a.

The consumption speed S_c is the speed at which reactants are being consumed, and is defined as $-\frac{1}{\rho_u Y_{f,u}} \int_{-\infty}^{+\infty} \dot{\omega}_f \, d\vec{n}$ where $\dot{\omega}_f$ is the consumption rate[9], ρ_u is the unburned gas density, $Y_{f,u}$ is the unburned fuel mass fraction, and $\vec{n}$ is a unit vector normal to the flame surface pointing towards the

[9] $\dot{\omega}_f$ has units of kg/(m^3 s) and has a value < 0 since it reflects the consumption of fuel.

unburned fresh gases. It is a global quantity that considers the net reaction rate integrated over the entire domain, and is therefore relatively insensitive to the choice of the flame surface. In contrast, the displacement speed S_d and absolute flame speed S_a are local quantities which vary spatially and are dependent on the chosen flame surface. S_d at a point $\vec{\mathbf{p}}$ on the flame surface is given as the difference between the gas flow speed $\vec{\mathbf{u}}(\vec{\mathbf{p}})$ and the flame front speed $\vec{\mathbf{w}}(\vec{\mathbf{p}})$, i.e. $(\vec{\mathbf{w}}(\vec{\mathbf{p}}) - \vec{\mathbf{u}}(\vec{\mathbf{p}})) \cdot \vec{\mathbf{n}}$. Given that $\vec{\mathbf{u}}(\vec{\mathbf{p}})$ is the unburned gas speed just upstream of the flame front, it is hard to measure experimentally. A more convenient choice, often by necessity in experiments, is to consider the flame front speed at point $\vec{\mathbf{p}}$ relative to a fixed spatial position, and not relative to the flow. This is known as the absolute flame speed S_a. The definition of S_a used in this thesis is described later in Flame speeds: S_a.

Next, these definitions are applied to the canonical case of a 1-D planar, unstretched laminar flame freely propagating in a premixed gas as depicted earlier in Figure 2.1 but with an inlet flow velocity of $\vec{\mathbf{u}}_x$ in the positive x direction, so $\vec{\mathbf{u}}_x = u_x\vec{\mathbf{n}} = -u_x\vec{\mathbf{x}}$.[10]

The consumption speed S_c is only dependent on the global fuel consumption rate, and is equal to the fuel burning rate of the laminar flame, which is S_L^0. Taking a point far upstream ($x = 0$) as the spatial reference (see Figure 2.1), the absolute flame speed S_a is simply: $S_\mathrm{a} = \vec{\mathbf{w}} \cdot \vec{\mathbf{n}} = -u_x + S_\mathrm{L}^0$. To compute the displacement speed S_d at the flame surface[11], Equation 2.1 is used to obtain the flow velocity component along $\vec{\mathbf{n}}$.

$$\underbrace{\rho\,(\vec{\mathbf{u}} - \vec{\mathbf{w}}) \cdot \vec{\mathbf{n}}}_{\text{flame surface}} = \underbrace{\rho_\mathrm{u}\,(\vec{\mathbf{u}}_\mathrm{u} - \vec{\mathbf{w}}) \cdot \vec{\mathbf{n}}}_{\substack{\text{unburned}\\ \text{reactants}}} \tag{2.1}$$

S_d is then defined as: $S_\mathrm{d} = S_\mathrm{L}^0\,(\rho/\rho_\mathrm{u})$. Readers may wish to refer to Poinsot and Veynante (2001) for the mathematical details. If we take the density ρ at flame front to be that of the hot burned products ρ_b, we retrieve the expression for density-weighted displacement speed: $S_\mathrm{d} = S_\mathrm{L}^0\,(\rho_\mathrm{b}/\rho_\mathrm{u})$ which quantifies acceleration through the flame front (Giannakopoulos et al. 2015, Ruetsch et al. 1995).

Flame speed concepts which have been briefly discussed in this section are summarised in Table 2.2.

[10] We recall that $\vec{\mathbf{n}}$ points towards the unburned fresh reactants.

[11] Since we consider a 1-D case, the notation $(\vec{\mathbf{p}})$ to denote a point $\vec{\mathbf{p}}$ on the flame surface is omitted in subsequent discussion.

Table 2.2: Table of flame speed definitions. Adapted from Poinsot and Veynante (2001).

Speed	Definition	Equation	Canonical case
consumption	speed at which reactants are consumed	$-\frac{1}{\rho_\mathrm{u} Y_\mathrm{f,u}} \int_{-\infty}^{+\infty} \dot{\omega}_\mathrm{f} \, \mathrm{d}\vec{\mathbf{n}}$	S_L^0
displacement	flame front speed relative to the flow	$(\vec{\mathbf{w}}(\vec{\mathbf{p}}) - \vec{\mathbf{u}}(\vec{\mathbf{p}})) \cdot \vec{\mathbf{n}}$	$S_\mathrm{L}^0 \left(\frac{\rho}{\rho_\mathrm{u}}\right)$
absolute	flame front speed relative to a fixed reference frame	$\vec{\mathbf{w}}(\vec{\mathbf{p}}) \cdot \vec{\mathbf{n}}$	$-u_x + S_\mathrm{L}^0$

Flame speeds: S_a

For the purpose of our research, we are concerned with the flame speed when propagating from one burner to another. The absolute flame speed S_a is taken to be the experimentally measured propagation speed relative to a fixed reference frame. An example is given below: consider a sector of an annular combustor with an arc length of l_s between injectors I_1 and I_2 as shown in Figure 2.2(a). PMT_1 and PMT_2 detect the normalised flame intensity along a line-of-sight (1D) exceeding 20% at time t_1 and t_2 respectively (see Figure 2.2(b)). S_a is then given as:

$$S_\mathrm{a} = \frac{\overbrace{l_\mathrm{s}}^{\text{distance}}}{\underbrace{(t_2 - t_1)}_{\text{time delay}}} \tag{2.2}$$

The choice of 20% as a threshold is arbitrary and other values such as 3% (Ciardiello et al. 2020a) or 100% (Töpperwien et al. 2022) are possible. The idea is that the chosen threshold is representative of an ignition event. For instance, a peak in flame intensity (which occurs at the end of light-around stage (III) as described earlier in Section 1.2.1) is indicative of the instant of successful flame stabilisation at an injector. Alternatively, a certain percentage of the measured peak intensity (e.g. 3% or 20%) is used to quantify the instant at which the flame kernel propagates past an injector and ignites a sufficient amount of unburned reactants. This may then be used to represent any time instant between stages I and III of the light-around process.

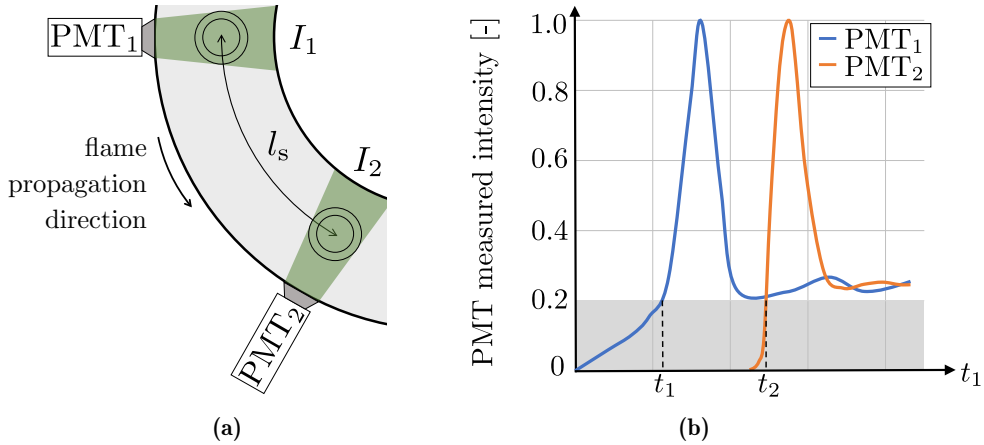

Figure 2.2: Figure showing: (a) schematic of setup for measuring absolute flame speed S_a and (b) plots of the 1-D line-of-sight intensity measured by PMTs positioned at injector sectors I_1 and I_2.

2.1.1 Flame stretch

One of the factors influencing flame speed is flame stretch κ which is the rate of change of a flame surface element A given by:

$$\kappa = \frac{1}{A}\frac{\mathrm{d}A}{\mathrm{d}t} \tag{2.3}$$

The reason why κ influences flame speed is mainly due to the inflow of fresh gas reactants when the flame is stretched which also inevitably subjects the flame to more cooling. This competing effect of reactant diffusivities into the flame and the heat transfer between the cold fresh reactants and the hot burned gaseous products then plays an important role in determining whether the flame speed accelerates or decreases. A detailed discussion may be found in Cant and Mastorakos (2007), Lieuwen (2012), Poinsot and Veynante (2001).

The rate of change of flame surface is affected by both (i) local flow (due to flow non-uniformity), and (ii) motion effects of a curved flame. κ may thus be expressed in the form of Equation 2.4 to reflect the contribution from these two factors (Candel and Poinsot 1990).

$$\kappa = \underbrace{-\vec{\mathbf{n}}\vec{\mathbf{n}} : \vec{\boldsymbol{\nabla}}\vec{\mathbf{u}} + \vec{\boldsymbol{\nabla}} \cdot \vec{\mathbf{u}}}_{\substack{\text{flow non-uniformity} \\ \text{or flame strain} \\ (\kappa_{\text{strain}})}} + \underbrace{S_{\mathrm{d}}\left(\vec{\boldsymbol{\nabla}} \cdot \vec{\mathbf{n}}\right)}_{\substack{\text{flame curvature} \\ (\kappa_{\text{curv}})}} \tag{2.4}$$

The two terms of κ_{strain} may be grouped into a single expression:

$$\kappa = (\vec{\mathbf{m}}\vec{\mathbf{m}} + \vec{\mathbf{q}}\vec{\mathbf{q}}) : \vec{\boldsymbol{\nabla}}\vec{\mathbf{u}} + S_{\text{d}}\left(\vec{\boldsymbol{\nabla}} \cdot \vec{\mathbf{n}}\right) \tag{2.5}$$

$$= \vec{\boldsymbol{\nabla}}_{\text{t}} \cdot \vec{\mathbf{u}} + S_{\text{d}}\left(\vec{\boldsymbol{\nabla}} \cdot \vec{\mathbf{n}}\right) \tag{2.6}$$

where $\vec{\mathbf{m}}$ and $\vec{\mathbf{q}}$ in Equation 2.5 are two orthonormal vectors lying in the tangent plane of the flame, and $(\cdot)_{\text{t}}$ in Equation 2.6 refers to the tangential components of the $\vec{\boldsymbol{\nabla}}$ operator. In a Cartesian coordinate (x, y, z) where the flame normal vector $\vec{\mathbf{n}}$ at a particular time instant is along the $\vec{\mathbf{x}}$ (axial direction), $\vec{\mathbf{y}}$ and $\vec{\mathbf{z}}$ are the two orthonormal vectors lying in the tangent plane, and $\vec{\boldsymbol{\nabla}}_{\text{t}} \cdot \vec{\mathbf{u}} = \partial u_y/\partial y + \partial u_z/\partial z$.

At weak flame stretch rates, flame strain and flame curvature have similar roles (Poinsot and Veynante 2001). This is a particularly useful property since in certain cases, one may then simply consider only the strain values which are obtainable from computationally inexpensive simulation of a 1-D velocity field using Equation 2.7 (Klarmann et al. 2016, Long et al. 2019).

$$\kappa_{\text{strain}} = -\frac{\partial u_x}{\partial x} \tag{2.7}$$

Note that Equation 2.7 is valid because of the incompressible assumption:

$$\vec{\boldsymbol{\nabla}} \cdot \vec{\mathbf{u}} = \frac{\partial u_x}{\partial x} + \underbrace{\frac{\partial u_y}{\partial y} + \frac{\partial u_z}{\partial z}}_{\kappa_{\text{strain}}} = 0 \tag{2.8}$$

The inherent complexity of measuring the flame curvature, which is multi-dimensional in nature, is thereby avoided (Klarmann et al. 2016). In highly turbulent flows, the contribution of flame curvature is also limited and may be neglected (Klarmann et al. 2016, Nassini et al. 2021).

2.1.2 Effective Lewis number

The response of laminar flame speed S_{L} to stretch κ is strongly dependent on the thermo-diffusive property of the mixture which may be quantified by the Lewis number Le. Le_i of a species i in a mixture is D_{th}/D_i where D_{th} is the thermal diffusivity of the mixture and D_i is the mass diffusivity of species i into the mixture. The overall or effective Lewis number of the mixture is known as the effective Lewis number Le_{eff} and is computed based on a two-reactant approach (Jackson 1987, Joulin and Mitani 1981) given

by:

$$Le_{\text{eff}} = 1 + \frac{(Le_{\text{E}} - 1) + (Le_{\text{D}} - 1) \cdot \mathcal{A}}{1 + \mathcal{A}} \tag{2.9}$$

The relevant variables are:

- Le_{E}: Lewis number of excess reactant
- Le_{D}: Lewis number of deficient reactant
- $\mathcal{A}$: mixture's strength which is defined as: $\mathcal{A} = 1 + Ze(\Phi - 1)$.

In a lean mixture ($\phi < 1$), the oxidiser (oxygen) is the excess reactant, and $Le_{\text{E}} = Le_{\text{ox}}$. Fuel is the deficient reactant, so $Le_{\text{D}} = Le_{\text{f}}$. In a fuel-rich mixture ($\phi > 1$), fuel is the excess reactant, and $Le_{\text{E}} = Le_{\text{f}}$. Oxygen is the deficient reactant, and Le_{D} becomes Le_{ox}.

Lewis numbers: Le_{ox} and Le_{f}

Computing the Lewis number of the oxidiser Le_{ox} is usually straightforward. The Lewis number of fuel Le_{f} however, requires careful consideration. If only a single fuel is used, Le_{f} is simply that of the single fuel species. In instances whereby two or more fuel types are used in a premix, .e.g. a CH_4-H_2 blend, a weighted Le_{f} has to be computed. Currently, there are three main approaches to compute a weighted Le_{f} but with no general consensus on a common definition (Bouvet et al. 2013). They are: heat release-based, volume-based, and diffusion-based.

Le_{f}: heat release-based

First introduced by Law et al. (2005), the heat release-based expression is:

$$Le_{\text{f}} = 1 + \frac{\sum_{i=1}^{N} q_i^* \, (Le_i - 1)}{\sum_{i=1}^{N} q_i^*} \quad \text{for } i = 1^{st}, \ldots, N^{th} \text{ fuel species} \tag{2.10}$$

where Le_i is the Lewis number of the i^{th} fuel species, and q^* is the non-dimensional heat release:

$$q_i^* = \frac{qY_i}{C_{\text{p}} T_{\text{u}}} \tag{2.11}$$

In Equation 2.11, q is the specific heat of reaction (kJ/kg), Y_i is the species mass fraction, c_{p} is the specific heat capacity of the mixture at constant pressure (kJ/(kg K)), and T_{u} is the unburned mixture temperature (K). Existing works by Vu et al. (2009, 2011) have applied Equation 2.10 for mixtures up to $N = 3$ fuel species.

Le_{f}: volume-based

Proposed by Muppala et al. (2009), the volume-based expression is:

$$Le_{\mathrm{f}} = \sum_{i=1}^{N} \chi_i Le_i, \quad \sum_{i=1}^{N} \chi_i = 1 \text{ for } i = 1^{st}, \ldots, N^{th} \text{ fuel species} \tag{2.12}$$

where χ_i refers to the mole fraction of each fuel species.

Le_{f}: diffusion-based

Introduced by Dinkelacker et al. (2011), the diffusion-based expression is:

$$Le_{\mathrm{f}} = \sum_{i=1}^{N} \frac{\chi_i}{Le_i}, \quad \sum_{i=1}^{N} \chi_i = 1 \text{ for } i = 1^{st}, \ldots, N^{th} \text{ fuel species} \tag{2.13}$$

Equation 2.13 is formulated on the assumption of a predominantly positively curved flame front.

Mixture strength $\mathcal{A}$

To compute $\mathcal{A} = 1 + Ze(\Phi - 1)$, the following expressions are used:

$$\Phi = \begin{cases} \frac{1}{\phi}, & \text{if } \phi < 1 \\ \phi & \text{otherwise} \end{cases} \tag{2.14}$$

$$Ze = \frac{E}{\mathcal{R}} \frac{(T_{\mathrm{b}} - T_{\mathrm{u}})}{T_{\mathrm{b}}^2}, \qquad \text{where } \frac{E}{\mathcal{R}} = -2 \frac{\mathrm{d} \ln\left(\rho_{\mathrm{u}} S_{\mathrm{L}}^0\right)}{\mathrm{d}(1/T_{\mathrm{b}})} \tag{2.15}$$

Equation 2.14 characterises the equivalence ratio ϕ of the mixture and is always ≥ 1. Equation 2.15 is the Zel'dovich number which is a non-dimensional quantity characterising the activation energy of a chemical reaction with $\mathcal{R}$ the universal gas constant, E the activation energy of the chemical reaction, T_{b} the burned mixture temperature, T_{u} the unburned mixture temperature, ρ_{u} the density of the unburned mixture, and S_{L}^0 the laminar flame speed. To compute $E/\mathcal{R}$, small increments of T_{u} were considered to vary T_{b} (Beeckmann et al. 2017, Bradley et al. 1998).

2.2 Swirling flow

In most engines, flames are stabilised by means of swirl which is achieved by imparting an azimuthal velocity component U_θ to the flow via swirler(s),

creating a 3-D flow with a number of large-scale flow structures (Candel et al. 2012, 2014). If the angular momentum is sufficiently large, i.e. U_θ is sufficiently high, vortex breakdown occurs, creating a central recirculation zone (CRZ)[12]. This flow region is characterised by a circulating hot flow of combustion products which helps to reignite fresh, cold reactants injected into the combustor. The swirling flow region is surrounded by a high velocity reactant flow which creates a shear layer where the flames can stabilise (Lieuwen 2012, Lilley 1977). An outer recirculation zone (ORZ) of hot burned gases is also formed in the region enclosed by the flame fronts and the confines of the combustor (chamber walls and back plane). A typical swirling flow field is shown in Figure 2.3.

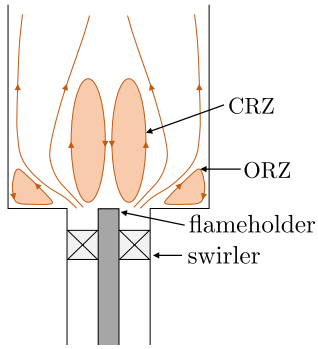

Figure 2.3: Illustration depicting the recirculation zones of a confined swirling flame. Adapted from Farisco et al. (2021).

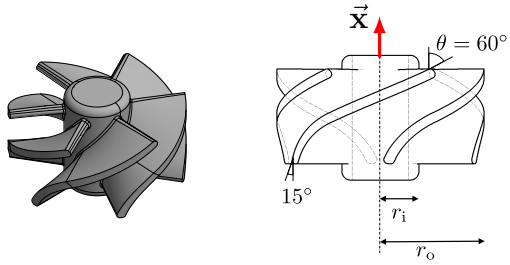

Figure 2.4: Isometric view of an axial swirler (left), and its relevant geometric dimensions (right). The red arrow denotes the axial flow direction, $\vec{\mathbf{x}}$.

In this thesis, an axial swirler is used to generate the swirling flow field and is shown in Figure 2.4.

[12] some literature use the term: internal recirculation zone.

The degree of swirl in a flow is characterised by the swirl number $\mathcal{S}$. It is a dimensionless number defined as: $G_\theta/(r_\mathrm{o}G_x)$ where G_θ is the axial flux of angular momentum, G_x is the axial flux of axial momentum, and r_o is the characteristic radius which is usually the swirler outlet radius (Chigier and Beér 1964). By neglecting pressure effects (Candel et al. 2014), the expression for $\mathcal{S}$ may be approximated as:

$$\begin{aligned}\mathcal{S} &= \frac{G_\theta}{r_\mathrm{o}G_x} \\ &\approx \frac{\int_0^R u_x u_\theta r^2 \,\mathrm{d}r}{r_\mathrm{o}\int_0^R u_x^2 r \,\mathrm{d}r}\end{aligned} \tag{2.16}$$

where u_θ is the azimuthal velocity component and u_x is the axial velocity component.

Equation 2.16 requires the knowledge of u_x and u_θ which are not always accessible. An alternative formulation may be used such that the swirl number of an axial swirler is defined solely by its relevant geometric dimensions in Figure 2.4.

$$\begin{aligned}\mathcal{S} &= \frac{\int_{r_\mathrm{i}}^{r_\mathrm{o}} u_x u_\theta r^2 \,\mathrm{d}r}{r_\mathrm{o}\int_{r_\mathrm{i}}^{r_\mathrm{o}} u_x^2 r \,\mathrm{d}r} \\ &= \frac{2}{3}\frac{1}{r_\mathrm{o}}\frac{u_\theta}{u_x}\frac{\left[r^3\right]_{r_\mathrm{i}}^{r_\mathrm{o}}}{\left[r^2\right]_{r_\mathrm{i}}^{r_\mathrm{o}}} \\ &= \frac{2}{3}\frac{u_\theta}{u_x}\left[\frac{1-\left(\frac{r_\mathrm{i}}{r_\mathrm{o}}\right)^3}{1-\left(\frac{r_\mathrm{i}}{r_\mathrm{o}}\right)^2}\right] \\ \mathcal{S}_\mathrm{g} &\approx \frac{2}{3}\tan\theta\left[\frac{1-\left(\frac{r_\mathrm{i}}{r_\mathrm{o}}\right)^3}{1-\left(\frac{r_\mathrm{i}}{r_\mathrm{o}}\right)^2}\right]\end{aligned} \tag{2.17}$$

The final expression Equation 2.17 approximates the velocity ratio U_θ/U_x using $\tan\theta$ where θ is the angle between the axial flow direction, x, and the trailing edge of the swirler. Comprising only geometric parameters, it is fittingly called the geometric swirl number $\mathcal{S}_\mathrm{g}$. For $\theta = 60°$, $r_\mathrm{i} = 5.1\,\mathrm{mm}$ and $r_\mathrm{o} = 18.8\,\mathrm{mm}$, this gives $\mathcal{S}_\mathrm{g} = 1.22$.

The critical swirl number $\mathcal{S}$ for vortex breakdown is $\mathcal{S} \geq 0.6$ (Lilley 1977, Palies et al. 2009). In this work, we have directly measured $\mathcal{S}$ of an axial

swirler under cold flow conditions by means of 2-dimensional, 3-component (2-D,3-C) stereoscopic particle image velocimetry (PIV). Details of it may be found in Section 3.8.2 which briefly describes the stereoscopic PIV performed. under Chapter 3 on experimental setup and diagnostics.

2.3 Spinning Combustion Technology

Part of this thesis focuses on investigating transient dynamics and characteristics of ignition light-around and lean blowoff in the presence of strong azimuthal swirl produced by a novel injector design of the SAFRAN Arrano 1A engine. Two simplified laboratory-scale combustors were built to investigate the physics of the novel injector design. Notably, it features:

(2.3.1) a mean azimuthal swirl flow round the annulus chamber,
(2.3.2) a Rich-Quench-Lean (RQL) combustion mode,
(2.3.3) and azimuthal fuel staging.

These three distinctive features are made possible with unique geometric designs such as angled injectors and perforated cooling plate. Images of these components are shown in Figure 2.5. The following sections briefly describe how these unique combustion modes of the engine help enhance its operational limits while realising reductions in greenhouse emissions.

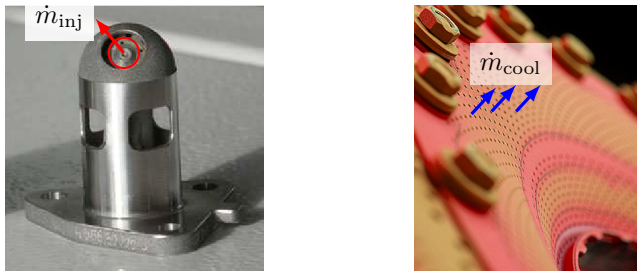

(a) (b)

Figure 2.5: Components of the SAFRAN Arrano spinning combustor: (a) an angled fuel injector for oblique air-fuel injection (of mass flow rate $\dot{m}_{\text{inj}}$) into the chamber, and (b) perforated cooling plate for tangential air dilution (of flow rate $\dot{m}_{\text{cool}}$) as part of the RQL process. Adapted from Savary and Taliercio (2016).

2.3.1 Mean azimuthal swirl

In the SAFRAN Arrano engine, angled injectors are installed along the outer circumferential wall of the chamber to inject air-fuel in an oblique angle. Air from the perforated plate is also introduced into the chamber through angled

slots to generate a tangential velocity component. This arrangement imparts a strong azimuthal velocity forming a pseudo-continuous spinning flame ring as shown in Figure 2.6. The tangential orientation of the flames and cooling air is in sharp contrast to the conventional axial injection of a typical combustor as illustrated in Figure 2.7, and is referred to as the Spinning Combustion Technology (SCT) by Safran Helicopter Engines (2016b).

Other strategies exist to induce a mean azimuthal flow round the annulus chamber, and is not unique to a SCT engine. Combustor designs like the Short Helical Combustor (SHC) (Ariatabar et al. 2016, 2017, Hoffmann et al. 2021), Compact Helical Arranged combustoRs with lean LIFTed flames (CHAIRLIFT) (Shamma et al. 2021), the angled flow combustor (Burd and Cheung 2007), the tangential flameless combustor (Toqan et al. 2015) or the recursive sequential combustor (Giuliani et al. 2022) also have similar fuel injection concepts. The increased popularity of this novel concept is due to its advantages over convention axial design described below.

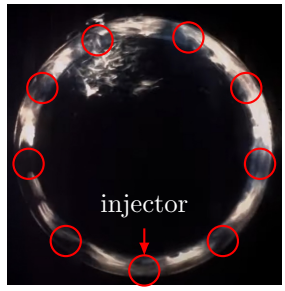

Figure 2.6: True-color image showing the annulus flame ring of the SAFRAN Arrano spinning combustor during ignition light-around. The approximate positions of the injectors are circled in red. Adapted from Safran Helicopter Engines (2016a).

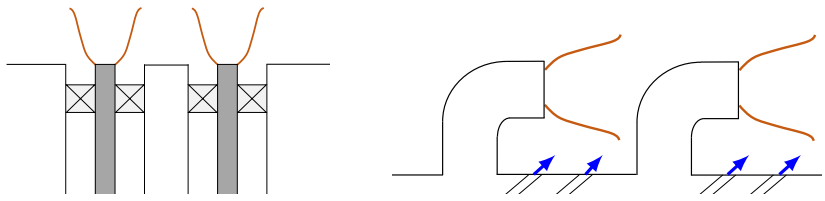

Figure 2.7: Schematic showing: (a) conventional axial fuel injection compared with (b) tangential injection of the SAFRAN Arrano engine utilising the SCT. The blue arrows represent cooling air effusing from the angled slots of the perforated plate.

Thermoacoustic stability

The mean azimuthal flow has a symmetry breaking effect which alters the thermo-acoustic azimuthal modes as suggested from analytical studies performed by Bauerheim et al. (2014, 2015). In some cases, this may lead to a dampening of self-sustained oscillations as shown in the experiments conducted by Humbert et al. (2021) on an annular combustor model with electroacoustic feedback. It was demonstrated that the introduction of a mean azimuthal flow alters the nature of self-sustained oscillations and in some cases, helps to dampen the instabilities.

Increased operational limits and reduced emissions

The SCT combustor design approach aims to promote flame-flame interaction since hot combustion products from each injector impinge on the next injector. A pseudo-continuous azimuthal flame is then generated. The continuous hot exhaust recirculation round the annulus helps sustain combustion especially in regions with lean fuel mixture (Ariatabar et al. 2016, 2017, Giuliani et al. 2022, Savary and Taliercio 2016). The lean blowoff limit may potentially be extended. Compared with conventional injectors, the enhanced mixing (of hot combustion products and fresh reactants) and increased residence time from the gas recirculation also increase the fuel homogeneity within the combustion chamber Giuliani et al. (2022), leading to (i) more complete combustion which reduces CO emissions, and (ii) reduction of hotspots, which reduces NOx emissions (Lefebvre and Ballal 2010, Lieuwen and Yang 2013).

Reduced costs

Engines utilising such a principle are more economical and the reasons are twofold. As mentioned, residence time of hot gas circulation in an angled flow configuration is longer than a conventional axial flow. The combustor could therefore be shortened in length (Ariatabar et al. 2016, Burd and Cheung 2007). Also, the angled injectors impart a significant azimuthal velocity component to the flow and require less turning by the turbine vanes downstream of the combustor chamber exit so vane design is simplified (Burd and Cheung 2007). Simpler vanes and shorter combustor height contribute to lighter engines which are more fuel efficient. In the case of the SAFRAN Arrano 1A engine, fuel consumption is reduced by 15 to 30% compared to conventional axial injection engines (Safran Helicopter Engines 2019).

2.3.2 Rich-Quench-Lean (RQL)

One of the challenges in combustor design is reducing both CO and NOx emissions. In general, design considerations to reduce CO leads to increase in NOx, and vice versa as pointed out by Lefebvre and Ballal (2010). This can be summarised in Figure 2.8 whereby high temperatures lead to formation of nitrogen oxides while low temperatures contribute to increased CO.

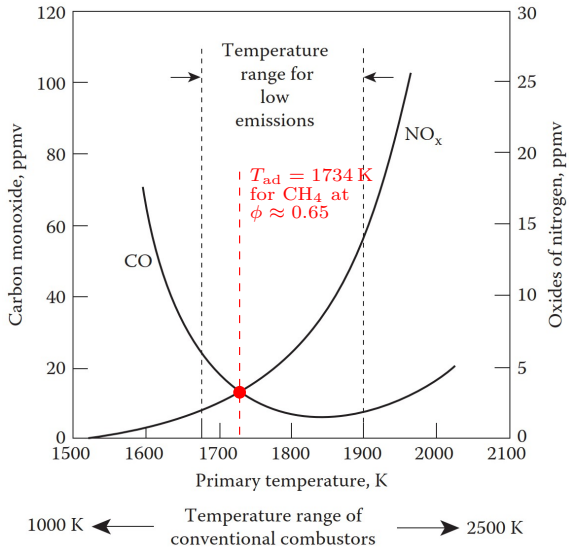

Figure 2.8: Plot showing CO and thermal NOx emissions in parts per million volume (ppmv) against temperature (K). The operating point at $T = 1734$ K (denoted in red) provides a good trade-off between CO and thermal NOx emissions. Adapted from Lefebvre and Ballal (2010).

The Rich-Quench-Lean is a successful strategy conceived in the 1970s to ensure high combustion efficiency and reduce NOx. The combustion mode can be described by the following stages and illustrated in Figure 2.9.

(I) Fuel-rich mixture is first injected into the combustor (*rich-burn, typically* $1.2 \leq \phi \leq 1.6$) leading to a stable diffusion flame.

(II) To reduce the temperature, substantial amount of dilution air is rapidly added to the fuel-rich zone to quench the fuel-rich flames (*quick-quench*) and create a lean premixed flame.

(III) The resultant lean mixture burns at a steady state with an air-fuel ratio greater than stoichiometric conditions (*lean-burn,* $\phi < 1$) at a

lower temperature to minimise NOx emissions.

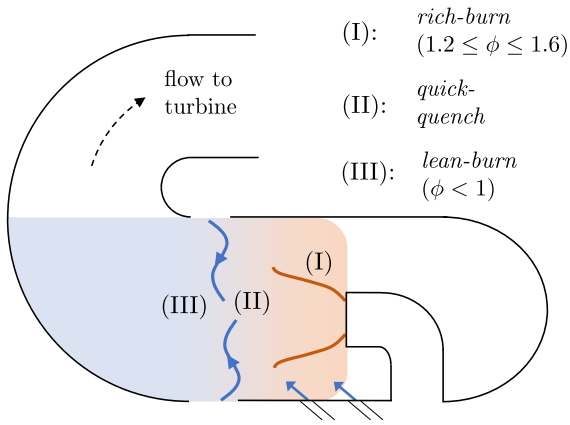

Figure 2.9: Illustration of the Rich-Quench-Lean (RQL) mode. The blue arrows represent the quenching air flow exiting the dilution holes and angled slots of the perforated cooling plate. The shaded colour gradient represents the equivalence ratio ϕ of the burning mixture with orange for $\phi > 1$, and blue for $\phi < 1$.

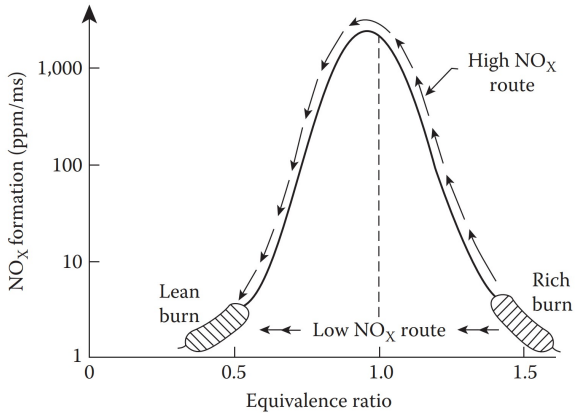

Figure 2.10: Plot showing NOx emissions in parts per million per millisecond (ppm/ms). Reproduced from Lefebvre and Ballal (2010).

The combustion pathway in a RQL process is represented in Figure 2.10 as the low NOx route. It is imperative that the progression from rich-burn to lean-burn happens rapidly so that the pathway of low NOx route is followed. If the transition is slow (i.e. progressive addition of air), the temperature within the combustor will rise, increasing NOx levels (see Figure 2.8). Aside from low NOx formation through quick-quenching of fuel-rich flames, the RQL procedure also minimises carbon monoxide (CO) and unburned hy-

drocarbon (UHC) emissions since the excess air oxidises any unburned or partially burned hydrocarbons (Tracey et al. 2018). It is worth noting that the combustor is globally lean, $\phi < 1$.

To realise the RQL mode, air jets are placed downstream of the primary combustion zone to dilute the fuel-rich mixture (Lefebvre and Ballal 2010, Lieuwen and Yang 2013). This is also the case for the SAFRAN Arrano 1A engine described in Section 3.5. Careful consideration needs to be given to various design aspects, such as the position of these dilution jets, mass flow rate ($\dot{m}_{\text{dil}}$) which may dramatically affect the efficacy of the RQL combustion mode in minimising emissions as shown in studies performed by Mastorakos and co-workers (El Helou et al. 2021, Gkantonas et al. 2020, Tracey et al. 2018).

2.3.3 Azimuthally staged combustion

In an annular combustion chamber, injector staging is another strategy employed to reduce emissions. Aside from lower emissions, Noiray et al. (2011) has also demonstrated that azimuthal staging may be used to control combustion (thermoacoustic) instabilities. To achieve this, localised variation of air or fuel in the combustion chamber is performed and Figure 2.11 shows the possible fuel staging configurations. The following description is useful to interpret the figure.

- A blue circle ● represents injector with a fuel mass flow rate of $\dot{m}_{\text{f,blue}}$, with the subscript $(\cdot)_{\text{f}}$ referring to the mass flow rate of fuel, and $(\cdot)_{\text{blue}}$ meaning that it is colour-coded blue.
- A white circle ○ represents injector with a fuel mass flow rate of $\dot{m}_{\text{f,black}}$, where $\dot{m}_{\text{f,black}} \neq \dot{m}_{\text{f,blue}}$. $(\cdot)_{\text{black}}$ means that it is colour-coded black(white).
- The air flow rate in each injector $\dot{m}_{\text{air}}$ is constant for all cases.

Figure 2.11(a) shows the conventional non-staged combustor where the same fuel mass flow rate ($\dot{m}_{\text{f,blue}}$) is supplied to each injector. The illustration of Figure 2.11(b) shows a sectorised staging whereby different fuel rates (either ($\dot{m}_{\text{f,black}}$ or $\dot{m}_{\text{f,blue}}$) are supplied to sectors of injectors. Fuel flow rates of $\dot{m}_{\text{f,black}}$ and $\dot{m}_{\text{f,blue}}$ may also be supplied in an alternate fashion as shown on Figure 2.11(c).

The non-uniform fuel flow distribution in a staged combustor may introduce potential hot spots which are not ideal for the material integrity of the engine and may result in increased NOx emissions. However, when the engine is operating at a low power where high flame temperature is not a

concern, fuel staging has been shown to be particularly effective in reducing UHC and CO emissions Bahr (1982, 1987). Consider an engine operating at idle or low power. In an unstaged configuration, there is a consistently low temperature around the chamber since an equally low fuel flow rate is supplied to all injectors and we recall that at low temperatures (power), CO emission levels are high (see Figure 2.8). With fuel staging however, the same power (fuel) may be delivered to only half of the injectors, for instance as in Figure 2.11(b), such that locally fuel-rich regions are present in the combustor. Having combustion take place in only these fuel-rich regions leads to a marked increase in temperature which are naturally much more favourable to low CO and UHC formation. Studies by Bahr (1982) have found that the reduction in emissions may be up to 98%. Locally fuel-rich regions in a staged combustor are also favourable in extending the lean blowoff limits (Lefebvre and Ballal 2010). In the current work, the effect of fuel staging on ignition and lean blowoff limits is investigated on the laboratory-scale combustor meant to replicate the SAFRAN Arrano engine.

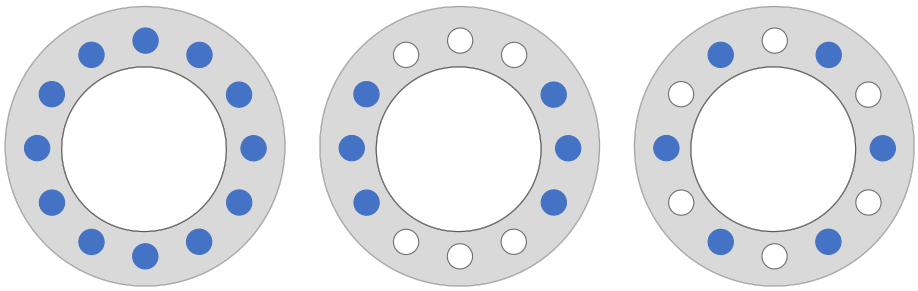

Figure 2.11: Schematic showing fuel staging configurations. Injectors which have the same colour codes have identical fuel flow rates. (a): unstaged uniform fuel injection for all injectors. (b): sectorised staging where sectors of two or more adjacent injectors have the same fuel mass flow rate. (c): repetitive staging in which fuel flow rates are alternated for adjacent injectors. Adapted from Bahr (1982), Lefebvre and Ballal (2010).

2.3.4 Study on Spinning Combustion Technology

Two laboratory-scale combustors have been conceived to study the physics of these combustor designs as stated in **O3. Studies more closely replicating physics of real combustors.** The first combustor, SCT V1, served as a preliminary test rig to study the effects of azimuthal swirl on flame dynamics. The staged combustor designs of Rich-Quench-Lean (RQL) and azimuthal

fuel staging were studied in a second version of the laboratory-scale combustor, known as SCT V2. In the following chapter, the laboratory setups which include SCT V1 and V2 combustors and the relevant diagnostics employed are presented.

3

Experimental setup and diagnostics

In this section, setups used in the current work are presented in the order:

(3.1) the single sector combustor
(3.2) flame stabilisation mechanisms in both single and annular setups
(3.3) general overview of the annular combustor and details of the NTNU atmospheric annular combustor
(3.4) details of version 1 (V1) of the simplified SCT combustor, SCT V1
(3.5) details of version 2 (V2) of the simplified SCT combustor, SCT V2

The chapter includes a rundown of the ignition procedure **(3.7)**, LBO procedure **(3.8)**, and relevant diagnostics **(3.9)** used to characterise ignition and lean blow-off dynamics. A brief discussion on experimental uncertainty and statistical convergence **(3.10)** concludes this section of the thesis.

3.1 Atmospheric single combustor

A single flame setup was used for lean blow-off studies. It represents a single injector sector of either the NTNU annular combustor or version 1 (V1) of the simplified SCT combustor, SCT V1. If a straight axial injector is used, it is assembled in an upright position as shown in Figure 3.1(a). In Figure 3.1(b), the setup is oriented 90° when a bend injector is used instead. A schematic representation in Figure 3.1(c) shows two impinging jets feeding

air-fuel premix into the plenum. Grids are placed for flow conditioning before converging into the injector tube. Pressure transducers or hot-wire probes may be inserted into either of the two ports at $h_{P1} = 105\,\text{mm}$ and $h_{P2} = 45\,\text{mm}$ upstream of the injector outlet for diagnostics. The injector exit ($d_{inj} = 19\,\text{mm}$) expands into a dump (back) plane which is enclosed by a quartz tube of diameter $d_i = 34\,\text{mm}$ and height $h_i = 130\,\text{mm}$. Different bluff bodies and swirlers can be installed. These are described in the next section.

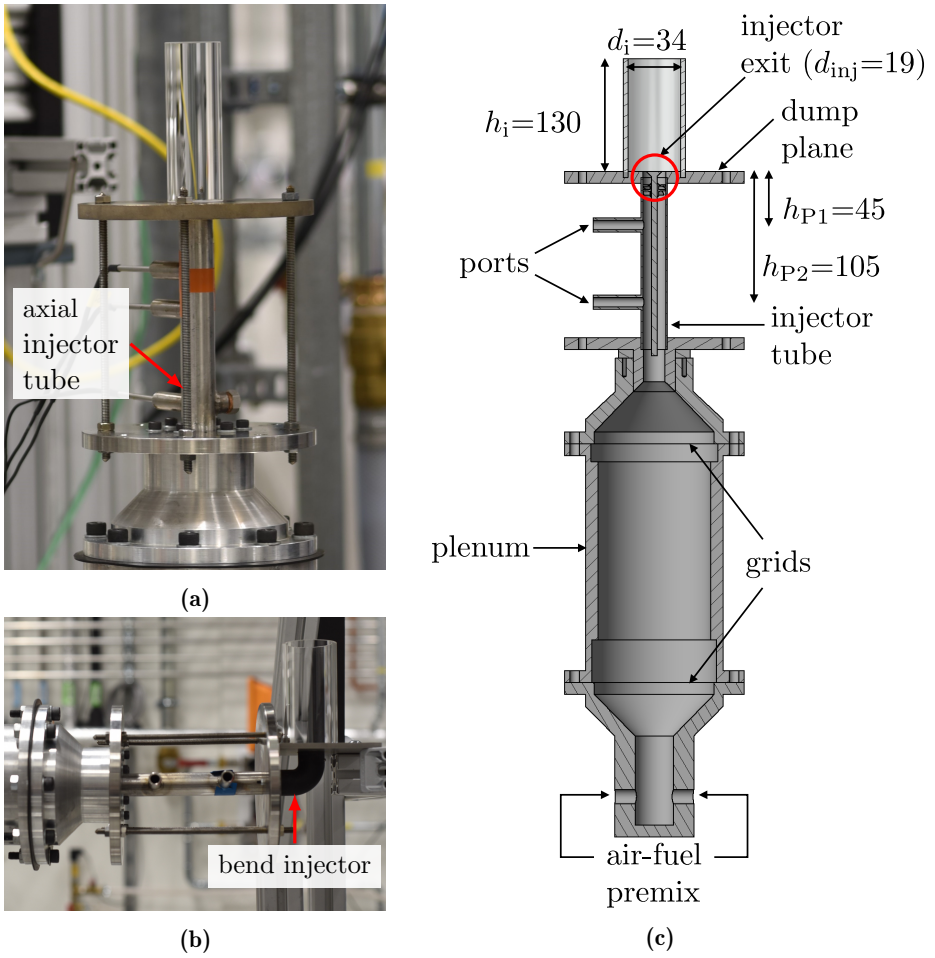

Figure 3.1: The NTNU atmospheric single combustor: (a) in an upright position when fitted with an axial injector, (b) oriented 90° when mounted with a bend injector, (c) schematic side view in upright position.

3.2 Injector configurations

Imperative to the design of combustors is the fuel injector and its role in flame stabilisation. The different injector configurations investigated were as follows:

(a) an inverted conical bluff body of $d_{\mathrm{bb}} = 13\,\mathrm{mm}$ mounted on a rod of diameter 5 mm, Figure 3.2(a)

(b) a swirler with a central rod of 5 mm at the injector exit plane Figure 3.2(b), or

(c) the combination of a bluff body and a swirler positioned $h = 10\,\mathrm{mm}$ upstream Figure 3.2(c).

Photos of the bluff body and swirler viewed from the injector outlet is shown in Figure 3.3, and rendered drawings of the swirler are in Figure 3.5.

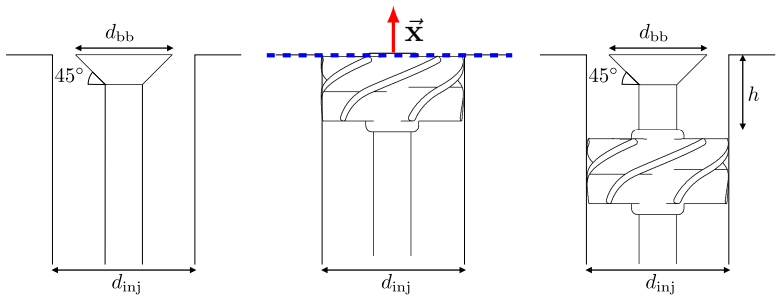

Figure 3.2: Different configurations of injectors for flame stabilisation using: (a) a bluff body, (b) an axial swirler, or (c) a combination of both. The red arrow denotes the mixture mass flow in the axial direction, $\vec{\mathbf{x}}$ and the blue dashed line represents the back plane axis.

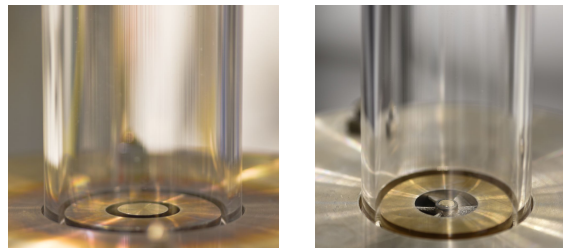

Figure 3.3: Photos of (a) a bluff body, (b) an axial swirler at the injector exit of a single flame setup.

To generate azimuthal swirl, new injectors were designed that were inclined at an angle β relative to the back plane as shown in Figure 3.4.

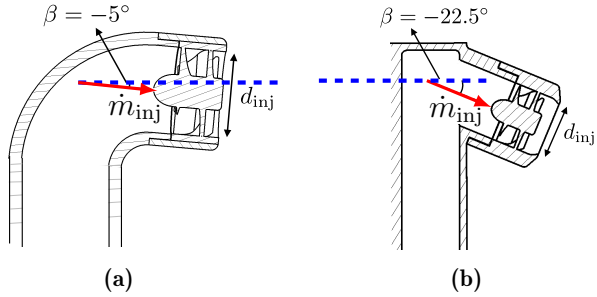

Figure 3.4: The oblique angled injectors designed for: (a) SCT V1 with $\beta = -5°$. 0 or 5° is also possible, and (b) SCT V2 with a fixed $\beta = -22.5°$. The blue lines denote the back plane axis, and the red arrows denote the fuel flow direction.

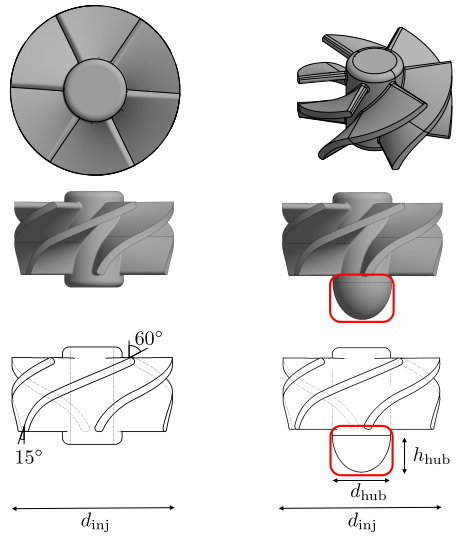

Figure 3.5: Rendered illustration of the swirler. Top row shows the top and isometric view. Middle and bottom left show the side view of a swirler used in straight axial injector, while middle and bottom right show the swirler with a semi-elliptic profile enclosed in red.

To improve flow uniformity through the injector's oblique bend, the swirler upstream has a semi-elliptic profile at the hub with major axis of h_{hub} and

minor axis of $d_{\text{hub}}/2$ as denoted in Figure 3.5. Barring that, the swirler is identical to the one used in the straight axial injectors of the NTNU combustor and previous studies of Ciardiello et al. (2020a,c), Dawson and Worth (2014, 2015), Nygård et al. (2019, 2021), Worth and Dawson (2013a,b). The six-vane axial swirler has a trailing edge angle of $\theta = 60°$ to the axial flow direction and a geometric swirl number of $\mathcal{S} = 1.22$, which is computed based on Equation 2.17. Details of the computation may be found in Section 2.2.

For the case of a swirler at $h = 10\,\text{mm}$ upstream of the back plane (see Figure 3.2(b)), stereo-PIV was performed in an unconfined, cold flow. The measured u_θ and u_x were used to compute $\mathcal{S}$, using Equation 2.16. $\mathcal{S}$ was found to be approximately 0.65 at $x/d_{\text{inj}} = 0.5$. And at $x/d_{\text{inj}} = 2$, S was at the maximum value of 1. Details are presented in Section 4.1.

Two variations of the swirler were used: one that induces a ACW swirling motion, or one that induces a CW swirling motion when viewed from the top. See Figure 3.6.

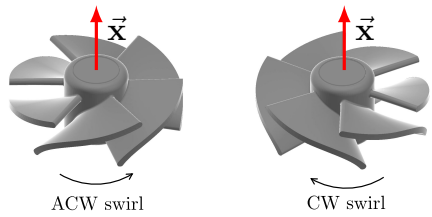

Figure 3.6: Possible geometric variations of the swirlers: (a) one that imparts a ACW swirl, (b) or one that imparts a CW swirl when viewed from top. The red arrows denote the axial flow direction, $\vec{\mathbf{x}}$.

3.3 Atmospheric annular combustor

A schematic depicting the side view of the annular combustor is shown in Figure 3.7. It shares similar features as the single sector setup, but a hemispherical body has been added at the plenum exit to evenly distribute the air-fuel mixture into injectors which are arranged circumferentially around the annulus. The back plane is enclosed by an inner tube ($d_{\text{i}} = 127\,\text{mm}$) and outer tube ($d_{\text{o}} = 212\,\text{mm}$) to form the combustion chamber walls. The inner and outer height of the chamber is $h_{\text{i}} = 130\,\text{mm}$ and $h_{\text{o}} = 200\,\text{mm}$ respectively. Different tubes may be used to vary the heights or to allow/block optical access. A transparent quartz outer wall and an opaque steel inner wall is depicted in this case. Its modular design allows geometric modification of the combustion chamber (enclosed in red) to perform ignition and

lean blow-off studies.

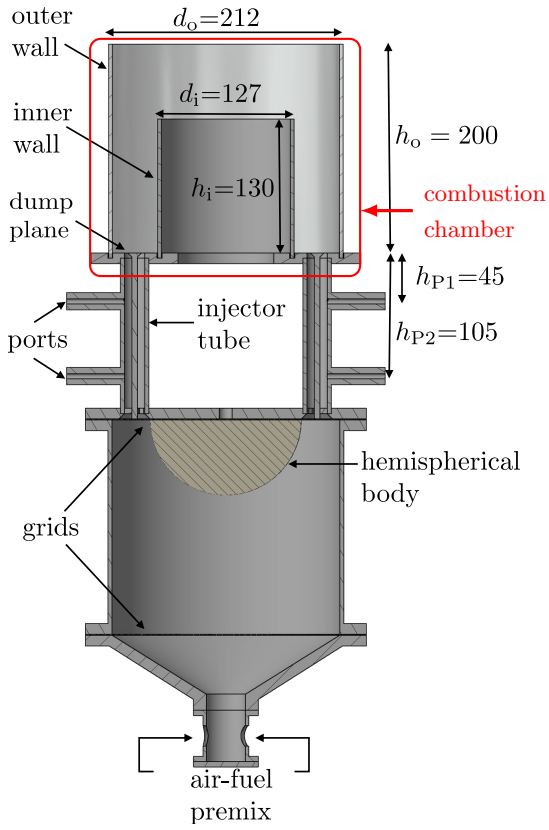

Figure 3.7: The NTNU atmospheric annular combustor. Geometric variations may be made on the combustion chamber (in red box) to perform any relevant parametric studies.

Modifications to the injection system were made to produce mean azimuthal swirl. Figure 3.8(a) shows the NTNU atmospheric annular combustor which consists of a number of bluff body or rod stabilised premixed flames with or without swirl. Figure 3.8(b) is an illustration of the SCT V1 combustor, and is described in Section 3.4. Finally, Figure 3.8(c) depicts the SCT V2 combustor presented in Section 3.5.

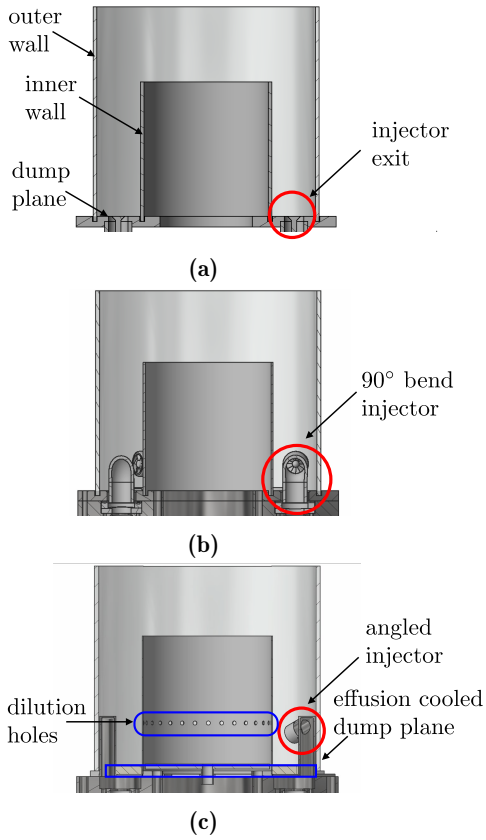

Figure 3.8: Different modular designs of the annular combustor: (a) premixed for a typical NTNU configuration, (b) spinning premixed for SCT V1, and (c) spinning RQL for SCT V2.

NTNU atmospheric annular combustor

The NTNU annular combustor has a simple annular geometry consisting of straight axial injectors fitted with simple flameholders and/or swirlers (Worth and Dawson 2013a,b) as described in Section 3.2 for fundamental studies concerning the physics of ignition and lean blowoff. A 6- or 12-injector configuration is used as shown in Figure 3.9. In addition to variable injector spacing, the global swirl dynamics may be modified as well. CW and ACW swirlers may be alternated round the chamber to produce a zero bulk swirl, as is the case in Figure 3.9(a). The swirlers may also be mounted in the same ACW (or CW) swirling orientation to produce a corresponding net ACW (or CW) swirl when viewed from downstream. To ensure the rotational symmetry between each injector sector, each swirler has two of

their trailing edges aligned radially towards the centre of the combustor (Nygård 2021). This is illustrated in Figure 3.9(a) whereby the red dotted lines show the swirlers' edges pointing towards the centre marked in red.

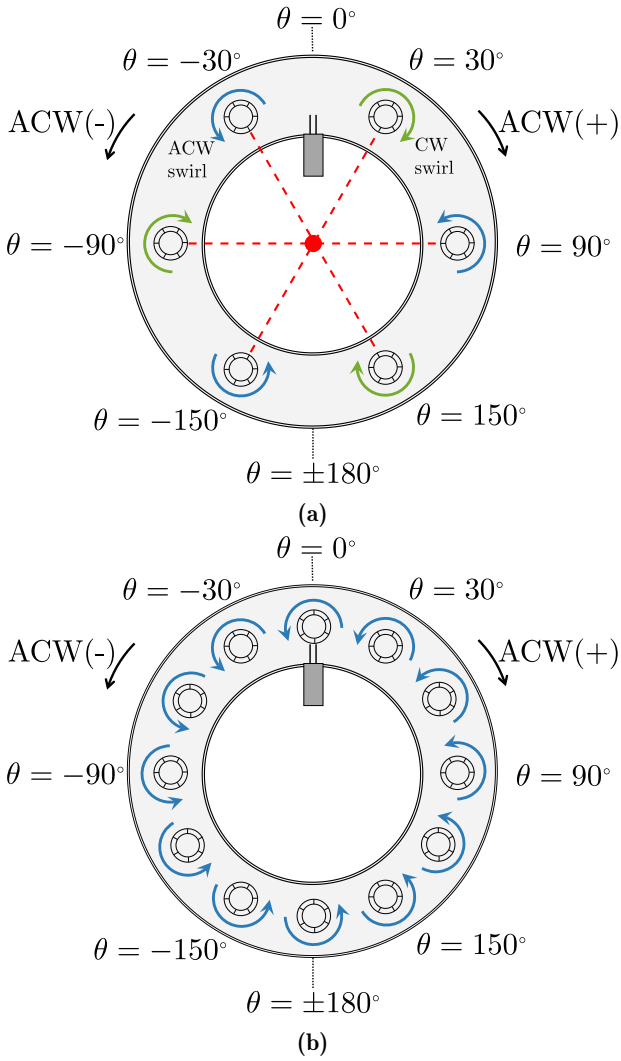

Figure 3.9: (a) Configurations of the NTNU annular combustor: (a) 6-injector with a zero net bulk swirl, (b) 12-injector with an ACW net bulk swirl. The grey rectangle positioned on the inner side of the combustor at $\theta = 0°$ represents the spark electrode. Blue (arc) arrows denote ACW swirl, and the green arrows denote CW swirl.

3.4 V1 of the spinning combustor (SCT V1)

A salient feature of the SAFRAN spinning combustor is the strong azimuthal swirling motion within the annular chamber. In this 1st iteration, strong azimuthal swirl is introduced by 90° bend injectors attached to the combustor back plane. Cooling ducts are also introduced to cool the combustor back plane. This setup served as a preliminary test bed to perform various parametric studies, and is named SCT V1. The eventual test bed is a culmination of more than 30 design iterations to ensure maximum flexibility in the variation of geometric parameters. Photos of the SCT V1 and instantaneous true-color flame images are shown in Figure 3.10(a) to Figure 3.10(d).

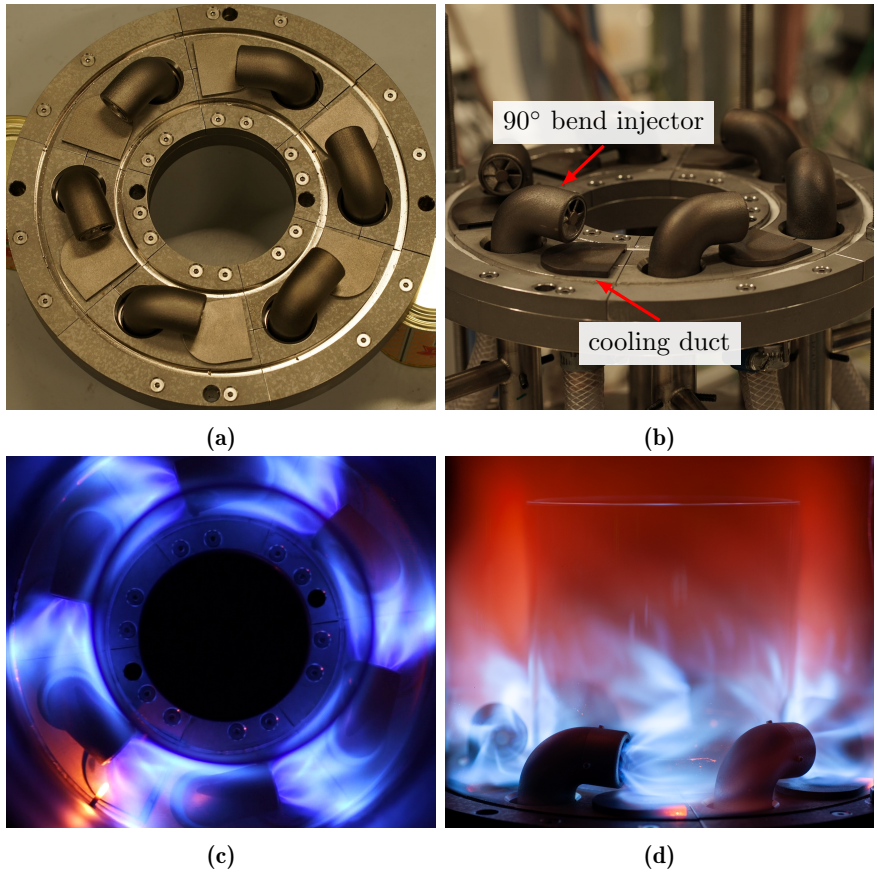

Figure 3.10: Photos of the SCT V1 combustor from (a): top, and (b) side view. The true-colour flame images from the corresponding views are shown in (c) and (d).

3.4.1 SCT V1 geometric details

Figure 3.11 shows key dimensions of the V1 configuration. Details of drawings are included in Appendix A. The fuel injector has two angles of inclination: angle α for the yaw, and angle β for the pitch. The pitch angle β is varied using a pair of inclined wedges which are shaded in red (for the bottom wedge), and grey (for the top wedge) as shown in Figure 3.11(c).

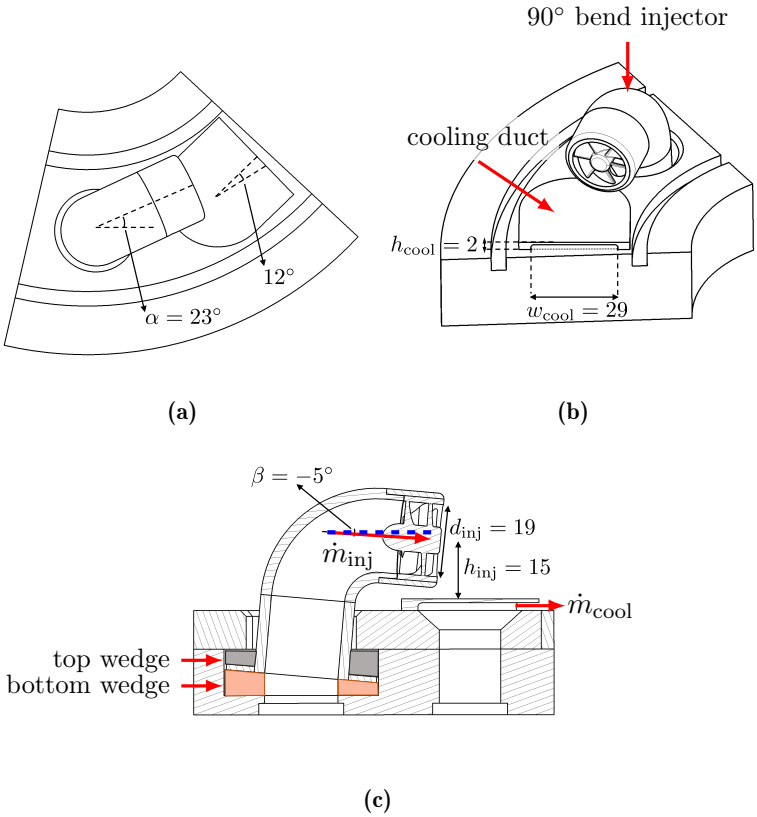

Figure 3.11: Relevant geometric dimensions (in mm) of the SCT V1.

Figure 3.12 illustrates the 3 possible wedge configurations to vary the pitch angle β. At the neutral position of angle $\beta = 0°$, the bend injector sits atop the top and bottom wedge. At angle $\beta = -5°$, the bend injector is placed on a wedge which has a declination of 5°. The same arrangement applies for angle $\beta = 5°$, but with the bottom wedge rotated to form an inclination instead.

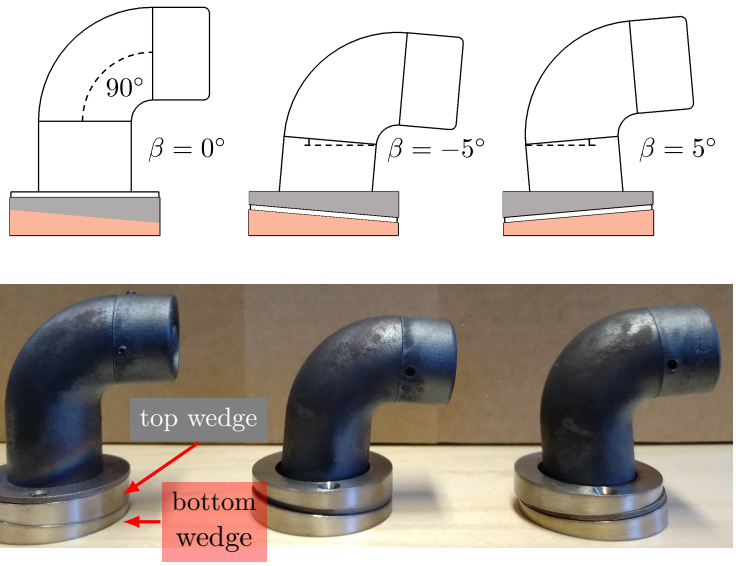

Figure 3.12: Schematics and photos showing the three different geometric configurations of the pitch angle β for the 90° bend injector in SCT V1. Left: $\beta = 0°$, middle: $\beta = -5°$, and right: $\beta = 5°$.

The adjustment of yaw angle α for both the 90° bend injector and the cooling duct is made possible via arc-shaped slots machined onto the combustor back plate shown in Figure 3.13. The cooling duct is fixed at $\alpha = 12°$ as seen in Figure 3.14(a). For the 90° bend injector, three yaw angles are considered: $\alpha = -23°$, 0°, and 23° which are depicted in Figure 3.14.

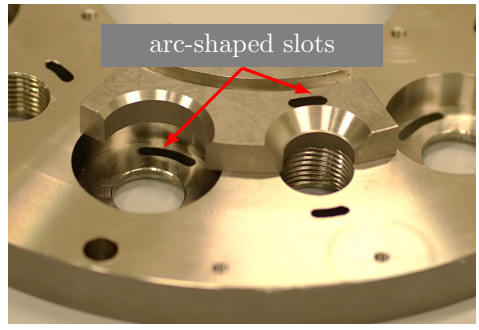

Figure 3.13: Arc-shaped slots are machined onto the combustor back plate so that the fuel injectors and cooling ducts may be attached at various positions, thereby varying the yaw angle α.

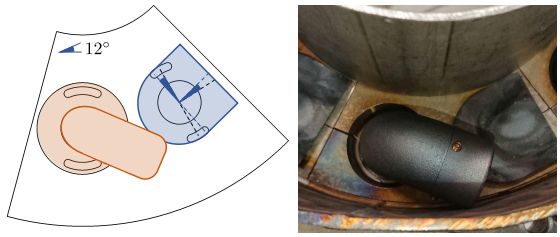

(a) Cooling duct fixed at 12°.

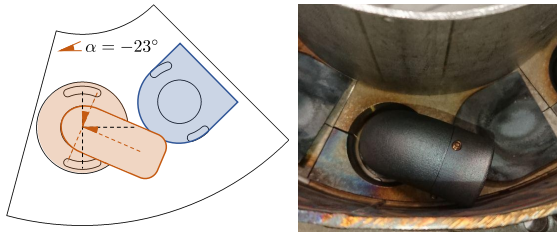

(b) Bend injector at $\alpha = -23°$.

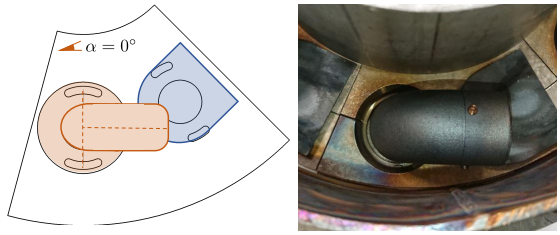

(c) Bend injector at $\alpha = 0°$.

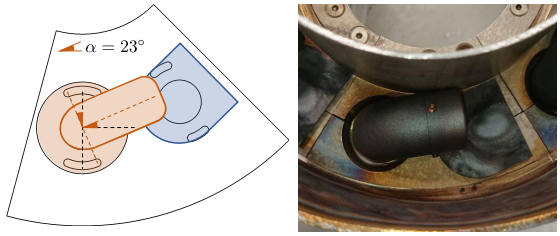

(d) Bend injector at $\alpha = 23°$.

Figure 3.14: Figure showing the possible pitch angle α of the SAFRAN spinning combustor V1. (a): cooling duct fixed at $\alpha = 12°$, and the 90° bend injector at (b) $\alpha = -23°$, (c) $\alpha = 0°$, and (d) $\alpha = 23°$.

3.4.2 SCT V1 assembly

The combustor back plane has three components: the bottom piece, the top inner piece, and the top outer piece. The assembly stages are shown in Figure 3.15 and the assembly is as follows:

(i) The 90° bend injector and wedges are placed into the recess of the bottom piece, and fastened through the arc slot to the desired yaw angle α.

(ii) The top inner piece of the combustor plate,

(iii) followed by the top outer piece, are both fastened onto the combustor bottom piece, forming the combustor back plane (outlined in blue).

(iv) The cooling ducts are then fastened onto the combustor back plane.

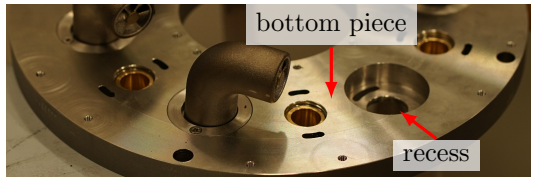

Stage (i): bend injectors and wedges positioned into recess of bottom piece.

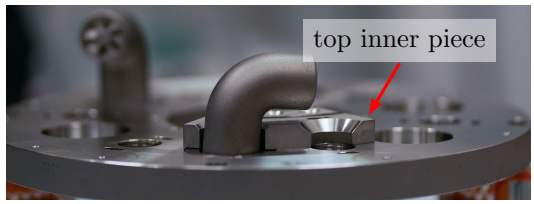

Stage (ii): top inner piece attached on top of bottom piece.

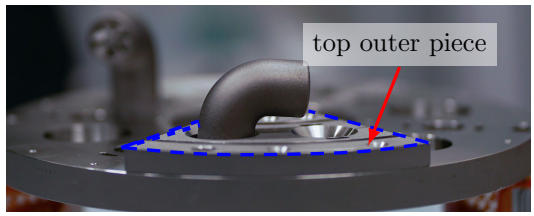

Stage (iii): top outer piece fastened onto bottom piece.

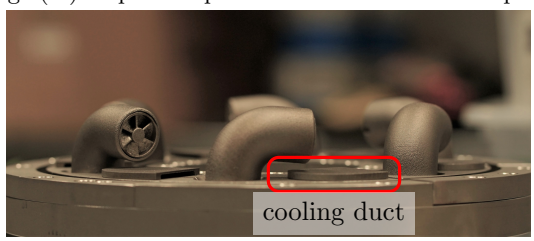

Stage (iv): cooling ducts affixed onto the top pieces.

Figure 3.15: Sequence of photos illustrating the different assembly stages of the SCT V1 combustor.

3.5 V2 of the spinning combustor (SCT V2)

To replicate the Rich-Quench-Lean (RQL) combustion mode used in the SAFRAN spinning combustor, a second version of the laboratory-scale setup, SCT V2, was developed and is presented in Figure 3.16. It features: (i) a circumferential array of dilution ports of diameter, $d_{\mathrm{dil}} = 4\,\mathrm{mm}$. The mass flow of dilution air, $\dot{m}_{\mathrm{dil}}$, could be independently varied. (ii) a back plane with a uniform distribution of elliptical holes (major axis of 2 mm and minor axis of 1 mm) for effusion air cooling of $\dot{m}_{\mathrm{cool}}$, (iii) and an oblique injection of air-fuel mixture at a flow rate of $\dot{m}_{\mathrm{inj}}$ to produce a strong azimuthal swirl. The geometric complexity of the perforated back plane meant that it had to be manufactured using 3-D metal printing with Inconel as material for rigidity and thermal resistance. The elliptical holes were also enlarged from the original size of 0.8 mm by 0.4 mm which proved too challenging to be fabricated.

Compared to the lean premixed flames ($\phi < 1$) in SCT V1 however, $\dot{m}_{\mathrm{inj}}$ exiting the injector is fuel-rich ($\phi > 1$) which is then rapidly quenched by the high air flow rate of $\dot{m}_{\mathrm{dil}}$ to provide a globally lean fuel mixture. Details of the RQL operation mode is the focus of Article II. The angled injector in this setup has a fixed value of $\beta = -22.5°$ and $\alpha = 45°$, and is positioned around the outer circumference of the combustion chamber to better mimic the actual engine's injection mechanism. Photos of the angled injector and the effusion-cooled back plane are in Figure 3.17 and their dimensions in Figure 3.18.

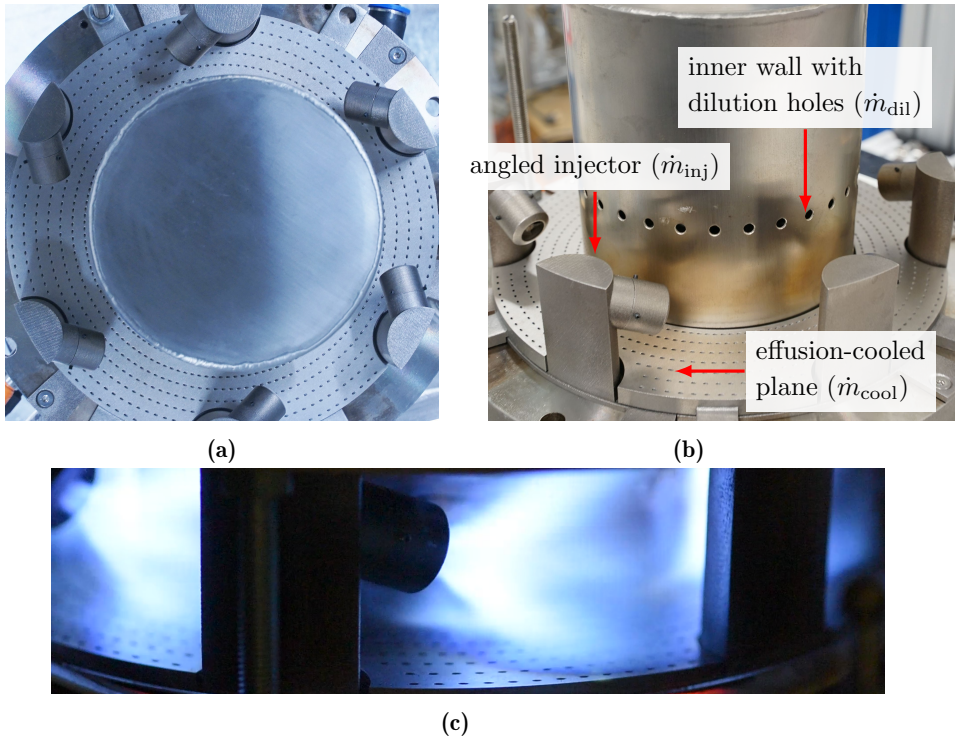

Figure 3.16: Photos of the SCT V2 combustor from the (a) top, and (b) side. The true-colour flame image is shown in (c).

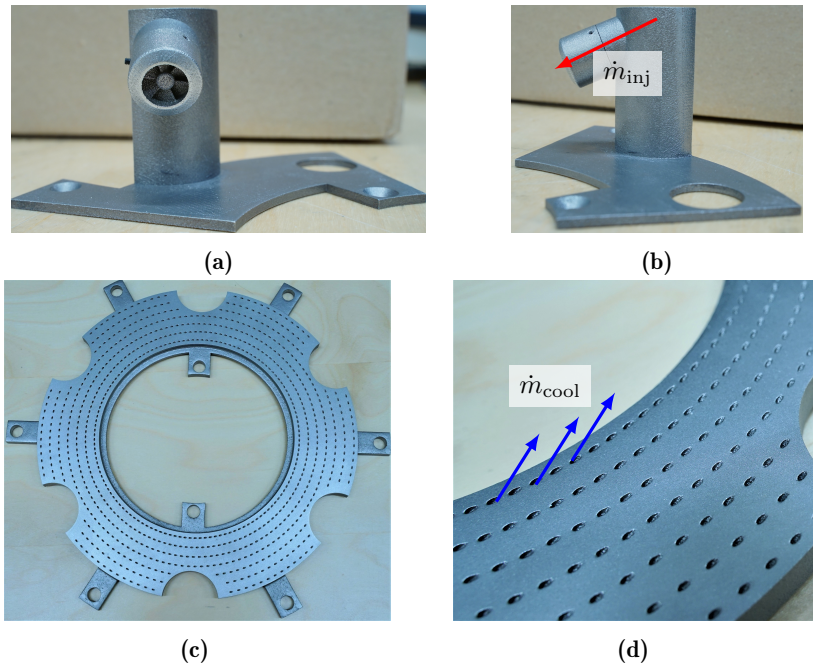

Figure 3.17: Photos of the angled injector from the (a) front view, and (b) side view. Photos of the perforated plate which permits tangential effusion cooling of the back plane seen (a) from the top, and (b) close-up. The red arrow depicts the air-fuel flow rate through the injector ($\dot{m}_{\text{inj}}$) and the blue arrows show the cooling air through the plate ($\dot{m}_{\text{cool}}$).

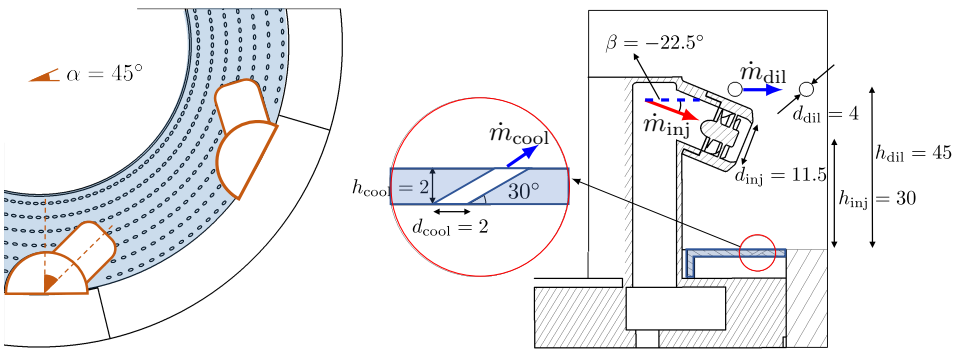

Figure 3.18: CAD of the angled injector and perforated plate. All dimensions in mm. The red arrows depict the fuel-rich (ϕ>1) premixed flow through the injector ($\dot{m}_{\text{inj}}$), the cooling air through the plate ($\dot{m}_{\text{cool}}$), and the dilution air through the holes of the inner combustor wall ($\dot{m}_{\text{dil}}$).

3.5.1 SCT V2 assembly

The SCT V2 is assembled in a 3-stage process which involves:

(i) positioning of the angled injected around the outer circumference of the combustion chamber,
(ii) fastening the perforated plate atop the combustor back plate, and
(iii) insertion of the inner combustor wall (with dilution ports).

Figure 3.19 illustrates this assembly.

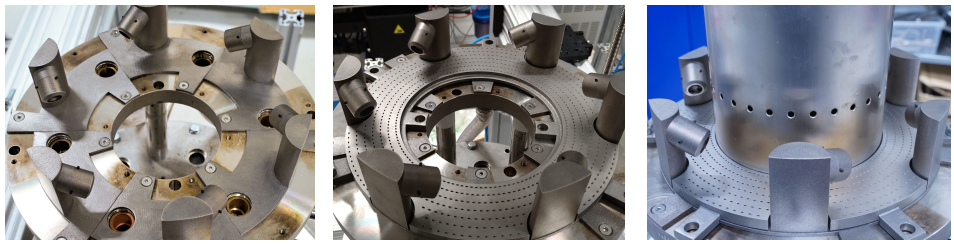

Stage (i) Stage (ii) Stage (iii)

Figure 3.19: Sequence of photos illustrating the different assembly stages of the SCT V2 combustor. Stage (i): angled injectors attached around the chamber circumference. Stage (ii): perforated plate fixed onto the combustor. Stage (iii): inner combustion wall (with dilution holes) is placed onto the setup.

3.5.2 SCT V2 staging

Aside from replication of the RQL mode, the concept of azimuthal fuel staging was also examined in SCT V2 to investigate the effect on the ignition limit. Fuel injectors are split into two sets: (i) the first set has a fuel mass flow rate of $\dot{m}_{\mathrm{f,blue}}$. The subscript $(\cdot)_{\mathrm{blue}}$ denotes that the fuel injector is color-coded blue. (ii) A second set of injectors has a fuel mass flow rate of $\dot{m}_{\mathrm{f,black}}$. The subscript $(\cdot)_{\mathrm{black}}$ denotes that the fuel injector is color-coded black. From Figure 3.20(a) and Figure 3.20(b), these two sets of injectors may be arranged with either (i) one half of the annulus having identical flow rates, or (ii) in an alternate manner respectively. As shown in Figure 3.20(c), fuel is introduced through the angled injectors via the upstream injector port at position h_{P2} (see Figure 3.7) with a black pipe providing $\dot{m}_{\mathrm{f,black}}$ and a blue pipe for $\dot{m}_{\mathrm{f,blue}}$.

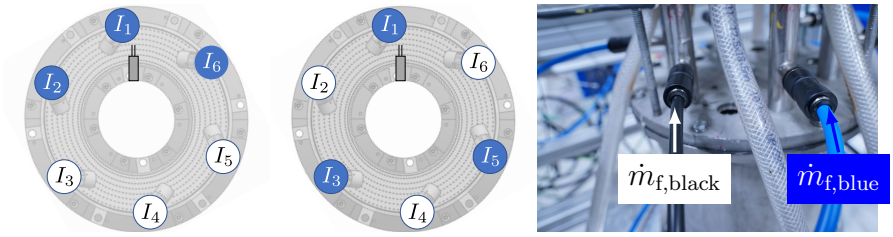

(a) (b) (c)

Figure 3.20: Azimuthal fuel staging on the SCT V2. (a) and (b) show the two different staging configurations considered in the current work. The grey rectangle positioned on the inner combustor at $\theta = 0°$ represents the spark electrode. (c) shows either a black or blue pipe carrying fuel mass flow rate of $\dot{m}_{\mathrm{f,black}}$ and $\dot{m}_{\mathrm{f,blue}}$ respectively to the injector tube port position at h_{P2}. Adapted from Article II.

3.6 Ignition studies

Electrical discharge from a spark was used to provide the necessary energy to initiate a flame kernel. The spark ignition system is similar to that of the MICCA in EM2C, France (Bourgouin et al. 2013). A single electrode was connected to a Danfoss transformer unit (Model: EBI4 1-Pole) and positioned about 10 mm above the back plane. The azimuthal position of the electrode has little to no influence on ignition system as found by Ciardiello et al. (2020a). In the case of the NTNU 6-injector combustor, the electrode was positioned equidistant between two injectors at $\theta = 0°$ (see Figure 3.9) to minimise any possible saturation resulting from the intense energy (mainly in the UV spectrum) of the spark deposits. This avoids any signal artifacts since optical diagnostics positioned at each injector sector are recording 1-D (photomultipliers) or 2-D signals (images) in the UV range. For the SCT V1 and V2 configurations, the electrode was positioned directly behind the bend or angled injectors as illustrated in Figure 3.20(a). The transformer unit and its connections are shown in Figure 3.21.

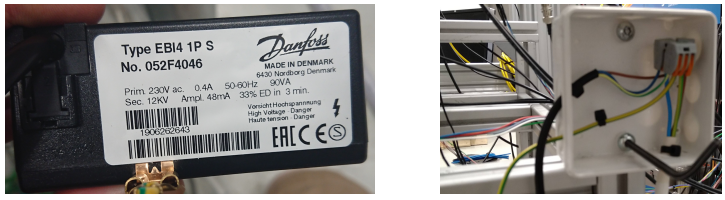

(a) (b)

Figure 3.21: Photos of (a): the igniter transformer unit and (b) the electrical connections powering the spark ignition.

Ignition was controlled via a LabView program. The spark was generated between the electrode tip and the inner steel wall with a gap of approximately 2 mm with an energy of approximately 50 mJ every 20 ms. The spark duration was 7.5 ms. Figure 3.22 shows the electrode position in the combustor and the spark instant.

The procedure of ignition is summarised as:

(i) Temperature was measured to ensure the thermal conditions of the combustor were fulfilled for the relevant study.
- For experiments meant to approximate a quick relight scenario (adiabatic conditions), the combustor was first preheated to a sufficiently high temperature T.
- For cold-start experiments, the combustor was cooled to room temperature.

(ii) Air-fuel mixture through the injectors (and any cooling or dilution flow if applicable) was started for 5 s.

(iii) Igniter system was switched on for 0.5 s.

(iv) There were two possible outcomes:
- A successful run whereby there was complete ignition and propagation around the annular combustor, or
- A failed run with no ignition or ignition of only one/some injector(s).

Steps (i) to (iv) were repeated between 10 to 30 times for a given operating point for repeatability. Details of statistical convergence are in Section 3.8.6.

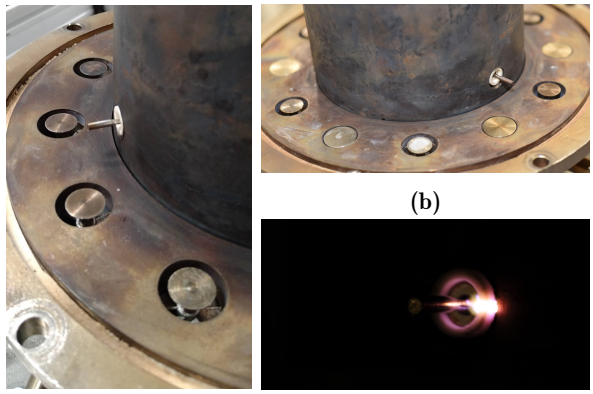

Figure 3.22: Photos showing the spark igniter in the NTNU atmospheric annular combustor (a): side view, (b) front view, (c) at sparking instant.

3.7 Lean blowoff studies

To determine the lean blow-off limit of each operating point, two main approaches are possible (Dawson et al. 2011, Zhang et al. 2021):

(i) Keeping the fuel mass flow rate $\dot{m}_{\mathrm{f}}$ constant, incrementally increase the air mass flow rate $\dot{m}_{\mathrm{air}}$.

(ii) Keeping $\dot{m}_{\mathrm{air}}$ constant, incrementally decrease $\dot{m}_{\mathrm{f}}$. The mixture velocity U and the thermal load $\mathcal{P}_{\mathrm{th}}$ is thus constant throughout the procedure.

The flow rates $\dot{m}_{\mathrm{f}}$ and $\dot{m}_{\mathrm{air}}$ at the instant of global flame extinction is the LBO limit. Dawson et al. (2011) noted that using any of the two approaches leads to similar if not identical LBO limits. The LBO trajectories representative of these methods are shown in Figure 3.23 and circled in red: solid arrow (⟶) for method (i), and dashed arrow (- - -▸) for method (ii).

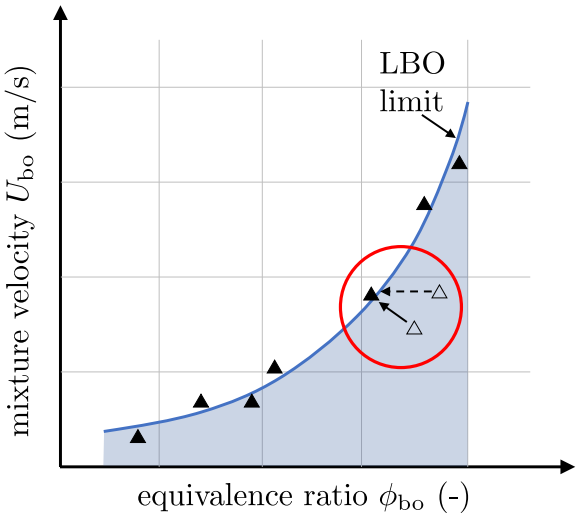

Figure 3.23: A typical LBO limit curve. The solid triangle markers represent the LBO limit at each operating point. The blue curve is the curve fit of LBO limit. Enclosed in the red circle are two hollow triangle markers with arrows representing the different possible trajectories to the eventual LBO limit.

Lean blow-off experiments were performed as follows using method (i) and as described in Wiseman et al. (2020):

(i) Combustor was ignited at a stable point far from the LBO limit.

(ii) The air flow rate $\dot{m}_{\mathrm{air}}$ was ramped up till about 90% of the estimated

LBO limit. The fuel flow rate $\dot{m}_f$ was kept constant.

(iii) Combustor was left operating at this point for 3 to 5 minutes to ensure steady state conditions.

(iv) $\dot{m}_A$ was increased in steps of 1 to 2% every 20 s until blow-off occurred.

For each value of $\dot{m}_f$, multiple runs were performed on separate occasions for repeatability. The associated mass flow uncertainties are in Section 3.8.6.

3.8 Measurements

Several different high-speed diagnostics were used to characterise the transient phenomena of ignition and lean blow-off. Figure 3.24 is a photo illustrating the diagnostics employed with Figure 3.25 providing additional details through the use of schematics. This section describes the various methods. Optical diagnostics using photomultipliers and high-speed imaging (for OH* chemiluminescence, PIV, and PLIF) are first discussed, followed by pressure measurements. Temperature measurements using thermocouples and pyrometer are then briefly presented. Experimental uncertainties and statistical convergence for some of the measurements are also discussed.

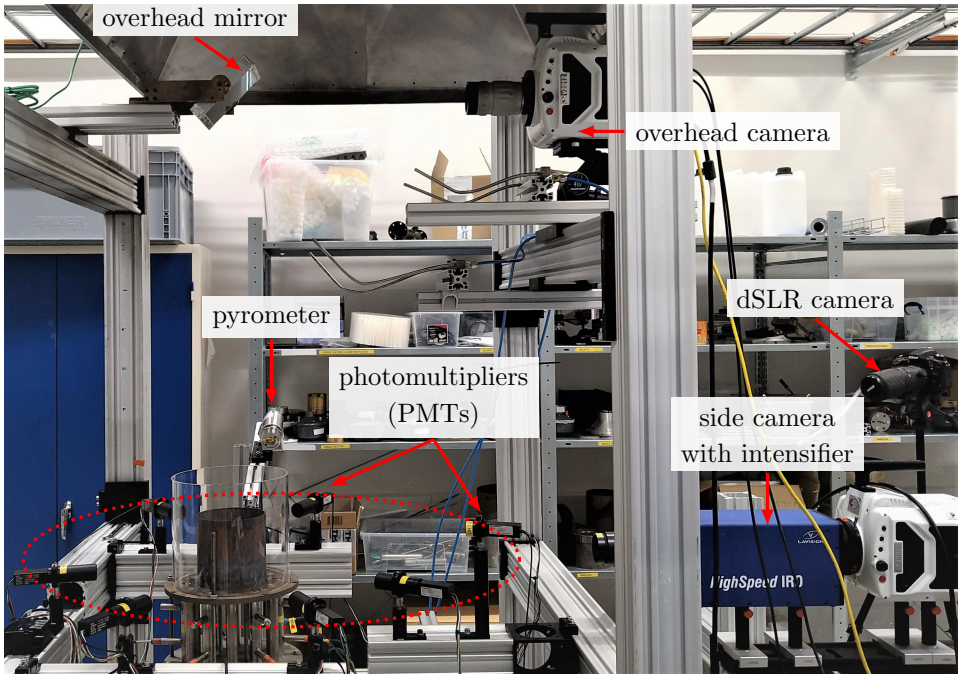

Figure 3.24: Photo annotated with the various diagnostics employed for ignition and LBO studies.

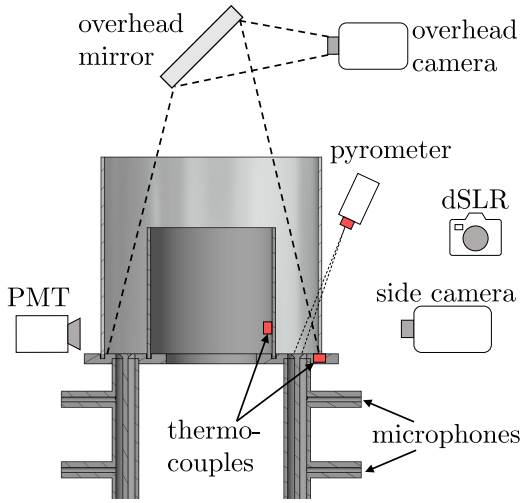

Figure 3.25: Schematics illustrating additional diagnostics (microphone positions and thermocouples) which are hidden from view on Figure 3.24. The dimensions of this schematic are not to scale to keep the figure compact.

3.8.1 Photomultipliers (PMT)

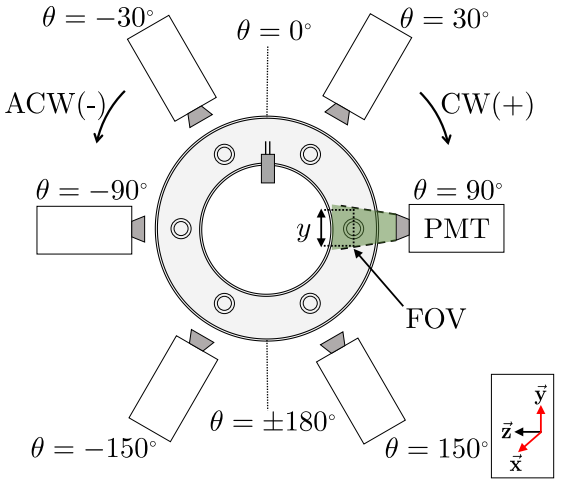

Figure 3.26: Schematics of PMT positions (not to scale) around the combustor with the coordinate system shown in inset. The field of view (FOV) of the PMT is shaded in green, and is defined at the centre of the bluff body, in terms of $(x \times y)$ mm. The vector $\vec{\mathbf{x}}$ is the axial flow direction and is out-of-plane.

One-dimensional (1-D) time series of global heat release rate (HRR) was measured using Hamamatsu PMTs of type H11902-113 with a spectral response of 185 to 700 nm with a high sampling frequency of 51.2 kHz. Each PMT was fitted with a UV filter which has a center wavelength of 310 nm, a full width at half maximum (FWHM) of 10 nm, and a transmission of $\geq 85\%$. The PMTs were placed in a circumferential array around the annulus at positions $\theta = \pm 30°$, $\pm 90°$, and $\pm 150°$ as depicted in Figure 3.26.

Alignment of the PMT's line-of-sight is critical to ensure consistent and repeatable flame detection of each flame. The field of view (FOV) shown in Figure 3.26 is defined as $(x \times y)$ mm measured at the centre of the bluff body. The FOV value $(x \times y)$ may be varied using extension tubes and slits with adjustable apertures to achieve the intended integrated line-of-sight. To achieve precise alignment, the vertical distance between the PMT and the combustor back plane was measured, and procedures were also in place to align the PMT's FOV to the intended injector sector as shown in Figure 3.27.

To amplify the 1-D signals recorded by the PMTs, the power supply control box (Hamamatsu model C7169) was used. Input voltage may be varied to adjust the signal gain. To individually adjust the gain of each PMT, a voltage control box (see Figure 3.28) was custom built. It features potentiometers with knob control and banana ports for ease of use.

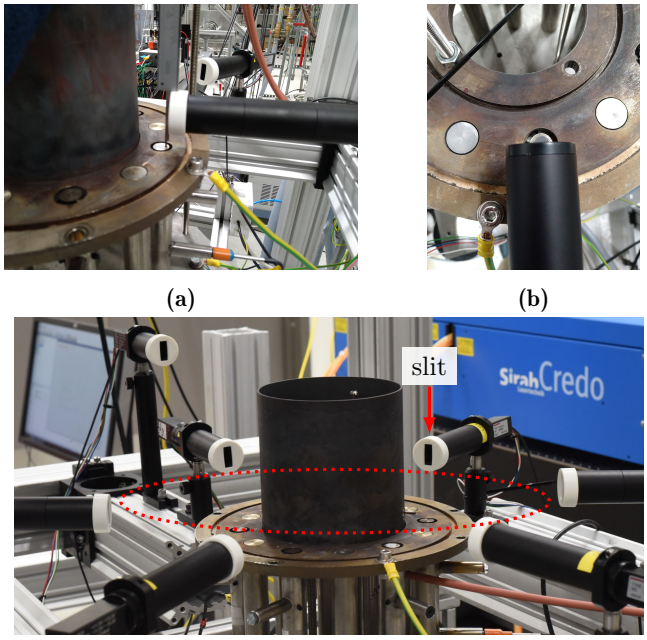

Figure 3.27: Photos showing the positioning of the PMTs: (a) a fixed vertical distance with respect to the injector exit plane, (b) alignment of the FOV to each injector sector. (c) shows the PMTs placed equidistant around the combustor (traced in red dots). The front of a PMT is covered by a slit (in white) to control the FOV.

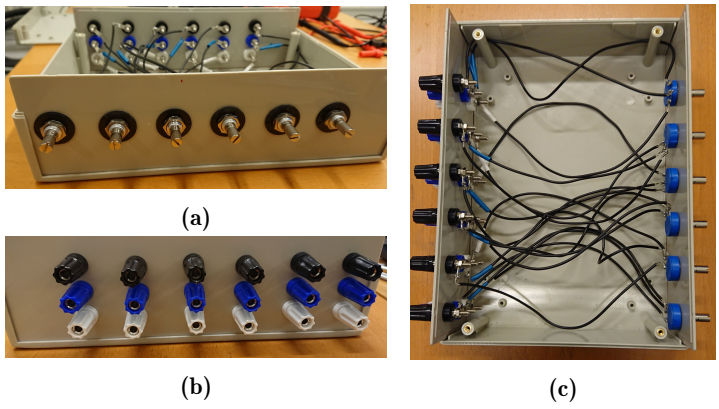

Figure 3.28: Photos of the custom-made PMT voltage (gain) control unit showing (a) front panel with knob for precise control, (b) back panel with banana ports for easy plug-and-play, and the (c) internal wire connections.

3.8.2 High-speed imaging

Either the Phantom V2012 or the Photron Fastcam SA1.1 camera was used for high-speed imaging. For all setups, simultaneous side and overhead imaging were performed as shown in Figure 3.25. To capture images of the entire annulus, a first surface mirror (Edmund Optics) with a peak-to-valley flatness of 4-6 λ[13] was mounted at an angle of 45° and positioned within the overhead camera's FOV. The camera trigger signals were recorded and widened according to the procedure described by Nygård (2021) to facilitate synchronisation with other acquired signals (1-D PMT and pressure transducer signals). High-speed images were recorded for OH* chemiluminescence, Planar Laser-Induced Fluorescence (PLIF), and stereoscopic Particle Image Velocimetry (stereoscopic PIV), and they are briefly discussed in the following paragraphs.

OH* chemiluminescence

In premixed flames, a reliable heat-release rate (HRR) marker is the emission of OH radicals (OH*) (Balachandran et al. 2005, Higgins et al. 2001). To capture OH* chemiluminescence images, a high-speed camera was connected to a LaVision high-speed intensified relay optics unit. This is to amplify the weak OH* chemiluminescence emissions from the short exposure time of the high frame rate shots. A UV lens (Sodern Cerco 2178, focal length = 100 mm, aperture F/2.8) fitted with a UV bandpass filter (310 nm with a FWHM of 10 nm) was used to block out emissions outside the intended wavelength. Samples of these images recording the integrated OH* intensity within the camera's line of sight (LOS) are shown in Figure 3.29.

Figure 3.29(a) shows the instantaneous side image. The normalised pixel intensity outlines the reaction zones (integrated LOS) with each of the bluff body stabilised flames assuming a V shape. Adjacent flames have limited flame interaction with flame brushes barely touching each other. Image taken simultaneously from the top provides an overview of the global flame dynamics. 12 distinct flame sectors can be identified in Figure 3.29(b), again indicative of limited flame-flame interaction. Each flame assumes an annulus shape when viewed downstream with minimal or no HRR detected directly above each bluff body (black circular disc), suggesting little or no reaction within the bluff body wakes.

[13] λ is the wavelength of the interferometer laser used for measuring surface flatness, and is usually taken to be 632.8 nm.

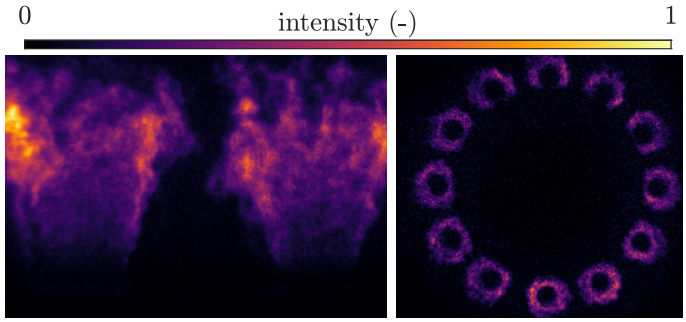

Figure 3.29: Example of instantaneous OH* chemiluminescence images of the 12-injector bluff body stabilised flames. (a) adjacent flames captured by side camera, and (b) global annulus view recorded using a top camera.

Planar Laser-Induced Fluorescence

OH-PLIF was performed on SCT V1 to validate the HRR computations predicted in the LES simulation. A detailed procedure on PLIF is given in Donbar et al. (2000). A brief description is given below with a schematic shown in Figure 3.30.

A diode-pumped, frequency-doubled Nd:YAG laser (Edgewave IS 400-2-L) with a pulse energy of 10 mJ and wavelength $\lambda = 532$ nm was operated at 10 kHz to pump a Sirah Credo dye laser using Rhodamine 6G dissolved in ethanol. A frequency conversion unit was used to generate a wavelength λ of approximately 283.55 nm. The wavelength was tuned to obtain the maximum signal, with the resultant pulse energy from the dye laser at approximately 0.3 mJ.

The sheet forming optics comprised a pair of cylindrical lenses, with focal lengths -8 mm and 100 mm. The laser sheet was focused to a width of approximately 0.2 mm by a plano-convex (PCX) lens with a focal length of 1 m. PLIF images were acquired with a gate width of 80 ns which is more than sufficient to capture the fluorescence from the 10 ns laser pulse but resulted in almost no contribution of chemiluminescence to the measured signal. Flame surface density (FSD) plots were calculated using the method described in Balachandran et al. (2005). An example of a FSD plot is shown in Figure 3.31.

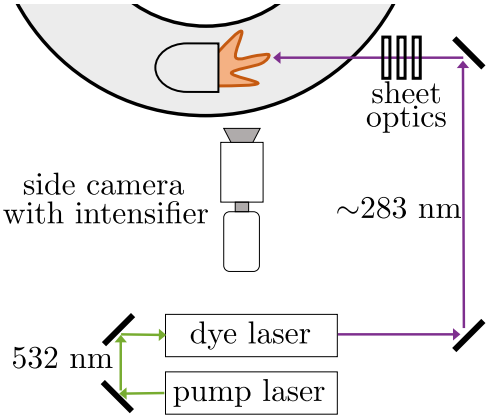

Figure 3.30: Schematic illustrating the OH-PLIF laser setup (not to scale). The green arrows represent the laser beam when wavelength $\lambda = 532\,\text{nm}$ while the purple ones depict the laser beam at $\lambda \sim 283\,\text{nm}$ (which is now in the UV range) after frequency conversion. The beam passes through the sheet (forming) optics which consists of a pair of cylindrical lens. A plano-convex (PCX) lens is used for adjusting the thickness of the laser sheet.

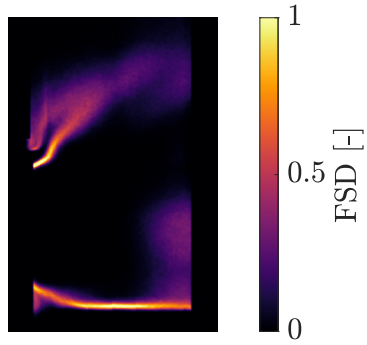

Figure 3.31: Example of a flame surface density (FSD) plot computed from OH-PLIF images.

Stereoscopic Particle Image Velocimetry

Local velocity components u_x and u_θ were measured using 2-dimensional, 3-component stereoscopic PIV for non-reacting, unconfined flow with swirler placed at $h = 10, 20,$ and $30\,\text{mm}$ upstream of the combustor back plane as depicted in Figure 3.2(c).

Details of a stereoscopic-PIV procedure may be found in Raffel et al. (2007). A schematic of the setup is shown in Figure 3.32 and is briefly discussed

below. Scheimpflug adapters were first attached to the high-speed cameras before the camera lens (Sigma 105 mm, F/2.8) were mounted. The adapters were then iteratively tilted until the entire field of view (FOV) was in focus. This was performed with the lens at the widest aperture of F/2.8. The laser sheet was aligned at the position $y = 0$ where a 2-level calibration plate (Davis Type 106-10) was placed. To correct for any laser sheet misalignment with respect to the calibration plate position, a self-calibration was performed using Davis 8.4.0. The non-reacting flow was seeded with olive oil particles using an in-house seeding unit. Double pulsed laser (Litron LDY303HE-PIV of 532 nm) was then fired at a rate of 1 kHz. Similar to the OH-PLIF setup, the laser beam passed through a pair of cylindrical lenses to form a laser sheet which then had its thickness adjusted by means of plano-convex (PCX) lens. The physical FOV was (89.3 × 90.4)mm and seeding images were acquired at a resolution of 896 x 896 pixels. Vector field was computed using the (dewarp) images in Davis 8.4.0 using a five pass method: two passes of 64 x 64 pixel window with 50% overlap followed by three passes of 32 x 32 pixel window with 75% overlap.

Details of the computation is presented in Section 2.2 and the data in Section 4.1.

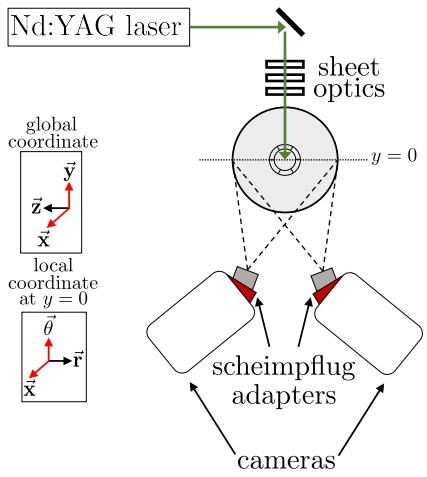

Figure 3.32: Schematic illustrating the stereoscopic PIV setup (not to scale). Scheimpflug adapters were mounted on the cameras to bring the camera's entire FOV to focus. The inset of figure shows the global coordinate system (x, y, z). The vector $\vec{\mathbf{x}}$ is the axial flow direction and is out-of-plane. The laser sheet was aligned at $y = 0$, and the corresponding (local) cylindrical coordinates (r, θ, x) showing the local vectors $\vec{\mathbf{x}}$ and $\vec{\theta}$ is in the second inset.

3.8.3 Hot-wire anemometry

Constant Temperature Anemometry (CTA) was also performed on the swirling flow. The Dantec 55P11 single hot-wire probe, which has a diameter of 5 µm and a length of 1.25 mm, was used in combination with the Dantec Streamline Pro system for this purpose. Details of the Dantec hot-wire setup may be found in Jørgensen (2002). In brief, the upstream unburned bulk mixture flows and cools the heated hot-wire. To maintain the temperature of the hot-wire, which is operating at an overheat ratio of 0.8, a voltage E is applied. Varying values of E are recorded depending on the extent of cooling by the mixture flow which is taken to be proportional to the bulk speed U. This relationship between voltage E and bulk speed U is known as the King's Law:

$$E^2 = (T_\mathrm{w} - T_\mathrm{u})\,(A + BU^{0.5}) \tag{3.1}$$

where T_w is the wire temperature, T_u is the (unburned) fluid mixture temperature, and A, B are constants. In the current work, voltage E was recorded across a range of known mixture flow velocity U. The values were fitted with a fourth order polynomial:

$$U = \sum_{i=0}^{4} c_i E^i \tag{3.2}$$

where c_i are constants. This polynomial calibration curve fit, with an example shown in Figure 3.33, was used to convert subsequent voltage readings measured from flows with unknown bulk velocity U.

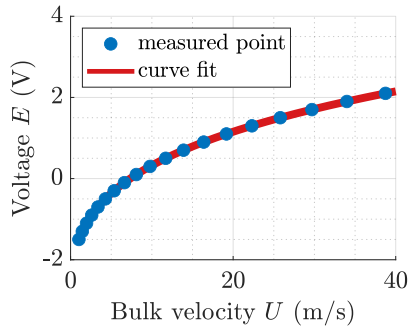

Figure 3.33: Hot-wire calibration curve correlating voltage E to bulk velocity U.

Calibration measurements were taken at the start and end of each day to check for repeatability. Since air was supplied from a central compressor

with a well-regulated temperature at all times, no temperature corrections were made.

3.8.4 Pressure measurements

Acoustic measurements were used to detect any onset of instability during ignition and LBO. They also served to supplement the 1-D PMT signals in detecting the successful ignition of an injector sector (Philip et al. 2014b). This was done using piezoelectric pressure transducers (type Kulite XCS-093 0.35bar) which were inserted into the ports of each injector tube at positions h_{P1} and h_{P2} (see Figure 3.7). The acoustic signals were amplified using a bridge amplifier (type Flyde FE-579-TA).

3.8.5 Temperature measurements

Thermal effects may drastically impact the ignition (Lancien et al. 2018, Philip et al. 2014b, Puggelli et al. 2020, Töpperwien et al. 2022) and lean blowoff dynamics (Korusoy and Whitelaw 2004, Russi et al. 1953, Zhang et al. 2011). Temperatures were therefore taken at various locations of the combustor throughout the entire ignition and LBO experiment run so that one may:

- Control the initial temperature before an experimental run for a well-defined boundary condition.
- Use the temperature profile as empirical input for relevant numerical simulation, and
- provide data for high fidelity numerical simulations (for our collaboration with SAFRAN and CERFACS).

Temperature may be measured using thermocouples and pyrometer, and is briefly presented as follows.

Thermocouple

Temperature profiles along the combustor wall were measured using Type-K thermocouples with a sheath diameter of 1 mm. They were welded on the inner combustor wall or inserted into slots on the combustor back plate as shown in Figure 3.34. The thermocouples are capable of measuring up to temperature $T = 1473\,\mathrm{K}$, with an accuracy of $\max\{1.5\,, 0.4\%\,T\}$ depending on the operating range.

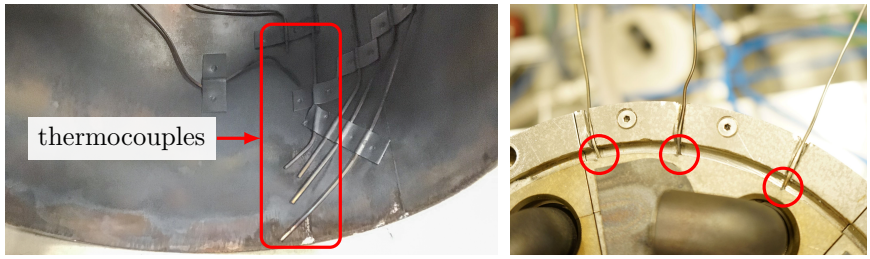

(a) (b)

Figure 3.34: Thermocouple positions on (a) combustor inner wall, and (b) the combustor back plate.

Pyrometer

Optical instruments may be used for non-intrusive temperature measurement of surfaces which are physically inaccessible, such as the flameholder. A pyrometer was used to ensure the same thermal conditions were used during ignition experiments. To do this, an infrared pyrometer (type Optris CTlaser 3MH) was mounted as shown in Figure 3.35. The target measurement spot in this case is the bluff body illuminated in red indicative light. The pyrometer is capable of measuring temperature T between 373 to 873 K, and provides a fast response time of approximately 1 ms. Readings are accurate up to $\pm(0.3\%)$ of reading + 2 K but requires user's input of the emissivity value of the measured surface, ε. To determine the emissivity ε, the following steps apply:

(i) An estimated value of ε for the target surface is used as input for the calibration of the pyrometer.

(ii) The intended area of measurement is first heated up to a sufficiently high temperature.

(iii) The heat source is then removed and the surface is left to cool.

(iv) Simultaneous temperature measurements of the cooling process are made from both the thermocouple (which acts as the reference temperature T_{ref}) and pyrometer (T_{pyro})

(v) The temperature profiles of T_{ref} and T_{pyro} are compared.

Steps (i) to (v) are repeated until a reasonable collapse of the temperature profiles are obtained as shown in Figure 3.35(c).

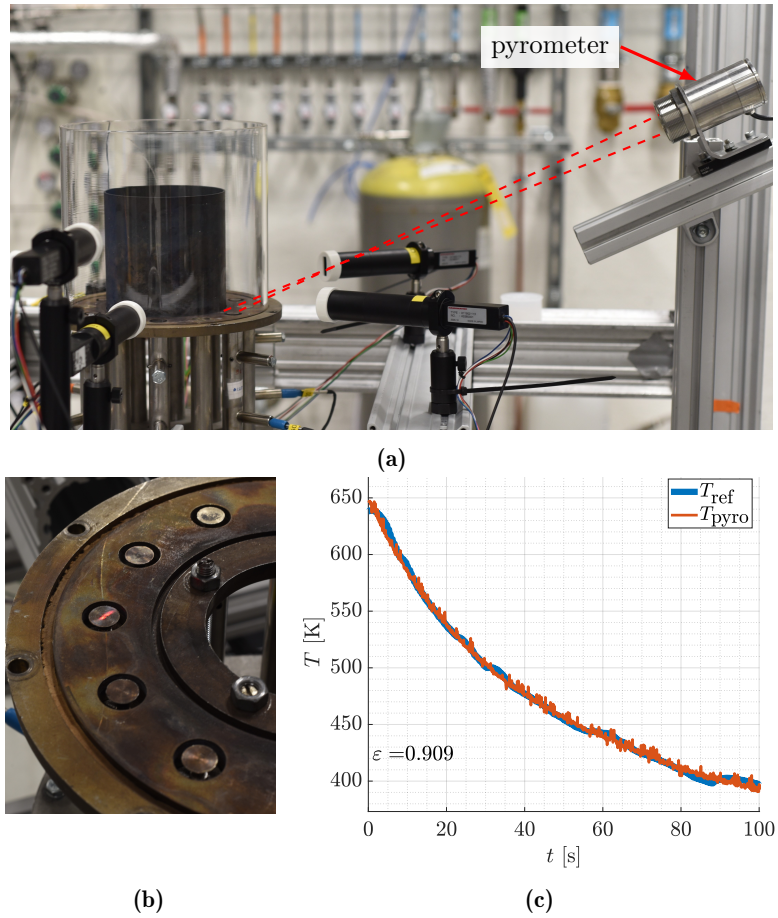

Figure 3.35: Images of pyrometric measurement: (a) shows a photo annotated with the infrared optical path from the pyrometer to the measurement spot which in this case is a flameholder. This is illuminated in red as shown in (b). (c) is a plot of the temperature profiles measured by a thermocouple (T_{ref}) and a pyrometer (T_{pyro}).

3.8.6 Experimental uncertainty and statistical convergence

Mass flow uncertainty

Air and fuel flow rates are regulated by Alicat MC and MCR series mass flow controllers (MFCs) which have an accuracy of ± (0.8% of the reading + 0.2% of the full scale). For each operating condition, the MFC is thus chosen to maximise its full scale flow rate whenever possible to minimise the uncertainty. This allows a more accurate determination of the bulk

flow velocity and the mixture equivalence ratio during instants of flame (re-)ignition and extinction. Table 3.1 lists the typical mass flow uncertainties in a single flame and a 12-injector annular setup for the lean blowoff studies. Flow rates of the MFCs are given in standard litres per minute (slpm)[14].

Table 3.1: Table showing mass flow uncertainties. The uncertainty errors (in %) for U and ϕ are written in brackets.

single bluff body stabilised flame at lowest bulk flow velocity
fuel: 1x 50 slpm MFC
air: 1x 250 slpm MFC

air flow rate (slpm)	fuel flow rate (slpm)	U (m/s)	ϕ (-)
75.00 ± 1.10	4.00 ± 0.13	8.73 ± 0.14 (1.56%)	0.51 ± 0.02 (4.84%)

annular bluff body stabilised flames at highest bulk flow velocity
fuel: 1x 250 slpm MFC
air: 1x 2000 slpm MFC, 1x 1000 slpm MFC

air flow rate (slpm)	fuel flow rate (slpm)	U (m/s)	ϕ (-)
2510.69 ± 26.09	143.93 ± 1.65	24.45 ± 0.26 (1.04%)	0.55 ± 0.01 (2.21%)

Statistical convergence

The stochastic nature of the light-around process requires multiple runs of the same operating condition for repeatability, and the term δ (expressed in %) is used to quantify the statistical convergence of the light-around time τ_{ign}. δ is defined in Equation 3.3 as:

$$\delta = \frac{\overline{\tau}_{\text{ign}}(N) - \overline{\tau}_{\text{ign}}(N-1)}{\overline{\tau}_{\text{ign}}(N)} \times 100 \tag{3.3}$$

[14]The mass reference condition is taken at 25 °C and 14.696 psia (pound-force per square inch absolute).

where $\overline{\tau}_{\text{ign}}(N)$ is the mean value of N measured runs. τ_{ign}^{j} is the light-around time for the j^{th} run.

$$\overline{\tau}_{\text{ign}}(N) = \frac{1}{N}\sum_{j=1}^{N}\tau_{\text{ign}}^{j}$$

Figure 3.36 shows the statistical convergence of a typical ignition experiment with 50 runs. At $N \gtrapprox 25$ runs, δ lies within $\pm 1\%$, as indicated by the grey shaded band.

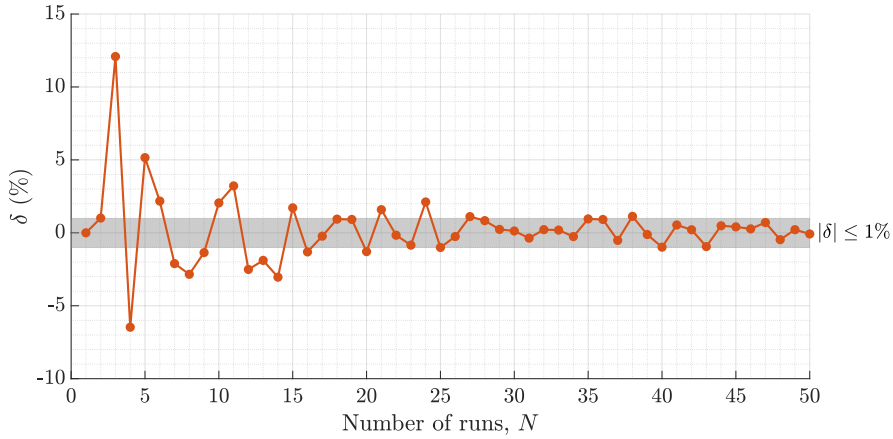

Figure 3.36: Plot showing the variation of δ (in %) with number of runs N. The grey shaded band represents $|\delta| \leq 1\%$.

4

Miscellaneous data

This chapter briefly covers some unpublished data.

Section 4.1 presents some data from the measurement of swirl number $\mathcal{S}$ by means of stereoscopic Particle Image Velocimetry (stereo-PIV) as described in Section 3.8.2.

The remaining chapter summarises some of the key findings of lean blowoff (LBO) dynamics in annular combustors. The presented LBO data is incomplete since data processing is still ongoing. An overview is first presented in Section 4.2.1 before concluding with a brief comparison of LBO limits between single and multi-injector combustors in Section 4.2.2.

4.1 Characterisation of swirling flow

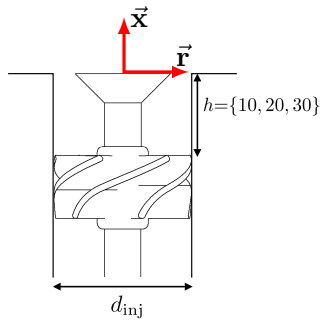

Figure 4.1: Injector configuration with swirler placed upstream of combustor back plane at $h = \{10, 20, 30\}$ mm. The red arrows denote the axes $\vec{\mathbf{x}}$ and $\vec{\mathbf{r}}$. All dimensions are in millimetres.

The swirl number $\mathcal{S}$ is measured for swirler placed at $h = \{10, 20, 30\}$ mm upstream of the combustor back plane as depicted in Figure 4.1. Data is presented for the cases $h = 10$ and 30 mm which are plotted in Figure 4.2. The 2-D velocity fields are shown in Figure 4.2(a). The axial velocity u_x and azimuthal velocity u_θ profiles along the radial direction at axial positions $x/d_{\text{inj}} = 1, 2, 3$ are shown in Figure 4.2(b) and Figure 4.2(c). The measured u_x and u_θ values from the stereo-PIV setup are used to compute the swirl number $\mathcal{S}$ using Equation 2.16 which is restated here for ease of reading.

$$\begin{aligned} \mathcal{S} &= \frac{G_\theta}{r_{\text{o}} G_x} \\ &\approx \frac{\int_0^R u_x u_\theta r^2 \, \mathrm{d}r}{r_{\text{o}} \int_0^R u_x^2 r \, \mathrm{d}r} \end{aligned} \tag{4.1}$$

The discretised form of Equation 2.16 is:

$$\mathcal{S} = \frac{\sum_{j=1}^{N} u_x u_\theta \left(\frac{r_j}{r_{\text{o}}}\right)^2 \Delta r}{\sum_{j=1}^{N} u_x^2 \left(\frac{r_j}{r_{\text{o}}}\right) \Delta r} \tag{4.2}$$

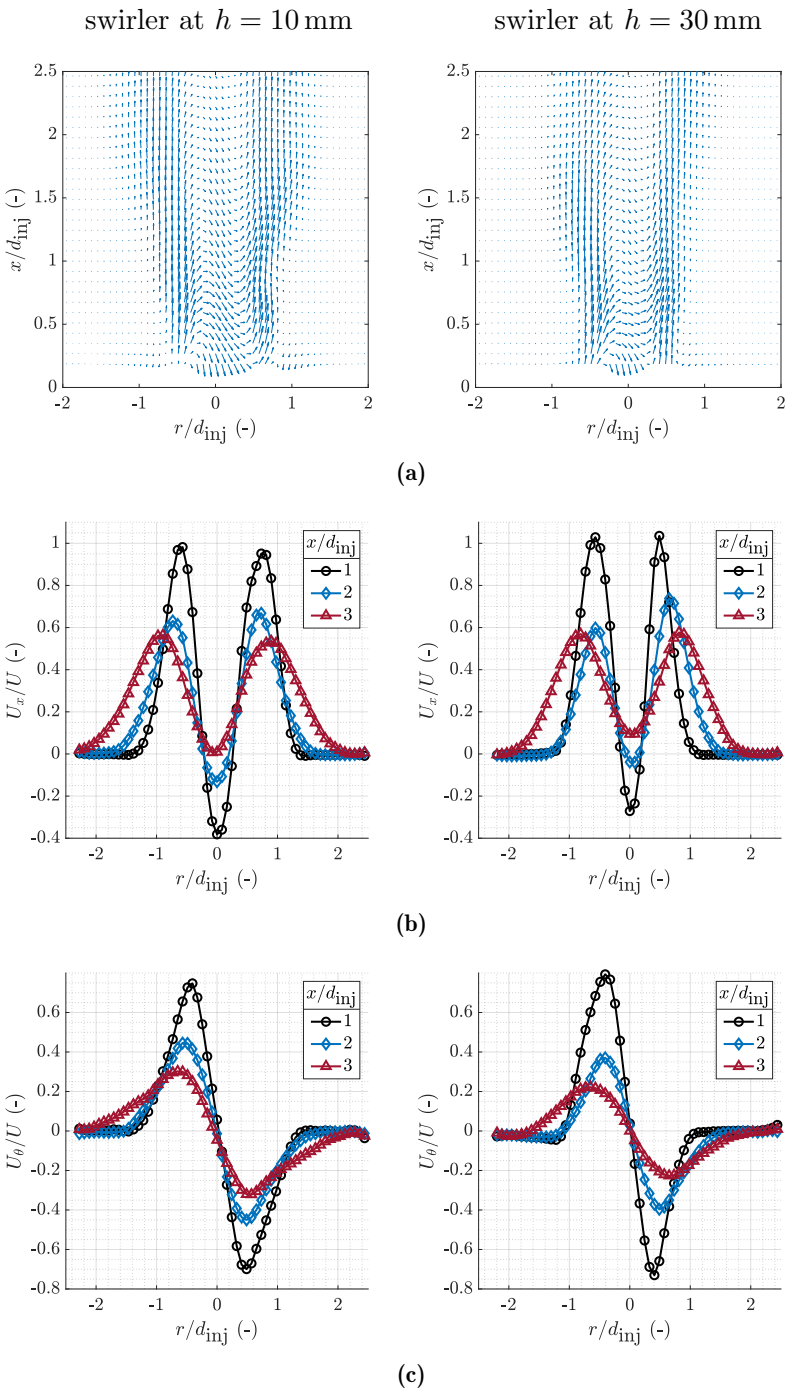

Figure 4.2: Velocity profiles for swirler placed at $h = 10\,\mathrm{mm}$ (left) and $h = 30\,\mathrm{mm}$ (right). (a) 2-D velocity field, (b) axial velocity u_x along the radial direction r at $x/d_{\mathrm{inj}} = \{1, 2, 3\}$, and (c) azimuthal velocity u_θ along the radial direction r at $x/d_{\mathrm{inj}} = \{1, 2, 3\}$.

In Equation 4.2, $r_{j=N} = r_o$ is the swirler outlet radius and is equal to radius of the injector exit $d_{inj}/2$. The radial direction is also uniformly discretised into N intervals so $\Delta r_{j=1,2,...,N} = \Delta r$. The calculated swirl number $\mathcal{S}$ is presented in Figure 4.3. $\mathcal{S}$ decreases when the swirler is placed further upstream, with the case of $h = 10\,\text{mm}$ having a maximum value of $\mathcal{S} \approx 1$ at $x/d_{inj} = 2$. When $h = 30\,\text{mm}$, the maximum value of $\mathcal{S}$ is 0.8 at $x/d_{inj} = 1.5$. The swirl number computed using solely geometric parameters (see Equation 2.17) assumes a spatially uniform value of $\mathcal{S}_g = 1.22$.

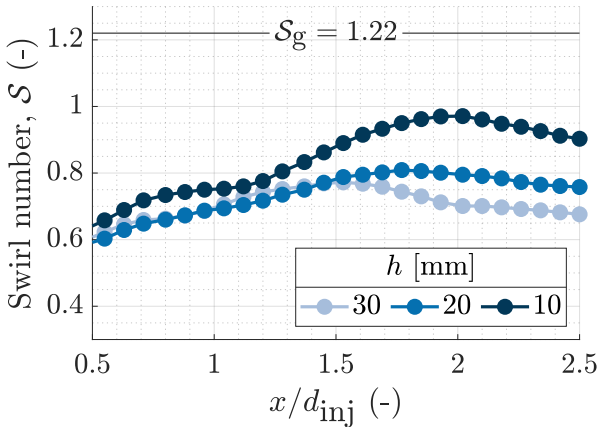

Figure 4.3: Computed swirl number $\mathcal{S}$ along the axial direction x for swirler at $h = \{10, 20, 30\}$ mm.

4.2 Lean blowoff dynamics

4.2.1 Lean blowoff sequence in annular combustors

True colour flame images taken with a DSLR camera are shown to illustrate the change in flame dynamics during the lean blowoff (LBO) sequence. All cases considered are air-methane premix. Figure 4.4 illustrates the LBO sequence of: (i) version 1 (V1) of the simplified Spinning Combustion Technology (SCT) combustor known as SCT V1, with $\alpha = 23°$, $\beta = 0°$ on the left, and (ii) the NTNU 12-injector combustor on the right. For the NTNU combustor, it was observed that with decreasing equivalence ratio ϕ, well-attached flames started to elongate. At some point of the LBO sequence, all flames were fully detached and stabilised at a certain axial distance downstream of the combustor back plane. Sporadic local flame liftoff (or local extinction) and subsequent reattachment at injector sectors were then observed. One such instant is shown in Figure 4.4 at $\phi = 0.57$. The red circles

show the region where local flame extinction and subsequent reattachment occurred. In the final instants leading up to global extinction, flames were stabilised almost at the downstream exit end of the inner combustor wall. In the SCT V1 combustor, the azimuthal flames were observed to stabilise downstream, forming a pseudo-continuous ring of azimuthally lifted flames around the circumference of the annulus chamber as seen from the visible heat patterns of the inner combustor wall.

Figure 4.5 shows the LBO sequence of: (i) the SAFRAN Arrano engine on the left, and (ii) version 2 (V2) of the simplified SCT, SCT V2 on the right. In both the actual engine and its laboratory-scale model, the flame stabilisation mechanism appears to be qualitatively similar, and also drastically different from those combustors depicted in Figure 4.4. At no point were flames noticed to stabilise downstream. There was strong indication of piloting effects whereby an extinguished injector (denoted E) was observed to reignite shortly if the preceding (pilot) injector (denoted P) has well-stabilised flames. More future investigations are required to conclusively demonstrate such a piloting effect.

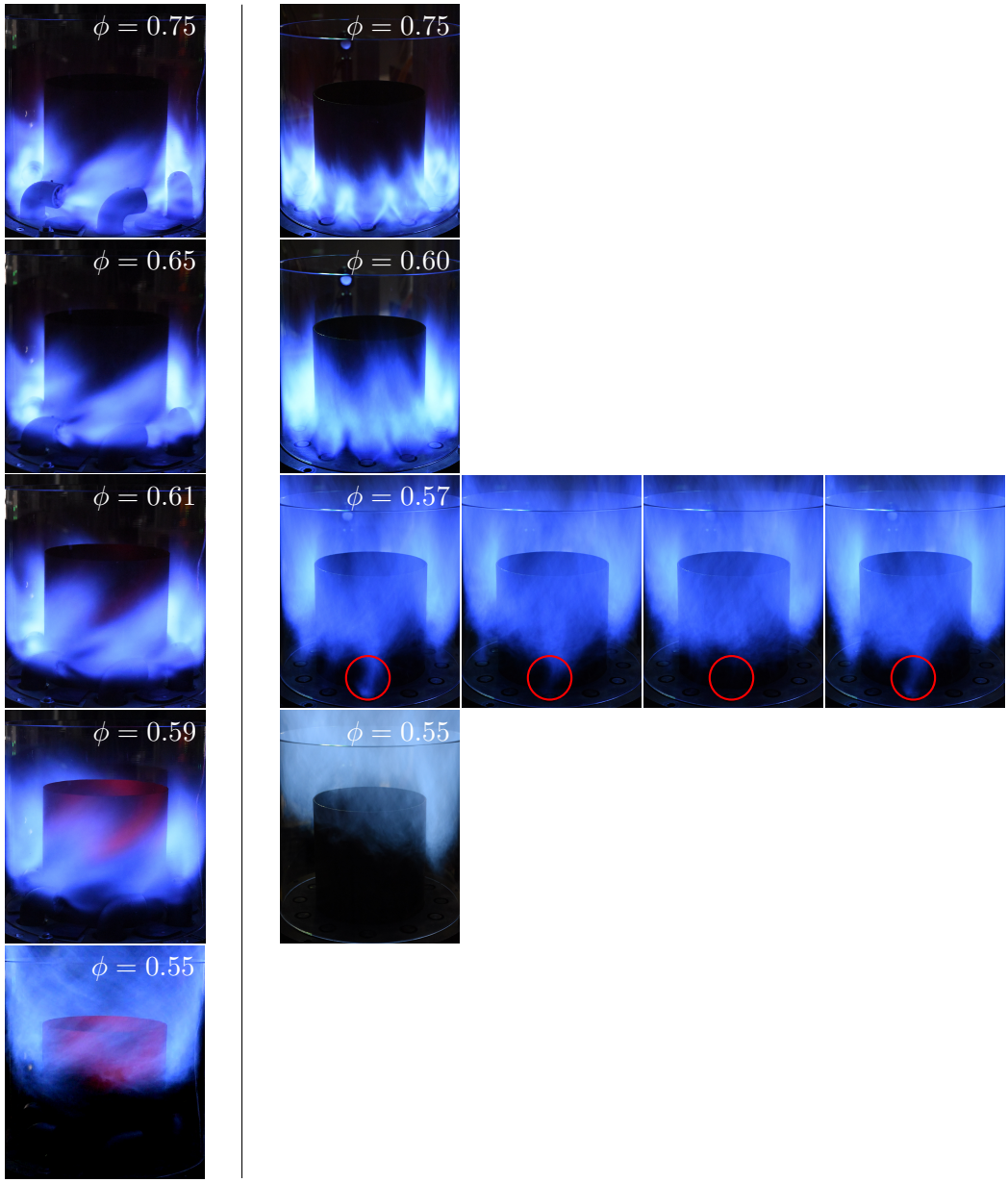

Figure 4.4: A typical lean blowoff image sequence. Left: SAFRAN SCT V1 with $\alpha = 23°$, $\beta = 0°$, and right: NTNU 12-injector combustor. A sequence of local extinction and subsequent reignition/flame reattachment is captured at $\phi = 0.57$ for the NTNU combustor and circled in red.

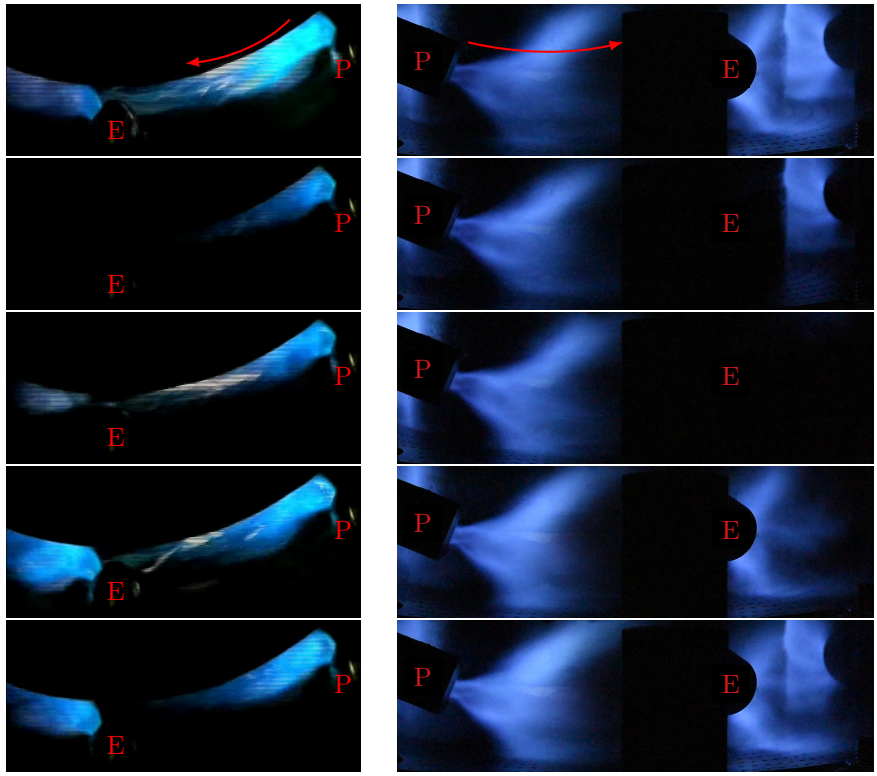

Figure 4.5: A typical lean blowoff image sequence. Left of the figure shows that of the SAFRAN Arrano engine, and right shows its laboratory-scale model SCT V2. In both cases, local extinction and reignition events suggest a piloting effect of a well-stabilised (pilot) flame injector labelled P on the extinguished injector denoted E. Direction of the net azimuthal swirl flow is indicated by a red arrow on the first image of each sequence. The LBO images of the Arrano engine adapted from Safran Helicopter Engines (2016a).

4.2.2 Lean blowoff curve

The LBO limit curves of both single and multi-injector combustor configurations are presented in Figure 4.6. The lip velocity upon global flame extinction U_{bo} is plotted against the equivalence ratio ϕ of the air-methane premix at that instant. In both the straight axial and 90° bend injector cases, the multi-injector configurations exhibit much more variability. Notably, the NTNU 6-injector combustor does not exhibit a monotonic relationship. For instance at a given blowoff velocity U_{bo} of 25 m/s, global extinction of flames may occur either at $\phi \approx 0.55$ or at a leaner value of $\phi \approx 0.50$. This is attributed to the stochastic behaviour of local flame extinction and reattachment

as discussed earlier in Section 4.2.1. A premature flame liftoff and failure in reattachment leads to a higher blowoff equivalence ratio ϕ_{bo} while the lean blowoff limit may be substantially extended if there is successful occurrence of flame reattachment. In the case of the NTNU 6-injector configuration, this effect is particularly pronounced, leading to a non-monotonic LBO curve relationship. For the 90° bend injectors, it is noted that either of the annular configuration leads to an improvement over the case of a single flame in terms of global flame extinction limit. A yaw angle value of $\alpha = 23°$ also leads to better LBO limits. This is likely due to increased flame interaction for the case of $\alpha = 23°$ as compared to $\alpha = 0°$. No concrete reasoning has been put forth but Large Eddy Simulations (LES) performed by CERFACS suggest that stronger flame interaction in the $\alpha = 23°$ configuration results in lower flame strain rate, and therefore better blowoff limits. This is presented in draft Article IV.

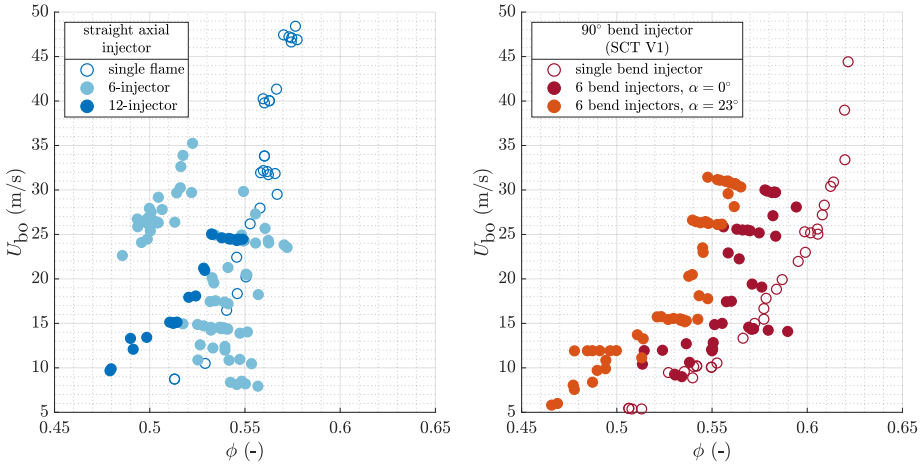

(a) **(b)**

Figure 4.6: Lean blowoff curves of: (a) straight axial injectors with swirlers at $h = 10\,\mathrm{mm}$ upstream of bluff body in single injector, 6-injector, and 12-injector configurations, and (b) 90° bend injectors in single and multi-injector annular configurations. Yaw angle $\alpha = 0$ and 23° were considered for the annular SCT V1 combustor. Hollow markers represent data points of single flames, while solid markers correspond to that of multi-injector combustors.

5

Summary of research articles and conclusions

5.1 Summary of articles

This chapter summarises four articles which are part of the thesis.

Two of the articles present numerical and experimental works performed on the laboratory-scale spinning combustor (SCT V1): in Article I, the general flame dynamics of spinning flames is characterised while in Article IV, the lean blowoff process is discussed. These studies were performed in collaboration with SAFRAN Helicopter Engines and CERFACS under the ANNULIGhT Innovative Training Network (ITN).

Article II and Article III focus on experimental ignition studies in annular combustors. In the former, we explored the ignition effects of strong azimuthal swirl and azimuthal fuel staging in SCT V2 operating under Rich-Quench-Lean (RQL) staging. In the latter, we investigated the light-around dynamics of non-carbon fuel blends in the NTNU annular combustor.

The thesis concludes with a discussion of how results presented in the articles, as well as in Chapter 4, have sought to address the three research objectives formulated in Section 1.4 concerning the *ignition and lean blowoff dynamics of turbulent flames in annular combustors*. Potential future

work is also briefly explored.

Article I

Numerical and experimental flame stabilization analysis in the new spinning combustion technology framework
Pasquale Walter Agostinelli, Yi Hao Kwah, Stephane Richard, Gorka Exilard, James R. Dawson, Laurent Gicquel, Thierry Poinsot
ASME Turbo Expo 2020: Turbomachinery Conference and Exposition, Volume 4A: Combustion, Fuels, and Emissions, Page V04At04A058

Article I is the first of two articles on the SCT V1. The azimuthally directed flames in this laboratory-scale combustor were studied experimentally and numerically. The characterisation involved temperature measurements along the combustor wall and pressure drop measurement across the bend injector. OH* chemiluminescence and OH-Planar Laser-Induced Fluorescence (PLIF) images were used to identify mean flame structures and compute flame surface density (FSD) respectively. Hot-wire anemometry (HWA) was also performed in a non-reacting flow field to obtain the velocity profiles. These relevant quantities of measure (temperature T, pressure P, bulk flow velocity U) and flame dynamics (mean flame structure and FSD) were used to validate the employed numerical method, providing groundwork for the subsequent numerical-experimental study on lean blowoff process in the same combustor (see Article IV). A preliminary investigation on the effect of combustor back plane cooling was also conducted to aid in the design process of the effusion-cooled back plane found in the second version of the laboratory-scale spinning combustor (SCT V2). It also allows for an assessment on the effectiveness of the geometry design in introducing a Rich-Quench-Lean (RQL) staged combustion which is later implemented in SCT V2.

Article II

Effect of strong azimuthal swirl on ignition and light-around in an annular combustor
Yi Hao Kwah, Pasquale Walter Agostinelli, Stephane Richard, Gorka Exilard, Stephane Pascaud, Laurent Gicquel, James R. Dawson
Journal of Engineering for Gas Turbines and Power, Volume 144, Issue 11, Pages 11010

Article II presents findings from ignition experiments conducted on the

second version of the laboratory-scale spinning combustor (SCT V2). Three aspects of the combustor design were considered: (i) Rich-Quench-Lean (RQL) staging, (ii) strong azimuthal swirl, and (iii) azimuthal fuel staging. Under RQL staging (see Section 3.5 for details), the spinning flames behave very similar to non-premixed flames: no clear correlation could be established between the ignition propagation speed S_a and mixture bulk velocity U. The presence of a strong azimuthal velocity component induced by the novel angled injector configuration results in a highly predictable ignition sequence around the annulus, with a considerably faster light-around speed compared to a typical straight injector combustor. In certain cases, a non-sequential order of ignition was observed. A novel ignition map was constructed to provide better visualisation of how ignition proceeds in SCT V2. Consideration of two different azimuthal fuel staging configurations as described in Section 3.5.2 leads to an improvement of the lean ignition limit due to a possible piloting effect which is inferred from overhead high-speed images.

Article III

The effect of methane-ammonia and methane-hydrogen blends on ignition and light-around in an annular combustor
Yi Hao Kwah, Samuel Wiseman, James R. Dawson
Submitted to: Journal of Engineering for Gas Turbines and Power

Article III considers the light-around phenomenon on a more fundamental level. Ignition experiments were conducted on the 6-injector NTNU annular combustor considering only bluff body stabilised premixed flames, and using a variety of hydrocarbon (CH_4, C_2H_4, and C_3H_8) and non-carbon (H_2 and NH_3) fuels. The choice of a much simple combustor geometry reduces flow complexity, and minimises the risk of flashback (compared to swirling flames) while the use of multiple fuel blends is motivated by recent interests in carbon-free fuel for reduced emissions and the ability to independently vary laminar flame speed S_L^0 and dilatation ratio ρ_u/ρ_b. To increase statistical certainty, each operating condition was repeated between 30 to 50 times, with a total of more than 3000 data sets of which 900 included high-speed imaging. Three fuel cases were considered as follows. (i) In pure hydrocarbon fuels cases where ρ_u/ρ_b and S_L^0 could not be independently varied, the light-around speeds were observed to have a positive correlation with the lumped parameter $(\rho_u/\rho_b) \cdot S_L^0$, coherent with previous studies. (ii) The equivalence ratio ϕ and blend ratio of CH_4-NH_3-H_2 were adjusted

to independently vary the laminar flame speed S_L^0 while keeping ρ_u/ρ_b constant. An empirically fit correlation considering Lewis number effects (with *Le* computed based on a heat release-based approach) results in good scaling between S_a and S_L^0. (iii) Similarly, the equivalence ratio ϕ and blend ratio of CH_4–H_2 were adjusted to only vary the dilatation ratio ρ_u/ρ_b without a change in S_L^0. Contrary to existing knowledge based upon prior studies on ignition of hydrocarbon fuels, a decrease in ρ_u/ρ_b results in an unexpected increase in S_a. No suitable explanation has yet been put forth but is likely attributed to the thermo-diffusive effects of H_2.

Draft article IV

On the lean blow-out dynamics in the Spinning Combustion Technology
Pasquale Walter Agostinelli, Yi Hao Kwah, Stephane Richard, Gorka Exilard, James R. Dawson, Laurent Gicquel
Planned submission to: Combustion and Flame

Article IV reports both numerical and experimental investigations of the lean blowff (LBO) process in SCT V1. Two different geometric configurations of SCT V1 were considered: (i) bend injector positioned at a yaw angle of $\alpha = 23°$, and (ii) at a yaw angle of $\alpha = 0°$. This is motivated by results of the LBO limit curve (Figure 4.6(b)) in Chapter 4 which shows a substantial difference in LBO limits depending on the yaw angle α of the injectors. It was observed that at sufficiently lean fuel-air mixtures, the presence of a strong azimuthal swirl in SCT V1 leads to the formation of a continuous, azimuthally lifted flame around the annulus downstream of the combustor back plane as depicted in Figure 4.4. This lifted flame ring has a piloting effect, helping to improve the LBO limits. At $\alpha = 23°$, there is a greater interaction between neighbouring flames, thereby enhancing this piloting effect. Consequentially, $\alpha = 23°$ fares better than the case of $\alpha = 0°$ in terms of LBO limit, with the flames being more resilient to the stretch rate (which is approximated by the flame strain rate) as suggested from numerical simulations.

5.2 Conclusions and future outlook

In the study of *ignition and lean blowoff dynamics of turbulent flames in annular combustors*, three main research goals have been identified. These have been previously summarised in Figure 1.9 and are reiterated here for ease for reading.

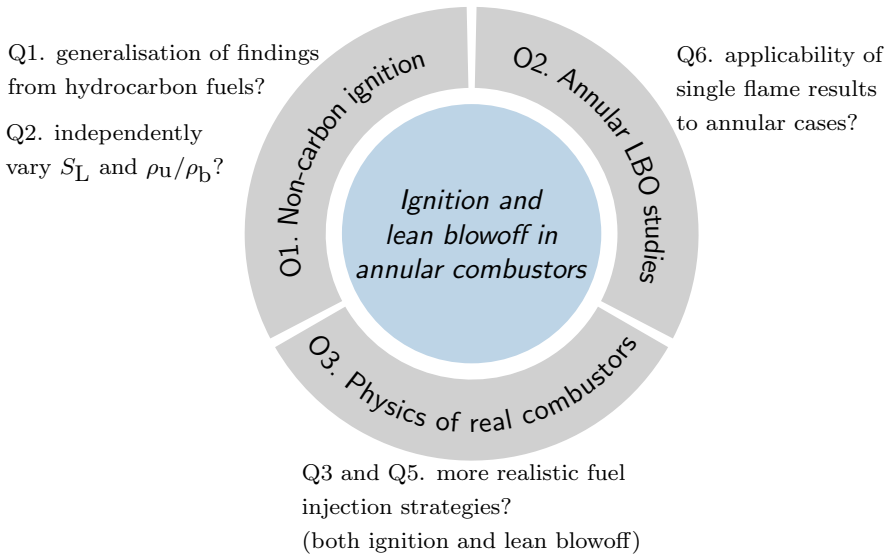

Figure 5.1: Chart reproduced from Figure 1.9 summarising the research objectives.

The research outcomes addressing these objectives are discussed in the following paragraphs.

O1. Ignition studies using non-carbon fuels

In Article III, we saw how the choice of fuel type can drastically influence the ignition light-around dynamics. The attempt to independently vary laminar flame speed S_L^0 and dilatation ratio ρ_u/ρ_b using non-carbon fuel blends led to the surprising finding that thermo-diffusive effect plays a crucial role in influencing the ignition propagation speed S_a. This has been previously reported by investigators measuring turbulent flame speed S_T in fan-stirred bombs (Karpov and Severin 1980, Lipatnikov and Chomiak 2005, 2002) but has never been studied in light-around experiments which as of present, have only used pure hydrocarbons as fuel. For CH_4-NH_3-H_2 blends with Lewis number $Le > 1$, an empirical correlation taking into account Le leads to good scaling between S_a and laminar flame speed S_L^0. However, applying the same correlation to CH_4-H_2 fuel blends failed to achieve any reasonable collapse of the datasets. The effect of increased S_a values with decreasing dilatation ratio ρ_u/ρ_b for CH_4-H_2 fuel blends runs contrary to existing knowledge based upon hydrocarbon fuels. This anomaly reflects the incomplete understanding of the ignition light-around phenomenon and warrants a more detailed investigation on fuel blends with flame properties which are different from that of conventional hydrocarbons. This is partic-

ularly pertinent when there is an ever increasing emphasis to transition to non-carbon fuels like NH_3 and H_2 for lower emissions. As seen in Article III, these fuels have drastically different flame properties which alter the ignition dynamics considerably. Light-around experiments may also be conducted in the intermediate pressurised annular (IPA) combustor in our lab under pressurised, choked flow conditions to even more closely replicate realistic engine conditions which relates to O3 of the thesis.

O2. Lean blowoff studies using different annular injector configurations

Lean blowoff (LBO) experiments have been conducted on both single flame and multiple flames arranged in an annular configuration. Due to time constraints, detailed analysis has not yet been performed but key findings are summarised in Chapter 4. The onset of a global pandemic also delayed the servicing of various equipment such as the OH-PLIF and the high-speed intensified relay optics unit, severely limiting the availability of various optical diagnostics for an extended period of time. The blowoff mechanism could therefore not be investigated in detail. However, the available measurements clearly indicate that flame interaction strongly influences the LBO dynamics, coherent with conclusions drawn from existing studies (Ciardiello et al. 2020c, 2022b, Kwong and Steinberg 2019a,b). The importance of flame interaction in influencing the LBO limits is also evident from the numerical and experimental study presented in Article IV. In this regard, future work may choose to study the role of multi-flame interaction during the LBO process, the physics of which cannot be replicated in a single flame setup. The limited LBO studies performed in a multi-flame configuration needs to be addressed via future experimental work as well.

O3. Studies more closely replicating real combustors

Two new laboratory-scale annular combustors (SCT V1 and SCT V2) have been designed and commissioned to replicate the relevant physics found in a SAFRAN spinning combustor which are: (i) Rich-Quench-Lean (RQL) staging, (ii) strong azimuthal swirl, and (iii) azimuthal fuel staging.

The effect of (i) RQL and (iii) azimuthal fuel staging on light-around ignition is presented in Article II. Compared to conventional laboratory annular combustors operating under premixed conditions, flames under RQL staging were observed to behave like non-premixed flames. This highlights the need for more light-around experimental data focusing on non-premixed combustion to more reliably predict ignition behaviour in real engines. NOx and CO emissions levels could also be measured in future experiments to evaluate the effectiveness of the implemented RQL staging. Azimuthal fuel staging

has been shown to improve the ignition limits and future works could be extended to evaluate whether blowoff limits may also be improved in the same manner.

The effect of (ii) strong azimuthal swirl on ignition and lean blowoff dynamics was investigated in Article II and Article IV respectively. Experimental results from both studies strongly suggest that these azimuthally directed flames have a piloting effect on the (re-)ignition of neighbouring injectors, and is likely to result in better ignition and blowoff limits. Studies may be performed to study the piloting effects of these flames in detail. In particular, the piloting effect during the blowoff process in SCT V2 bears much qualitative similarity to the actual SAFRAN engine as seen in Figure 4.5. This is a promising indication that the blowoff physics in a spinning combustor has been successfully replicated in a laboratory scale.

5.3 Final remarks

It is hoped that the works presented in this thesis have helped contribute to a better understanding of *ignition and lean blowoff dynamics of turbulent flames in annular combustors*. As is typical of a research journey, the process of addressing the main research objectives summarised in Section 1.4 have only led to more queries being raised. It is then the aim of future research to seek better insights on these emerging questions. On a more fundamental point of view, findings from Article III and Chapter 4 are but one of the numerous steps to be taken to elucidate the complex transient phenomena of *ignition and lean blowoff dynamics* while the numerical and experimental investigations reported in Article I, Article II and Article IV represent the first of many works which may be performed on the experimental rigs SCT V1 and SCT V2 to better understand the workings of a combustion engine.

Bibliography

S. Aggarwal. A review of spray ignition phenomena: present status and future research. *Progress in Energy and Combustion Science*, 24(6):565–600, Jan. 1998. ISSN 0360-1285. doi: 10.1016/S0360-1285(98)00016-1.

S. Ahmed and E. Mastorakos. Spark ignition of lifted turbulent jet flames. *Combustion and Flame*, 146(1-2):215–231, July 2006. ISSN 00102180. doi: 10.1016/j.combustflame.2006.03.007.

S. Ahmed, R. Balachandran, T. Marchione, and E. Mastorakos. Spark ignition of turbulent nonpremixed bluff-body flames. *Combustion and Flame*, 151(1-2):366–385, Oct. 2007. ISSN 00102180. doi: 10.1016/j.combustflame.2007.06.012.

P. M. Allison and E. Mastorakos. Forced response of flames in a bluff-body stabilized annular combustor. In *55th AIAA Aerospace Sciences Meeting*, Grapevine, Texas, Jan. 2017. American Institute of Aeronautics and Astronautics. ISBN 978-1-62410-447-3. doi: 10.2514/6.2017-1337.

B. Ariatabar, R. Koch, H.-J. Bauer, and D.-A. Negulescu. Short Helical Combustor: concept study of an innovative gas turbine combustor with angular air supply. *Journal of Engineering for Gas Turbines and Power*, 138(3):031503, Mar. 2016. ISSN 0742-4795, 1528-8919. doi: 10.1115/1.4031362.

B. Ariatabar, R. Koch, and H.-J. Bauer. Short Helical Combustor: dynamic flow analysis in a combustion system with angular air supply. *Journal of Engineering for Gas Turbines and Power*, 139(4):041505, Apr. 2017. ISSN 0742-4795, 1528-8919. doi: 10.1115/1.4034688.

E. Bach, J. Kariuki, J. R. Dawson, E. Mastorakos, and H.-J. Bauer. Spark ignition of single bluff-body premixed flames and annular combustors. In *51st AIAA Aerospace Sciences Meeting including the New Horizons Forum and Aerospace Exposition*, pages 1–12, Grapevine (Dallas/Ft.

Worth Region), Texas, Jan. 2013. American Institute of Aeronautics and Astronautics. ISBN 978-1-62410-181-6. doi: 10.2514/6.2013-1182.

D. W. Bahr. HC and CO emission abatement via selective fuel injection. In *Volume 3: Coal, Biomass and Alternative Fuels; Combustion and Fuels; Oil and Gas Applications; Cycle Innovations*, page V003T06A026, London, England, Apr. 1982. American Society of Mechanical Engineers. ISBN 978-0-7918-7958-0. doi: 10.1115/82-GT-178.

D. W. Bahr. Technology for the design of high temperature rise combustors. *Journal of Propulsion and Power*, 3(2):179–186, Mar. 1987. ISSN 0748-4658, 1533-3876. doi: 10.2514/3.22971.

R. Balachandran, B. Ayoola, C. Kaminski, A. Dowling, and E. Mastorakos. Experimental investigation of the nonlinear response of turbulent premixed flames to imposed inlet velocity oscillations. *Combustion and Flame*, 143(1-2):37–55, Oct. 2005. ISSN 00102180. doi: 10.1016/j.combustflame.2005.04.009.

D. Ballal and A. Lefebvre. The influence of flow parameters on minimum ignition energy and quenching distance. *Symposium (International) on Combustion*, 15(1):1473–1481, Jan. 1975a. ISSN 00820784. doi: 10.1016/S0082-0784(75)80405-X.

D. Ballal and A. Lefebvre. The influence of spark discharge characteristics on minimum ignition energy in flowing gases. *Combustion and Flame*, 24: 99–108, Feb. 1975b. ISSN 00102180. doi: 10.1016/0010-2180(75)90132-7.

D. Ballal and A. Lefebvre. Ignition and flame quenching in flowing gaseous mixtures. *Proceedings of the Royal Society A: Mathematical, Physical and Engineering Sciences*, 357(1689):163–181, Oct. 1977. ISSN 1364-5021, 1471-2946. doi: 10.1098/rspa.1977.0161.

D. Ballal and A. Lefebvre. A general model of spark ignition for gaseous and liquid fuel-air mixtures. *Symposium (International) on Combustion*, 18(1):1737–1746, 1981. ISSN 00820784. doi: 10.1016/S0082-0784(81)80178-6.

A. Barnett. Aviation safety: a whole new world? *Transportation Science*, 54(1):84–96, Jan. 2020. ISSN 0041-1655, 1526-5447. doi: 10.1287/trsc.2019.0937.

D. Barré, L. Esclapez, M. Cordier, E. Riber, B. Cuenot, G. Staffelbach, B. Renou, A. Vandel, L. Y. Gicquel, and G. Cabot. Flame propagation in

aeronautical swirled multi-burners: experimental and numerical investigation. *Combustion and Flame*, 161(9):2387–2405, Sept. 2014. ISSN 00102180. doi: 10.1016/j.combustflame.2014.02.006.

M. Bauerheim, P. Salas, F. Nicoud, and T. Poinsot. Symmetry breaking of azimuthal thermo-acoustic modes in annular cavities: a theoretical study. *Journal of Fluid Mechanics*, 760:431–465, Dec. 2014. ISSN 0022-1120, 1469-7645. doi: 10.1017/jfm.2014.578.

M. Bauerheim, M. Cazalens, and T. Poinsot. A theoretical study of mean azimuthal flow and asymmetry effects on thermo-acoustic modes in annular combustors. *Proceedings of the Combustion Institute*, 35(3):3219–3227, 2015. ISSN 15407489. doi: 10.1016/j.proci.2014.05.053.

J. Beeckmann, R. Hesse, S. Kruse, A. Berens, N. Peters, H. Pitsch, and M. Matalon. Propagation speed and stability of spherically expanding hydrogen/air flames: experimental study and asymptotics. *Proceedings of the Combustion Institute*, 36(1):1531–1538, 2017. ISSN 15407489. doi: 10.1016/j.proci.2016.06.194.

A. Bhattacharya, B. Gupta, S. Hansda, Z. Haque, A. Kumar, M. K. Mishra, S. De, A. Mukhopadhyay, and S. Sen. Lean blowout phenomena and prior detection of lean blowout in a premixed model annular combustor. In *Volume 2: Combustion, Fuels, and Emissions*, page V002T04A009, Chennai, Tamil Nadu, India, Dec. 2019. American Society of Mechanical Engineers. ISBN 978-0-7918-8353-2. doi: 10.1115/GTINDIA2019-2491.

M. V. Blanc, P. G. Guest, G. von Elbe, and B. Lewis. Ignition of explosive gas mixtures by electric sparks. i. minimum ignition energies and quenching distances of mixtures of methane, oxygen, and inert gases. *The Journal of Chemical Physics*, 15(11):798–802, Nov. 1947. ISSN 0021-9606, 1089-7690. doi: 10.1063/1.1746337.

M. V. Blanc, P. Guest, G. v. Elbe, and B. Lewis. Ignition of explosive gas mixtures by electric sparks: iii. minimum ignition energies and quenching distances of mixtures of hydrocarbons and ether with oxygen and inert gases. *Third Symposium on Combustion and Flame and Explosion Phenomena*, 3(1):363–367, Jan. 1948. ISSN 1062-2896. doi: 10.1016/S1062-2896(49)80044-4.

M. Boileau, G. Staffelbach, B. Cuenot, T. Poinsot, and C. Berat. LES of an ignition sequence in a gas turbine engine. *Combustion and Flame*, 154 (1-2):2–22, July 2008. ISSN 00102180. doi: 10.1016/j.combustflame.2008.02.006.

J.-F. Bourgouin, D. Durox, T. Schuller, J. Beaunier, and S. Candel. Ignition dynamics of an annular combustor equipped with multiple swirling injectors. *Combustion and Flame*, 160(8):1398–1413, Aug. 2013. ISSN 00102180. doi: 10.1016/j.combustflame.2013.02.014.

J.-F. Bourgouin, D. Durox, J. P. Moeck, T. Schuller, and S. Candel. Characterization and modeling of a spinning thermoacoustic instability in an annular combustor equipped with multiple matrix injectors. *Journal of Engineering for Gas Turbines and Power*, 137(2):021503, Sept. 2014. ISSN 0742-4795. doi: 10.1115/1.4028257.

J.-F. Bourgouin, D. Durox, J. Moeck, T. Schuller, and S. Candel. A new pattern of instability observed in an annular combustor: The slanted mode. *Proceedings of the Combustion Institute*, 35(3):3237–3244, 2015. ISSN 15407489. doi: 10.1016/j.proci.2014.06.029.

N. Bouvet, F. Halter, C. Chauveau, and Y. Yoon. On the effective Lewis number formulations for lean hydrogen/hydrocarbon/air mixtures. *International Journal of Hydrogen Energy*, 38(14):5949–5960, May 2013. ISSN 03603199. doi: 10.1016/j.ijhydene.2013.02.098.

D. Bradley, R. Hicks, M. Lawes, C. Sheppard, and R. Woolley. The measurement of laminar burning velocities and Markstein numbers for iso-octane–air and iso-octane–n-heptane–air mixtures at elevated temperatures and pressures in an explosion bomb. *Combustion and Flame*, 115 (1-2):126–144, Oct. 1998. ISSN 00102180. doi: 10.1016/S0010-2180(97) 00349-0.

S. W. Burd and A. K. Cheung. Angled flow annular combustor for turbine engine. Sept. 2007. Patent No WO 2007/102807 Al.

S. Candel, D. Durox, T. Schuller, P. Palies, J.-F. Bourgouin, and J. P. Moeck. Progress and challenges in swirling flame dynamics. *Comptes Rendus Mécanique*, 340(11-12):758–768, Nov. 2012. ISSN 16310721. doi: 10.1016/j.crme.2012.10.024.

S. Candel, D. Durox, T. Schuller, J.-F. Bourgouin, and J. P. Moeck. Dynamics of swirling flames. *Annual Review of Fluid Mechanics*, 46 (1):147–173, Jan. 2014. ISSN 0066-4189, 1545-4479. doi: 10.1146/annurev-fluid-010313-141300.

S. M. Candel and T. J. Poinsot. Flame stretch and the balance equation for the flame area. *Combustion Science and Technology*, 70(1-3):1–15, Mar. 1990. ISSN 0010-2202, 1563-521X. doi: 10.1080/00102209008951608.

R. S. Cant and E. Mastorakos. *An introduction to turbulent reacting flows*. Imperial College Press, Dec. 2007. ISBN 978-1-86094-778-0. doi: 10.1142/p498.

D. E. Cavaliere. *Blow-off in gas turbine combustors*. PhD thesis, University of Cambridge, June 2013. doi: 10.17863/CAM.11753.

D. E. Cavaliere, J. Kariuki, and E. Mastorakos. A comparison of the blow-off behaviour of swirl-stabilized premixed, non-premixed and spray flames. *Flow, Turbulence and Combustion*, 91(2):347–372, Sept. 2013. ISSN 1386-6184, 1573-1987. doi: 10.1007/s10494-013-9470-z.

S. Chaudhuri and B. M. Cetegen. Blowoff characteristics of bluff-body stabilized conical premixed flames with upstream spatial mixture gradients and velocity oscillations. *Combustion and Flame*, 153(4):616–633, June 2008. ISSN 00102180. doi: 10.1016/j.combustflame.2007.12.008.

S. Chaudhuri, S. Kostka, M. W. Renfro, and B. M. Cetegen. Blowoff dynamics of bluff body stabilized turbulent premixed flames. *Combustion and Flame*, 157(4):790–802, Apr. 2010. ISSN 00102180. doi: 10.1016/j.combustflame.2009.10.020.

S. Chaudhuri, S. Kostka, S. G. Tuttle, M. W. Renfro, and B. M. Cetegen. Blowoff mechanism of two dimensional bluff-body stabilized turbulent premixed flames in a prototypical combustor. *Combustion and Flame*, 158 (7):1358–1371, July 2011. ISSN 00102180. doi: 10.1016/j.combustflame.2010.11.012.

N. A. Chigier and J. M. Beér. Velocity and static-pressure distributions in swirling air jets issuing from annular and divergent nozzles. *Journal of Basic Engineering*, 86(4):788–796, Dec. 1964. ISSN 0098-2202. doi: 10.1115/1.3655954.

R. Ciardiello. *Transient phenomena in annular combustors*. PhD thesis, University of Cambridge, May 2021. doi: 10.17863/CAM.70267.

R. Ciardiello, P. M. de Oliveira, A. W. Skiba, E. Mastorakos, and P. M. Allison. Effect of spark location and laminar flame speed on the ignition transient of a premixed annular combustor. *Combustion and Flame*, 221: 296–310, Nov. 2020a. ISSN 00102180. doi: 10.1016/j.combustflame.2020.08.001.

R. Ciardiello, R. Pathania, P. Allison, P. M. de Oliveira, and E. Mastorakos. Ignition probability and lean ignition behaviour of a swirled premixed

bluff-body stabilised annular combustor. *Journal of Engineering for Gas Turbines and Power*, Sept. 2020b. ISSN 0742-4795, 1528-8919. doi: 10.1115/1.4048461.

R. Ciardiello, A. Skiba, R. Gordon, and E. Mastorakos. Experimental assessment of the lean blow-off in a fully premixed annular combustor. *Experimental Thermal and Fluid Science*, 112:109994, Apr. 2020c. ISSN 08941777. doi: 10.1016/j.expthermflusci.2019.109994.

R. Ciardiello, L. C. Mesquita, and E. Mastorakos. Low-order modelling of the light-round ignition transient in a premixed annular combustor. *Combustion Theory and Modelling*, pages 1–23, Jan. 2022a. ISSN 1364-7830, 1741-3559. doi: 10.1080/13647830.2022.2027524.

R. Ciardiello, R. S. Pathania, I. E. Helou, and E. Mastorakos. Lean blow-off investigation in a linear multi-burner combustor operated in premixed and non-premixed modes. *Applications in Energy and Combustion Science*, 9: 100041, Mar. 2022b. ISSN 2666352X. doi: 10.1016/j.jaecs.2021.100041.

M. Cordier, A. Vandel, G. Cabot, B. Renou, and A. M. Boukhalfa. Laser-induced spark ignition of premixed confined swirled flames. *Combustion Science and Technology*, 185(3):379–407, Mar. 2013. ISSN 0010-2202, 1563-521X. doi: 10.1080/00102202.2012.725791.

J. Dawson, R. Gordon, J. Kariuki, E. Mastorakos, A. Masri, and M. Juddoo. Visualization of blow-off events in bluff-body stabilized turbulent premixed flames. *Proceedings of the Combustion Institute*, 33(1):1559–1566, 2011. ISSN 15407489. doi: 10.1016/j.proci.2010.05.044.

J. R. Dawson and N. A. Worth. Flame dynamics and unsteady heat release rate of self-excited azimuthal modes in an annular combustor. *Combustion and Flame*, 161(10):2565–2578, Oct. 2014. ISSN 00102180. doi: 10.1016/j.combustflame.2014.03.021.

J. R. Dawson and N. A. Worth. The effect of baffles on self-excited azimuthal modes in an annular combustor. *Proceedings of the Combustion Institute*, 35(3):3283–3290, 2015. ISSN 15407489. doi: 10.1016/j.proci.2014.07.011.

F. Dinkelacker, B. Manickam, and S. Muppala. Modelling and simulation of lean premixed turbulent methane/hydrogen/air flames with an effective Lewis number approach. *Combustion and Flame*, 158(9):1742–1749, Sept. 2011. ISSN 00102180. doi: 10.1016/j.combustflame.2010.12.003.

J. M. Donbar, J. F. Driscoll, and C. D. Carter. Reaction zone structure in turbulent nonpremixed jet flames—from CH-OH PLIF images. *Combustion and Flame*, 122(1-2):1–19, July 2000. ISSN 00102180. doi: 10.1016/S0010-2180(00)00098-5.

J. Driscoll. Turbulent premixed combustion: Flamelet structure and its effect on turbulent burning velocities. *Progress in Energy and Combustion Science*, 34(1):91–134, Feb. 2008. ISSN 03601285. doi: 10.1016/j.pecs.2007.04.002.

D. Dunn-Rankin, M. M. Miyasato, and T. K. Pham. Chapter 1 - Introduction and perspectives. In D. Dunn-Rankin, editor, *Lean Combustion*, pages 1–18. Academic Press, Burlington, Jan. 2008. ISBN 978-0-12-370619-5. doi: 10.1016/B978-012370619-5.50002-9.

T. Echekki and J. H. Chen. Structure and propagation of methanol–air triple flames. *Combustion and Flame*, 114(1-2):231–245, July 1998. ISSN 00102180. doi: 10.1016/S0010-2180(97)00287-3.

I. El Helou, A. W. Skiba, and E. Mastorakos. Experimental investigation of soot production and oxidation in a lab-scale rich–quench–lean (rql) burner. *Flow, Turbulence and Combustion*, 106(4):1019–1041, Apr. 2021. ISSN 1386-6184, 1573-1987. doi: 10.1007/s10494-020-00113-5.

European Commission. *Flightpath 2050: europe's vision for aviation : maintaining global leadership and serving society's needs*. European Commission, 2012. doi: doi/10.2777/15458.

European Union Aviation Safety Agency. Certification memorandum turbine engine relighting in flight. Technical Report EASA CM No.: CM-PIFS-010 Issue 01, European Union Aviation Safety Agency, Apr. 2015. URL https://www.easa.europa.eu/en/downloads/18544/en.

European Union Aviation Safety Agency. Certification specifications and acceptable means of compliance for engines cs-e. Technical Report CS-E - Amendment 6, European Union Aviation Safety Agency, June 2020. URL https://www.easa.europa.eu/en/downloads/116287/en.

F. Farisco, L. Castellanos, J. Woisetschläger, and W. Sanz. Numerical steady and transient evaluation of a confined swirl stabilized burner. *International Journal of Turbomachinery, Propulsion and Power*, 6(4):46, Nov. 2021. ISSN 2504-186X. doi: 10.3390/ijtpp6040046.

Federal Aviation Adminstation. In-flight all-engines-out restart guidance. Technical Report CWI TCCA-002, U.S. Federal Aviation Adminstation, July 2020. URL https://www.faa.gov/sites/faa.gov/files/aircraft/air_cert/design_approvals/transport/TCCA-002_in-flight_all_engines_out_restart_guidance.pdf.

W. Gao, J. Yang, F. Liu, Y. Mu, C. Liu, and G. Xu. Experimental investigation on the flame propagation pattern of a staged partially premixed annular combustor. *Combustion and Flame*, 230:111445, Aug. 2021a. ISSN 00102180. doi: 10.1016/j.combustflame.2021.111445.

W. Gao, J. Yang, Y. Mu, F. Liu, S. Wang, Q. Zhao, K. Wang, C. Liu, and G. Xu. Experimental investigation on spark ignition of a staged partially premixed annular combustor. *Fuel*, 302:121062, Oct. 2021b. ISSN 00162361. doi: 10.1016/j.fuel.2021.121062.

G. K. Giannakopoulos, A. Gatzoulis, C. E. Frouzakis, M. Matalon, and A. G. Tomboulides. Consistent definitions of "Flame Displacement Speed" and "Markstein Length" for premixed flame propagation. *Combustion and Flame*, 162(4):1249–1264, Apr. 2015. ISSN 00102180. doi: 10.1016/j.combustflame.2014.10.015.

F. Giuliani, N. Paulitsch, A. Hofer, and B. Akin. Recursive sequential combustion: an innovative and high-performance combustion technology, aimed at the fuels of the future. In *17. Symposium Energieinnovation 2022*, Feb. 2022.

S. Gkantonas, M. Sirignano, A. Giusti, A. D'Anna, and E. Mastorakos. Comprehensive soot particle size distribution modelling of a model Rich-Quench-Lean burner. *Fuel*, 270:117483, June 2020. ISSN 00162361. doi: 10.1016/j.fuel.2020.117483.

I. Glassman. *Combustion*. Combustion. Elsevier Science, 1997. ISBN 978-0-08-052941-7. tex.lccn: 96003069.

D. G. Goodwin, R. L. Speth, H. K. Moffat, and B. W. Weber. Cantera: an object-oriented software toolkit for chemical kinetics, thermodynamics, and transport processes, 2018. URL https://www.cantera.org.

J. Hertzberg, I. Shepherd, and L. Talbot. Vortex shedding behind rod stabilized flames. *Combustion and Flame*, 86(1-2):1–11, July 1991. ISSN 00102180. doi: 10.1016/0010-2180(91)90051-C.

B. Higgins, M. Q. McQuay, F. Lacas, J. C. Rolon, N. Darabiha, and S. Candel. Systematic measurements of OH chemiluminescence for fuel-lean, high-pressure, premixed, laminar flames. *Fuel*, 80:67–74, 2001.

S. Hoffmann, R. Koch, and H.-J. Bauer. Numerical investigation of the low-swirl flow in an aeronautical combustor with angular air supply. In *Volume 2C: Turbomachinery — Design Methods and CFD Modeling for Turbomachinery; Ducts, Noise, and Component Interactions*, page V02CT34A019, Virtual, Online, June 2021. American Society of Mechanical Engineers. ISBN 978-0-7918-8492-8. doi: 10.1115/GT2021-59286.

S. C. Humbert, J. P. Moeck, A. Orchini, and C. O. Paschereit. Effect of an azimuthal mean flow on the structure and stability of thermoacoustic modes in an annular combustor model with electroacoustic feedback. *Journal of Engineering for Gas Turbines and Power*, 143(6):061026, June 2021. ISSN 0742-4795, 1528-8919. doi: 10.1115/1.4048693.

H. G. Im and J. H. Chen. Structure and propagation of triple flames in partially premixed hydrogen–air mixtures. *Combustion and Flame*, 119 (4):19, Dec. 1999.

International Civil Aviation Organization. Units of measurement to be used in air and ground operations. Annex, International Civil Aviation Organization, July 2010.

T. L. Jackson. Effect of thermal expansion on the stability of two-reactant flames. *Combustion Science and Technology*, 53(1):51–54, May 1987. ISSN 0010-2202, 1563-521X. doi: 10.1080/00102208708947018.

S. Jella and J. Bergthorson. Injector spacing influences on flame blow-off in a linear array. *Proceedings of the Combustion Institute*, page S1540748922004862, Nov. 2022. ISSN 15407489. doi: 10.1016/j.proci.2022.10.001.

S. Jella, W. Kwong, A. Steinberg, J.-W. Park, T. Lu, J. Bergthorson, and G. Bourque. Attached and lifted flame stabilization in a linear array of swirl injectors. *Proceedings of the Combustion Institute*, 38(4):6279–6287, 2021. ISSN 15407489. doi: 10.1016/j.proci.2020.06.009.

W. Jerzak and M. Kuźnia. Experimental study of impact of swirl number as well as oxygen and carbon dioxide content in natural gas combustion air on flame flashback and blow-off. *Journal of Natural Gas Science and Engineering*, 29:46–54, Feb. 2016. ISSN 18755100. doi: 10.1016/j.jngse.2015.12.054.

L. Ji, J. Wang, W. Zhang, R. Mao, G. Hu, and Z. Huang. Effect of confinement ratio on flame structure and blow-off characteristics of swirl flames. *Experimental Thermal and Fluid Science*, 135:110630, July 2022. ISSN 08941777. doi: 10.1016/j.expthermflusci.2022.110630.

G. Joulin and T. Mitani. Linear stability analysis of two-reactant flames. *Combustion and Flame*, 40:235–246, Jan. 1981. ISSN 00102180. doi: 10.1016/0010-2180(81)90127-9.

F. Jørgensen. How to measure turbulence with hot-wire anemometers - a practical guide. Technical report, Dantec Dynamics, 2002. URL https://www.dantecdynamics.com/wp-content/uploads/2020/08/pratical-guide-how-to-measure-turbulence.pdf.

Jürgen Warnatz, Ulrich Maas, and Robert W. Dibble. *Combustion: physical and chemical fundamentals, modeling and simulation, experiments, pollutant formation*. Springer Berlin Heidelberg, 4 edition, 2006. ISBN 978-3-540-25992-3.

J. Kariuki, D. Cavaliere, C. Letty, and E. Mastorakos. A comparison of the blow-off behaviour of swirl-stabilized premixed and spray flames. In *50th AIAA Aerospace Sciences Meeting including the New Horizons Forum and Aerospace Exposition*, Nashville, Tennessee, Jan. 2012a. American Institute of Aeronautics and Astronautics. ISBN 978-1-60086-936-5. doi: 10.2514/6.2012-505.

J. Kariuki, J. R. Dawson, and E. Mastorakos. Measurements in turbulent premixed bluff body flames close to blow-off. *Combustion and Flame*, 159 (8):2589–2607, Aug. 2012b. ISSN 00102180. doi: 10.1016/j.combustflame.2012.01.005.

J. Kariuki, N. Worth, J. Dawson, and E. Mastorakos. Visualisation of blow-off events of two interacting turbulent premixed flames. In *51st AIAA Aerospace Sciences Meeting including the New Horizons Forum and Aerospace Exposition*, Grapevine (Dallas/Ft. Worth Region), Texas, Jan. 2013. American Institute of Aeronautics and Astronautics. ISBN 978-1-62410-181-6. doi: 10.2514/6.2013-692.

V. P. Karpov and E. S. Severin. Effects of molecular-transport coefficients on the rate of turbulent combustion. *Combustion, Explosion, and Shock Waves*, 16(1):41–46, 1980. ISSN 0010-5082, 1573-8345. doi: 10.1007/BF00756242.

N. Klarmann, T. Sattelmayer, W. Geng, and F. Magni. Flamelet generated manifolds for partially premixed, highly stretched and non-adiabatic combustion in gas turbines. In *54th AIAA Aerospace Sciences Meeting*, San Diego, California, USA, Jan. 2016. American Institute of Aeronautics and Astronautics. ISBN 978-1-62410-393-3. doi: 10.2514/6.2016-2120.

H. Klinger, S. Bake, H.-F. Vogt, D. Knieschke, and P. Schober. Altitude testing of the E3E core engine. In *Volume 1: Aircraft Engine; Ceramics; Coal, Biomass and Alternative Fuels; Wind Turbine Technology*, pages 223–232, Vancouver, British Columbia, Canada, Jan. 2011. ASMEDC. ISBN 978-0-7918-5461-7. doi: 10.1115/GT2011-45876.

E. Korusoy and J. H. Whitelaw. Effects of wall temperature and fuel on flammability, stability, and control of ducted premixed flames. *Combustion Science and Technology*, 176(8):1217–1241, Aug. 2004. ISSN 0010-2202, 1563-521X. doi: 10.1080/00102200490457411.

R. M. Kumar, I. Chterev, D. Stepien, M. Sirignano, B. L. Emerson, C. A. Fugger, N. Jiang, S. Roy, and T. C. Lieuwen. Near blowout dynamics of a premixed, swirl stabilized flame. *Proceedings of the Combustion Institute*, page S1540748920302273, Aug. 2020. ISSN 15407489. doi: 10.1016/j.proci.2020.06.147.

W. Y. Kwong and A. M. Steinberg. Blowoff and reattachment dynamics of a linear multinozzle combustor. *Journal of Engineering for Gas Turbines and Power*, 141(1):011015, Jan. 2019a. ISSN 0742-4795, 1528-8919. doi: 10.1115/1.4041070.

W. Y. P. Kwong and A. M. Steinberg. Effect of inter-nozzle spacing on lean blowoff performance of a linear multi-nozzle combustor. In *AIAA Scitech 2019 Forum*, San Diego, California, Jan. 2019b. American Institute of Aeronautics and Astronautics. ISBN 978-1-62410-578-4. doi: 10.2514/6.2019-2244.

T. Lancien, K. Prieur, D. Durox, S. Candel, and R. Vicquelin. Large Eddy Simulation of light-round in an annular combustor with liquid spray injection and comparison with experiments. *Journal of Engineering for Gas Turbines and Power*, 140(2):021504, Feb. 2018. ISSN 0742-4795, 1528-8919. doi: 10.1115/1.4037827.

T. Lancien, K. Prieur, D. Durox, S. Candel, and R. Vicquelin. Leading point behavior during the ignition of an annular combustor with liquid n-heptane injectors. *Proceedings of the Combustion Institute*, 37(4):5021–5029, 2019. ISSN 15407489. doi: 10.1016/j.proci.2018.05.160.

C. Law, G. Jomaas, and J. Bechtold. Cellular instabilities of expanding hydrogen/propane spherical flames at elevated pressures: theory and experiment. *Proceedings of the Combustion Institute*, 30(1):159–167, Jan. 2005. ISSN 15407489. doi: 10.1016/j.proci.2004.08.266.

C. K. Law. *Combustion physics*. Cambridge University Press, Cambridge, 2006. ISBN 978-0-521-15421-5. doi: 10.1017/CBO9780511754517.

A. Lefebvre and D. Ballal. *Gas turbine combustion: alternative fuels and emissions, third edition*. Taylor & Francis, 2010. ISBN 978-1-4200-8604-1. tex.lccn: 2010005450.

T. C. Lieuwen. *Unsteady combustor physics*. Cambridge University Press, Cambridge, 2012. ISBN 978-1-139-05996-1. doi: 10.1017/CBO9781139059961.

T. C. Lieuwen and V. Yang, editors. *Gas turbine emissions*. Cambridge Aerospace Series. Cambridge University Press, Cambridge, 2013. ISBN 978-0-521-76405-6. doi: 10.1017/CBO9781139015462.

D. G. Lilley. Swirl flows in combustion: a review. *AIAA Journal*, 15(8): 1063–1078, Aug. 1977. ISSN 0001-1452, 1533-385X. doi: 10.2514/3.60756.

A. Lipatnikov and J. Chomiak. Molecular transport effects on turbulent flame propagation and structure. *Progress in Energy and Combustion Science*, 31(1):1–73, Jan. 2005. ISSN 03601285. doi: 10.1016/j.pecs.2004.07.001.

A. N. Lipatnikov and J. Chomiak. Turbulent flame speed and thickness: phenomenology, evaluation, and application in multi-dimensional simulations. *Progress in Energy and Combustion Science*, page 74, 2002.

A. E. Long, H. Burbano, R. L. Speth, A. Movaghar, F. N. Egolfopoulos, and W. H. Green. An apparatus-independent extinction strain rate in counterflow flames. *Proceedings of the Combustion Institute*, 37(2):1979–1987, 2019. ISSN 15407489. doi: 10.1016/j.proci.2018.06.130.

J. Longwell. Flame stabilization by bluff bodies and turbulent flames in ducts. *Symposium (International) on Combustion*, 4(1):90–97, Jan. 1953. ISSN 00820784. doi: 10.1016/S0082-0784(53)80012-3.

J. P. Longwell, E. E. Frost, and M. A. Weiss. Flame stability in bluff body recirculation zones. *Industrial & Engineering Chemistry*, 45(8):1629–1633, Aug. 1953. ISSN 0019-7866, 1541-5724. doi: 10.1021/ie50524a019.

E. Machover and E. Mastorakos. Spark ignition of annular non-premixed combustors. *Experimental Thermal and Fluid Science*, 73:64–70, May 2016. ISSN 08941777. doi: 10.1016/j.expthermflusci.2015.09.008.

E. Machover and E. Mastorakos. Experimental investigation on spark ignition of annular premixed combustors. *Combustion and Flame*, 178: 148–157, Apr. 2017a. ISSN 00102180. doi: 10.1016/j.combustflame.2017.01.013.

E. Machover and E. Mastorakos. Numerical Investigation of the Stochastic Behavior of Light-Round in Annular Non-Premixed Combustors. *Combustion Science and Technology*, 189(9):1467–1485, Sept. 2017b. ISSN 0010-2202, 1563-521X. doi: 10.1080/00102202.2017.1305366.

M. S. Mansour. Stability characteristics of lifted turbulent partially premixed jet flames. *Combustion and Flame*, 133(3):263–274, May 2003. ISSN 00102180. doi: 10.1016/S0010-2180(02)00566-7.

E. Mastorakos. Ignition of turbulent non-premixed flames. *Progress in Energy and Combustion Science*, 35(1):57–97, 2009.

E. Mastorakos. Forced ignition of turbulent spray flames. *Proceedings of the Combustion Institute*, 36(2):2367–2383, 2017. ISSN 15407489. doi: 10.1016/j.proci.2016.08.044.

A. Mellor. Semi-empirical correlations for gas turbine emissions, ignition, and flame stabilization. *Progress in Energy and Combustion Science*, 6(4): 347–358, Jan. 1980. ISSN 03601285. doi: 10.1016/0360-1285(80)90010-6.

A. Mellor. *Design of modern turbine combustors*. Academic Press, 1990. ISBN 0-12-490055-0.

A. J. Morales, I. M. Lasky, M. K. Geikie, C. A. Engelmann, and K. A. Ahmed. Mechanisms of flame extinction and lean blowout of bluff body stabilized flames. *Combustion and Flame*, 203:31–45, May 2019. ISSN 00102180. doi: 10.1016/j.combustflame.2019.02.002.

S. Muppala, M. Nakahara, N. Aluri, H. Kido, J. Wen, and M. Papalexandris. Experimental and analytical investigation of the turbulent burning velocity of two-component fuel mixtures of hydrogen, methane and propane. *International Journal of Hydrogen Energy*, 34(22):9258–9265, Nov. 2009. ISSN 03603199. doi: 10.1016/j.ijhydene.2009.09.036.

T. Muruganandam and J. Seitzman. Origin of lean blow out precursors in swirled gas turbine combustors. In *43rd AIAA Aerospace Sciences Meeting and Exhibit*, Reno, Nevada, Jan. 2005. American Institute of Aeronautics and Astronautics. ISBN 978-1-62410-064-2. doi: 10.2514/6.2005-1163.

S. Nair and T. Lieuwen. Acoustic detection of blowout in premixed flames. *Journal of Propulsion and Power*, 21(1):32–39, Jan. 2005. ISSN 0748-4658, 1533-3876. doi: 10.2514/1.5658.

S. Nair and T. Lieuwen. Near-Blowoff Dynamics of a Bluff-Body Stabilized Flame. *Journal of Propulsion and Power*, 23(2):421–427, Mar. 2007. ISSN 0748-4658, 1533-3876. doi: 10.2514/1.24650.

P. C. Nassini, D. Pampaloni, R. Meloni, and A. Andreini. Lean blow-out prediction in an industrial gas turbine combustor through a LES-based CFD analysis. *Combustion and Flame*, 229:111391, July 2021. ISSN 00102180. doi: 10.1016/j.combustflame.2021.02.037.

A. Neophytou, E. Richardson, and E. Mastorakos. Spark ignition of turbulent recirculating non-premixed gas and spray flames: A model for predicting ignition probability. *Combustion and Flame*, 159(4):1503–1522, Apr. 2012. ISSN 00102180. doi: 10.1016/j.combustflame.2011.12.015.

N. Noiray, M. Bothien, and B. Schuermans. Investigation of azimuthal staging concepts in annular gas turbines. *Combustion Theory and Modelling*, 15(5):585–606, Oct. 2011. ISSN 1364-7830, 1741-3559. doi: 10.1080/13647830.2011.552636.

H. T. Nygård. *Experimental measurement of flame describing functions in an azimuthally forced annular combustor*. PhD thesis, Norwegian University of Science and Technology, June 2021. URL https://hdl.handle.net/11250/2755792.

H. T. Nygård, M. Mazur, J. R. Dawson, and N. A. Worth. Flame dynamics of azimuthal forced spinning and standing modes in an annular combustor. *Proceedings of the Combustion Institute*, 37(4):5113–5120, 2019. ISSN 15407489. doi: 10.1016/j.proci.2018.08.034.

H. T. Nygård, G. Ghirardo, and N. A. Worth. Azimuthal flame response and symmetry breaking in a forced annular combustor. *Combustion and Flame*, 233:111565, Nov. 2021. ISSN 00102180. doi: 10.1016/j.combustflame.2021.111565.

P. Palies, D. Durox, T. Schuller, P. Morenton, and S. Candel. Dynamics of premixed confined swirling flames. *Comptes Rendus Mécanique*, 337(6-7): 395–405, June 2009. ISSN 16310721. doi: 10.1016/j.crme.2009.06.001.

S. S. Penner and F. Williams. Recent studies on flame stabilization of premixed turbulent gases. *Applied Mechanics Reviews*, page 9, June 1957.

M. Philip. *Dynamique de l'allumage circulaire dans les foyers annulaires multi-injecteurs*. PhD thesis, EM2C, Ecole Centrale Paris, 2016. URL https://tel.archives-ouvertes.fr/tel-01349362.

M. Philip, M. Boileau, R. Vicquelin, T. Schmitt, D. Durox, J.-F. Bourgouin, and S. Candel. Ignition sequence of an annular multi-injector combustor. *Physics of Fluids*, 26(9):091106, Sept. 2014a. ISSN 1070-6631, 1089-7666. doi: 10.1063/1.4893452.

M. Philip, M. Boileau, R. Vicquelin, T. Schmitt, D. Durox, J.-F. Bourgouin, and S. Candel. Simulation of the ignition process in an annular multiple-injector combustor and comparison with experiments. *Journal of Engineering for Gas Turbines and Power*, 137(3):031501, Sept. 2014b. ISSN 0742-4795. doi: 10.1115/1.4028265.

M. Philip, M. Boileau, R. Vicquelin, E. Riber, T. Schmitt, B. Cuenot, D. Durox, and S. Candel. Large Eddy Simulations of the ignition sequence of an annular multiple-injector combustor. *Proceedings of the Combustion Institute*, 35(3):3159–3166, 2015. ISSN 15407489. doi: 10.1016/j.proci.2014.07.008.

T. Poinsot and D. P. Veynante. *Theoretical and numerical combustion*. R.T. Edwards, third edition, 2001.

K. Prieur, D. Durox, J. Beaunier, T. Schuller, and S. Candel. Ignition dynamics in an annular combustor for liquid spray and premixed gaseous injection. *Proceedings of the Combustion Institute*, 36(3):3717–3724, 2017. ISSN 15407489. doi: 10.1016/j.proci.2016.08.008.

K. Prieur, D. Durox, G. Vignat, T. Schuller, and S. Candel. Flame and spray dynamics during the light-round process in an annular system equipped with multiple swirl spray injectors. *ASME Turbo Expo 2018: Turbomachinery Technical Conference and Exposition*, page 13, 2018.

S. Puggelli, T. Lancien, K. Prieur, D. Durox, S. Candel, and R. Vicquelin. Impact of wall temperature in large eddy simulation of light-round in an annular liquid fueled combustor and assessment of wall models. *Journal*

of Engineering for Gas Turbines and Power, 142(1):011018, Jan. 2020. ISSN 0742-4795, 1528-8919. doi: 10.1115/1.4045341.

S. Puggelli, D. Veynante, and R. Vicquelin. Impact of dynamic modelling of the flame subgrid scale wrinkling in large-Eddy simulation of light-round in an annular combustor. *Combustion and Flame*, 230:111416, Aug. 2021. ISSN 00102180. doi: 10.1016/j.combustflame.2021.111416.

K. Radhakrishnan, J. B. Heywood, and R. J. Tabaczynski. Premixed turbulent flame blowoff velocity correlation based on coherent structures in turbulent flows. *Combustion and Flame*, 42:19–33, Jan. 1981. ISSN 00102180. doi: 10.1016/0010-2180(81)90139-5.

M. Raffel, C. Willert, S. Wereley, and J. Kompenhans. *Particle image velocimetry: a practical guide*. Springer, third edition, Jan. 2007. ISBN 978-3-540-72307-3. doi: 10.1007/978-3-540-72308-0.

M. Rieth, A. Gruber, F. A. Williams, and J. H. Chen. Enhanced burning rates in hydrogen-enriched turbulent premixed flames by diffusion of molecular and atomic hydrogen. *A dedication to Professor Kenneth Noel Corbett Bray*, 239:111740, May 2022. ISSN 0010-2180. doi: 10.1016/j.combustflame.2021.111740.

G. R. Ruetsch and J. E. Broadwell. Effects of confinement on partially premixed flames. Annual Research Briefs, Centre for Turbulence Research, Stanford University, 1995. URL https://ntrs.nasa.gov/api/citations/19960022319/downloads/19960022319.pdf.

G. R. Ruetsch, L. Vervisch, and A. Liñán. Effects of heat release on triple flames. *Physics of Fluids*, 7(6):1447–1454, June 1995. ISSN 1070-6631, 1089-7666. doi: 10.1063/1.868531.

M. Russi, I. Cornet, and R. Cornog. The influence of flame holder temperature on flame stabilization. *Symposium (International) on Combustion*, 4(1):743–748, Jan. 1953. ISSN 00820784. doi: 10.1016/S0082-0784(53)80097-4.

Safran Helicopter Engines. The revolution of helicopters engines, July 2016a. URL https://www.youtube.com/watch?v=cuCisE1gDnQ.

Safran Helicopter Engines. Turbomeca triumphant at Safran Innovation Awards 2016, Apr. 2016b. URL https://www.safran-group.com/news/turbomeca-triumphant-safran-innovation-awards-2016-2016-04-27.

Safran Helicopter Engines. Datasheet Arrano 1A, Jan. 2019. URL https://www.ila-berlin.de/sites/default/files/2020-07/Datasheet_Arrano_1A.pdf.

N. Savary and G. Taliercio. The SAFRAN helicopter engine spinning flame combustor concept to meet customer needs. In *42nd European Rotorcraft Forum 2016*, volume 2, page 1447, Lille, France, 2016. Association Aeronautique et Astronautique de France.

M. Shamma, S. Hoffmann, S. R. Harth, N. Zarzalis, D. Trimis, R. Koch, H.-J. Bauer, L. Langone, S. Galeotti, and A. Andreini. Investigation of adjacent lifted flames interaction in an inline and inclined multi-burner arrangement. In *Volume 3B: Combustion, Fuels, and Emissions*, page V03BT04A020, Virtual, Online, June 2021. American Society of Mechanical Engineers. ISBN 978-0-7918-8495-9. doi: 10.1115/GT2021-59941.

S. J. Shanbhogue, S. Husain, and T. Lieuwen. Lean blowoff of bluff body stabilized flames: Scaling and dynamics. *Progress in Energy and Combustion Science*, 35(1):98–120, Feb. 2009. ISSN 03601285. doi: 10.1016/j.pecs.2008.07.003.

C. Soares. Chapter 4 - Gas turbine major components and modules. In C. Soares, editor, *Gas Turbines (Second Edition)*, pages 173–254. Butterworth-Heinemann, Oxford, Jan. 2015. ISBN 978-0-12-410461-7. doi: 10.1016/B978-0-12-410461-7.00004-3.

C. C. Swett. Spark ignition of flowing gases using long-duration discharges. *Symposium (International) on Combustion*, 6(1):523–532, Jan. 1957. ISSN 00820784. doi: 10.1016/S0082-0784(57)80069-1.

N. Syred, A. Giles, J. Lewis, M. Abdulsada, A. Valera Medina, R. Marsh, P. Bowen, and A. Griffiths. Effect of inlet and outlet configurations on blow-off and flashback with premixed combustion for methane and a high hydrogen content fuel in a generic swirl burner. *Applied Energy*, 116:288–296, Mar. 2014. ISSN 03062619. doi: 10.1016/j.apenergy.2013.11.071.

Y. Tong, M. Li, M. Thern, and J. Klingmann. An Experimental Study of Effects of Confinement Ratio on Swirl Stabilized Flame Macrostructures. In *Volume 1: Boilers and Heat Recovery Steam Generator; Combustion Turbines; Energy Water Sustainability; Fuels, Combustion and Material Handling; Heat Exchangers, Condensers, Cooling Systems, and Balance-of-Plant*, page V001T04A007, Charlotte, North Carolina, USA, June 2017. American Society of Mechanical Engineers. ISBN 978-0-7918-5760-1. doi: 10.1115/POWER-ICOPE2017-3064.

M. Toqan, A. Dhabi, A. Gregory, J. D. Regele, F. Hills, and R. S. Yamane. Tangential and flameless annular combustor for use on gasturbine engines. July 2015. Patent No US 9,091.446 B1.

T. E. Tracey, J. A. Sidey, and E. Mastorakos. A lab-scale Rich-Quench-Lean (RQL) combustor for stability and soot investigations. In *2018 AIAA Aerospace Sciences Meeting*, Kissimmee, Florida, Jan. 2018. American Institute of Aeronautics and Astronautics. ISBN 978-1-62410-524-1. doi: 10.2514/6.2018-1880.

K. Töpperwien and R. Vicquelin. Numerical analysis of relight in an annular spray-flame combustor with preheated walls. *Proceedings of the Combustion Institute*, page S1540748922002589, Sept. 2022. ISSN 15407489. doi: 10.1016/j.proci.2022.07.234.

K. Töpperwien, S. Puggelli, and R. Vicquelin. Analysis of flame propagation mechanisms during light-round in an annular spray flame combustor: the impact of wall heat transfer and two-phase flow. *Combustion and Flame*, 241:112105, July 2022. ISSN 00102180. doi: 10.1016/j.combustflame.2022.112105.

A. Valera-Medina, H. Xiao, M. Owen-Jones, W. I. F. David, and P. J. Bowen. Ammonia for power. *Progress in Energy and Combustion Science*, 69:63–102, Nov. 2018. ISSN 0360-1285. doi: 10.1016/j.pecs.2018.07.001.

G. Vignat, D. Durox, T. Schuller, and S. Candel. Combustion dynamics of annular systems. *Combustion Science and Technology*, 192(7):1358–1388, July 2020. ISSN 0010-2202, 1563-521X. doi: 10.1080/00102202.2020.1734583.

T. M. Vu, J. Park, O. B. Kwon, and J. S. Kim. Effects of hydrocarbon addition on cellular instabilities in expanding syngas–air spherical premixed flames. *International Journal of Hydrogen Energy*, 34(16):6961–6969, Aug. 2009. ISSN 03603199. doi: 10.1016/j.ijhydene.2009.06.067.

T. M. Vu, J. Park, J. S. Kim, O. B. Kwon, J. H. Yun, and S. I. Keel. Experimental study on cellular instabilities in hydrocarbon/hydrogen/carbon monoxide–air premixed flames. *International Journal of Hydrogen Energy*, 36(11):6914–6924, June 2011. ISSN 03603199. doi: 10.1016/j.ijhydene.2011.02.085.

G. Wang, L. Zhong, Y. Yang, Y. Zheng, Y. Fang, Y. Xia, and C. Ye. Experimental investigation of the ignition dynamics in an annular premixed

combustor with oblique-injecting swirling burners. *Fuel*, 287:119494, Mar. 2021. ISSN 00162361. doi: 10.1016/j.fuel.2020.119494.

H. Wang, L. Zhong, E. Barakat, Y. Xia, W. Tao, X. Tong, and G. Wang. Experimental investigation on the ignition dynamics of an annular combustor with multiple centrally staged swirling burners. *Physics of Fluids*, 34(7):075103, July 2022. ISSN 1070-6631, 1089-7666. doi: 10.1063/5.0095756.

S. Wiseman, M. Rieth, A. Gruber, J. R. Dawson, and J. H. Chen. A comparison of the blow-out behavior of turbulent premixed ammonia/hydrogen/nitrogen-air and methane–air flames. *Proceedings of the Combustion Institute*, page S1540748920301887, Dec. 2020. ISSN 15407489. doi: 10.1016/j.proci.2020.07.011.

N. A. Worth and J. R. Dawson. Modal dynamics of self-excited azimuthal instabilities in an annular combustion chamber. *Combustion and Flame*, 160(11):2476–2489, Nov. 2013a. ISSN 00102180. doi: 10.1016/j.combustflame.2013.04.031.

N. A. Worth and J. R. Dawson. Self-excited circumferential instabilities in a model annular gas turbine combustor: global flame dynamics. *Proceedings of the Combustion Institute*, 34(2):3127–3134, Jan. 2013b. ISSN 15407489. doi: 10.1016/j.proci.2012.05.061.

Y. Xia, C. Linghu, Y. Zheng, C. Ye, C. Ma, H. Ge, and G. Wang. Experimental investigation of the flame front propagation characteristic during light-round ignition in an annular combustor. *Flow, Turbulence and Combustion*, 103(1):247–269, June 2019. ISSN 1386-6184, 1573-1987. doi: 10.1007/s10494-019-00018-y.

S. Yamaguchi, N. Ohiwa, and T. Hasegawa. Structure and blow-off mechanism of rod-stabilized premixed flame. *Combustion and Flame*, 62(1): 31–41, Oct. 1985. ISSN 00102180. doi: 10.1016/0010-2180(85)90091-4.

C. Ye, G. Wang, Y. Fang, C. Ma, L. Zhong, and S. Moreau. Ignition dynamics in an annular combustor with gyratory flow motion. In *Volume 4B: Combustion, Fuels, and Emissions*, page V04BT04A030, Oslo, Norway, June 2018. American Society of Mechanical Engineers. ISBN 978-0-7918-5106-7. doi: 10.1115/GT2018-76624.

M. Zhang, X. Wei, J. Wang, Z. Huang, and H. Tan. The blow-off and transient characteristics of co-firing ammonia/methane fuels in a swirl

combustor. *Proceedings of the Combustion Institute*, 38(4):5181–5190, 2021. ISSN 15407489. doi: 10.1016/j.proci.2020.08.056.

Q. Zhang, S. J. Shanbhogue, Shreekrishna, T. Lieuwen, and J. O'Connor. Strain characteristics near the flame attachment point in a swirling flow. *Combustion Science and Technology*, 183(7):665–685, Apr. 2011. ISSN 0010-2202, 1563-521X. doi: 10.1080/00102202.2010.537288.

D. Zhao, Y. Xia, H. Ge, Q. Lin, and G. Wang. Large eddy simulation of flame propagation during the ignition process in an annular multiple-injector combustor. *Fuel*, 263:116402, Mar. 2020. ISSN 00162361. doi: 10.1016/j.fuel.2019.116402.

L. Zhong, Y. Yang, T. Jin, Y. Xia, Y. Fang, Y. Zheng, and G. Wang. Local flame and flow properties of propagating premixed turbulent flames during light-round process in a MICCA-type annular combustor. *Combustion and Flame*, 231:111494, Sept. 2021. ISSN 00102180. doi: 10.1016/j.combustflame.2021.111494.

V. L. Zimont. Theory of turbulent combustion of a homogeneous fuel mixture at high reynolds numbers. *Combustion, Explosion, and Shock Waves*, 15(3):305–311, 1979. ISSN 0010-5082, 1573-8345. doi: 10.1007/BF00785062.

E. Zukoski and F. Marble. Experiments concerning the mechanism of flame blowoff from bluff bodies. Technical Report 82A, California Institute of Technology, Guggenheim Jet Propulsion Center, 1956. URL https://resolver.caltech.edu/CaltechAUTHORS:20110203-125953778.

Article I

Numerical and experimental flame stabilization analysis in the new spinning combustion technology framework

Pasquale Walter Agostinelli, Yi Hao Kwah, Stephane Richard, Gorka Exilard, James R. Dawson, Laurent Gicquel, Thierry Poinsot

Published in: Proceedings of ASME Turbo Expo 2020: Turbomachinery Conference and Exposition, Volume 4A: Combustion, Fuels, and Emissions, Page V04At04A058

Article II

Effect of strong azimuthal swirl on ignition and light-around in an annular combustor

Yi Hao Kwah, Pasquale Walter Agostinelli, Stephane Richard, Gorka Exilard, Stephane Pascaud, Laurent Gicquel, James R. Dawson

Published in: Journal of Engineering for Gas Turbines and Power, Volume 144, Issue 11, Pages 11010

Article III

The effect of methane-ammonia and methane-hydrogen blends on ignition and light-around in an annular combustor

Yi Hao Kwah, Samuel Wiseman, James R. Dawson

Accepted to: Turbomachinery Technical Conference and Exposition 2023
Recommended for publication in: Journal of Engineering for Gas Turbines and Power

This paper is awaiting publication and is not included

Article IV

The impact of azimuthal swirl on the lean blow-out dynamics in an annular combustor

Pasquale Walter Agostinelli, Yi Hao Kwah, Stephane Richard, Gorka Exilard, James R. Dawson, Laurent Gicquel

Submitted to: Combustion and Flame

This paper is awaiting publication and is not included

A

Technical drawings

Table A.1: List of technical drawings in the appendix.

Drawings for SAFRAN SCT V1

Combustor: SAFRAN SCT V1
Item part: components of back plate
Material: stainless steel
Description: visualisation of plate assembly

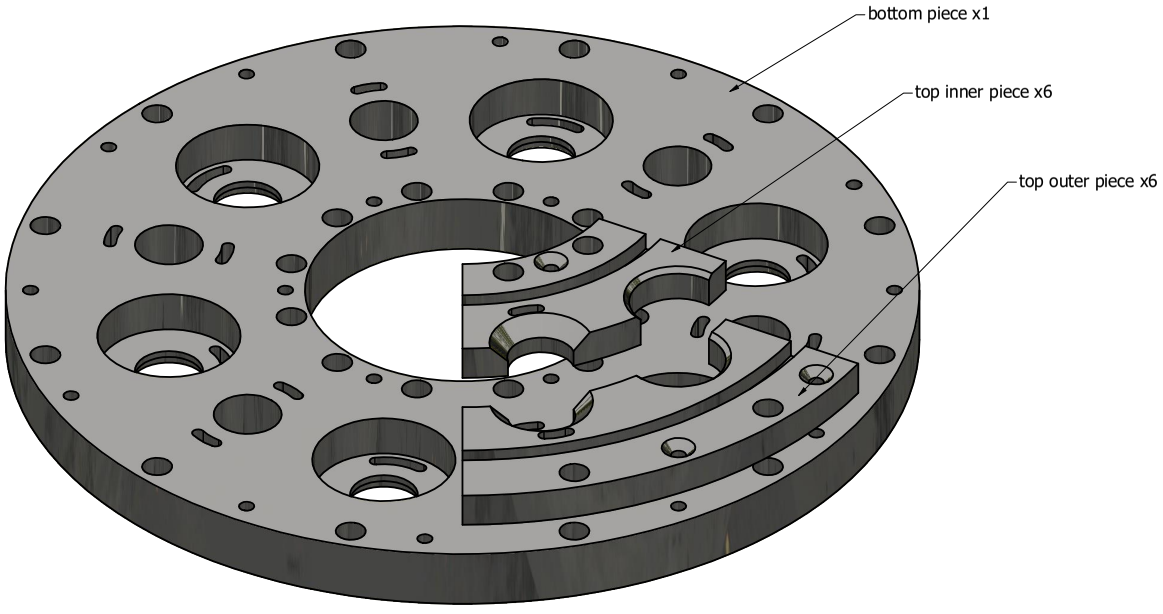

Designed by	Checked by	Approved by	Date		Date	
YI HAO						

	Edition	Sheet

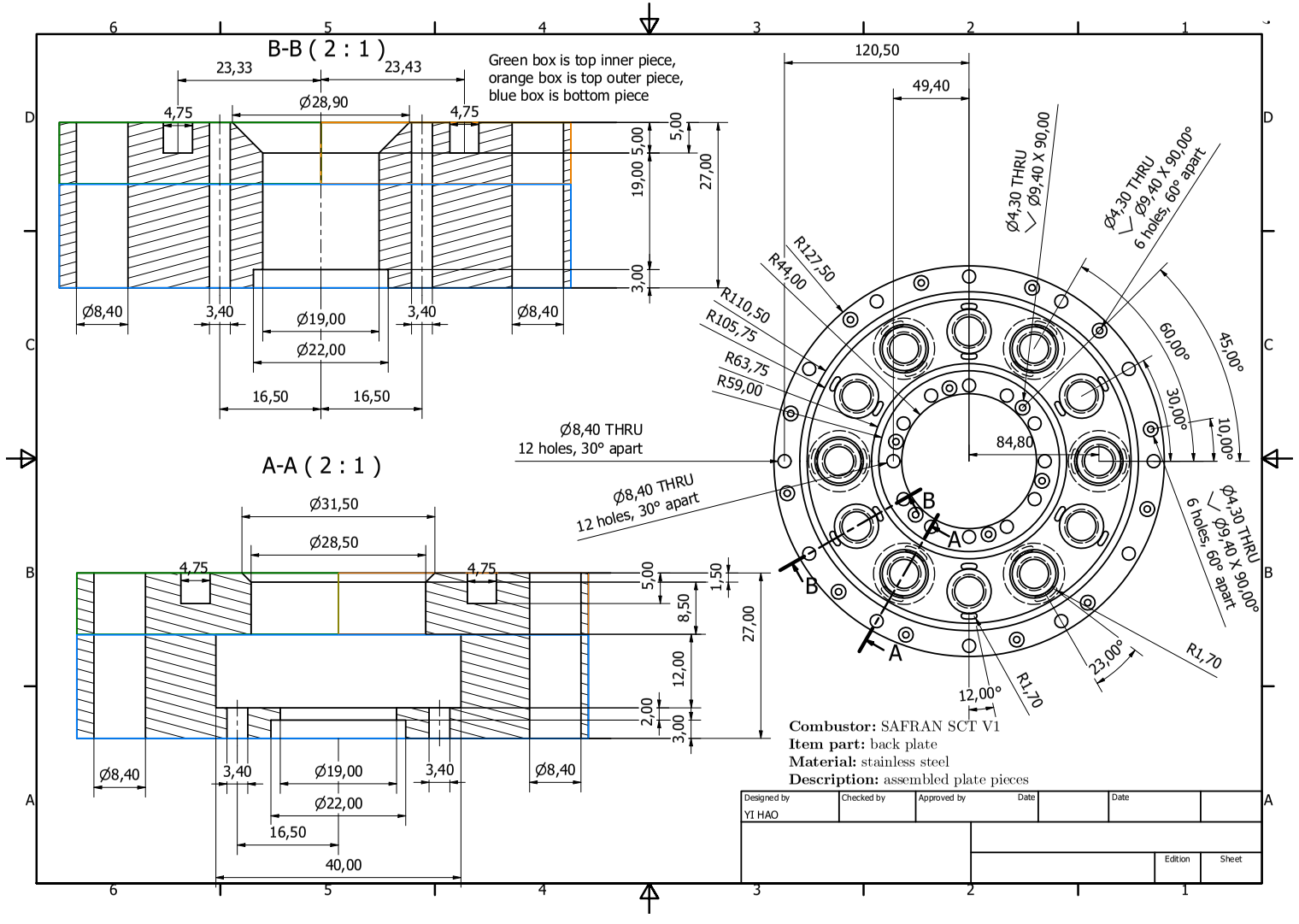
B-B (2 : 1)
Green box is top inner piece,
orange box is top outer piece,
blue box is bottom piece
23,33
23,43
Ø28,90
4,75
4,75
5,00
19,00
5,00
27,00
3,00
Ø8,40
3,40
Ø19,00
3,40
Ø8,40
Ø22,00
16,50
16,50
A-A (2 : 1)
Ø31,50
Ø28,50
4,75
4,75
5,00
1,50
8,50
27,00
12,00
2,00
3,00
Ø8,40
3,40
Ø19,00
3,40
Ø8,40
Ø22,00
16,50
40,00
120,50
49,40
Ø4,30 THRU
⌵ Ø9,40 X 90,00
Ø4,30 THRU
⌵ Ø9,40 X 90,00°
6 holes, 60° apart
R127,50
R44,00
R110,50
R105,75
R63,75
R59,00
60,00°
45,00°
30,00°
10,00°
84,80
Ø8,40 THRU
12 holes, 30° apart
Ø8,40 THRU
12 holes, 30° apart
Ø4,30 THRU
⌵ Ø9,40 X 90,00°
6 holes, 60° apart
B
A
B
A
23,00°
R1,70
R1,70
12,00°
Combustor: SAFRAN SCT V1
Item part: back plate
Material: stainless steel
Description: assembled plate pieces
Designed by
YI HAO
Checked by
Approved by
Date
Date
Edition
Sheet

Combustor: SAFRAN SCT V1
Item part: bottom piece of back plate
Material: stainless steel

B-B (2 : 1)

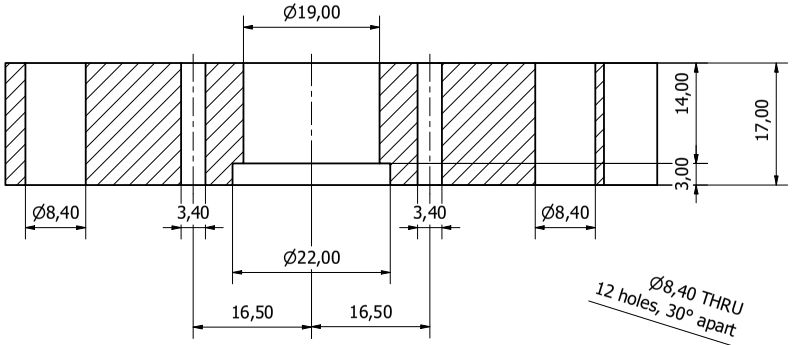

A-A (2 : 1)

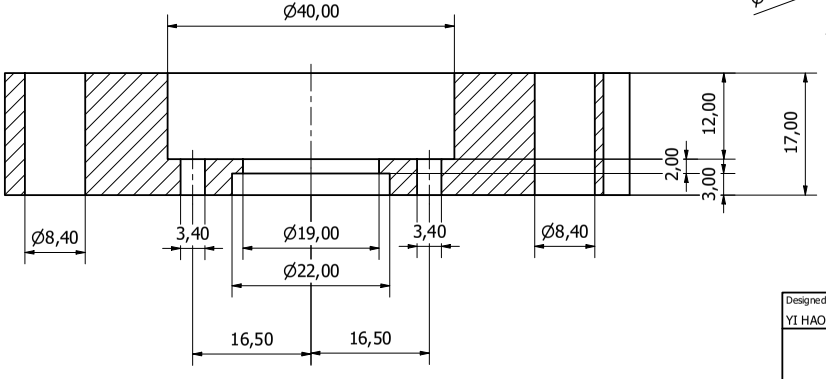

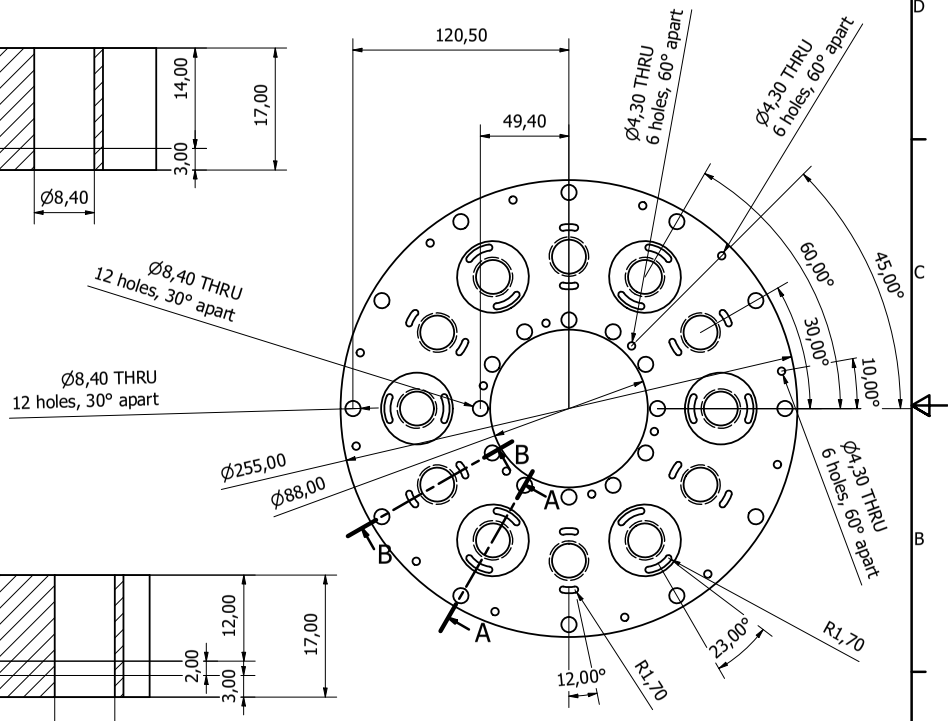

Designed by	Checked by	Approved by	Date		Date	
YI HAO						
					Edition	Sheet

Combustor: SAFRAN SCT V1
Item part: top inner piece of back plate
Material: stainless steel

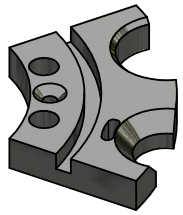

B-B (4 : 1)

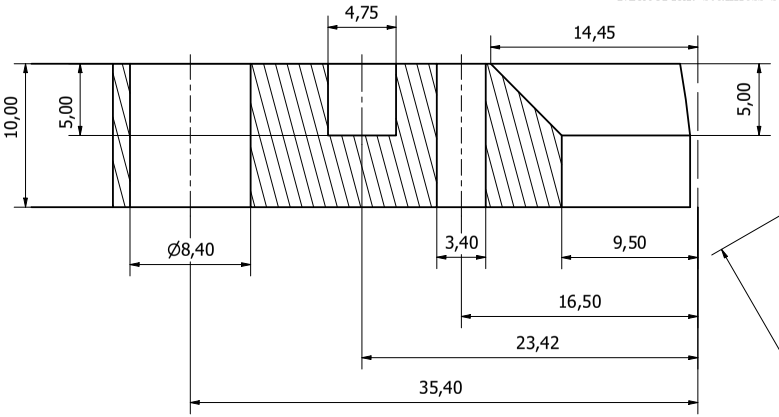

A-A (4 : 1)

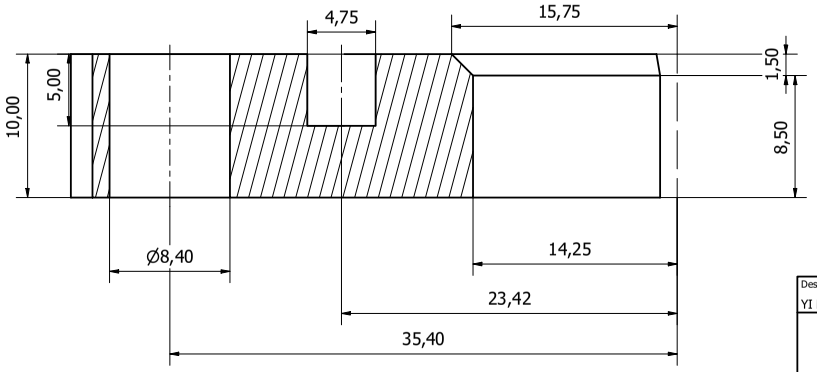

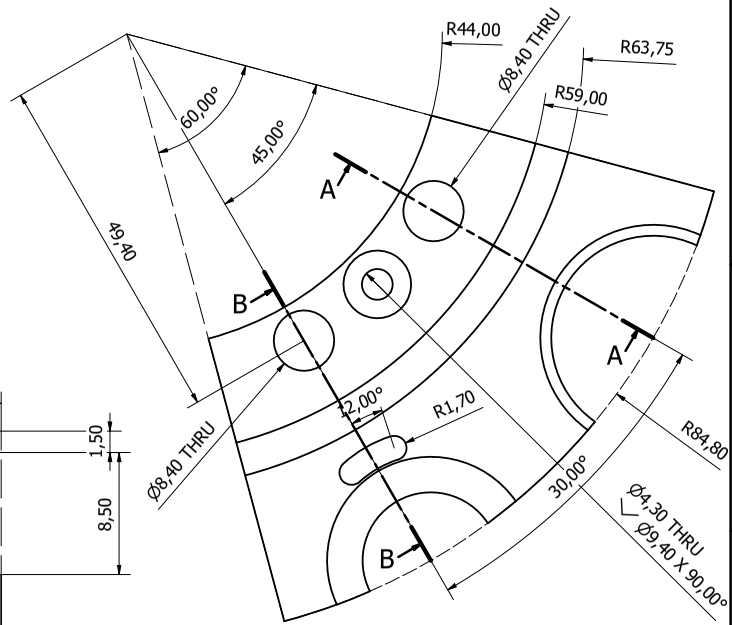

Designed by	Checked by	Approved by	Date		Date	
YI HAO						
					Edition	Sheet

Combustor: SAFRAN SCT V1
Item part: top outer piece of back plate
Material: stainless steel

B-B (4 : 1)

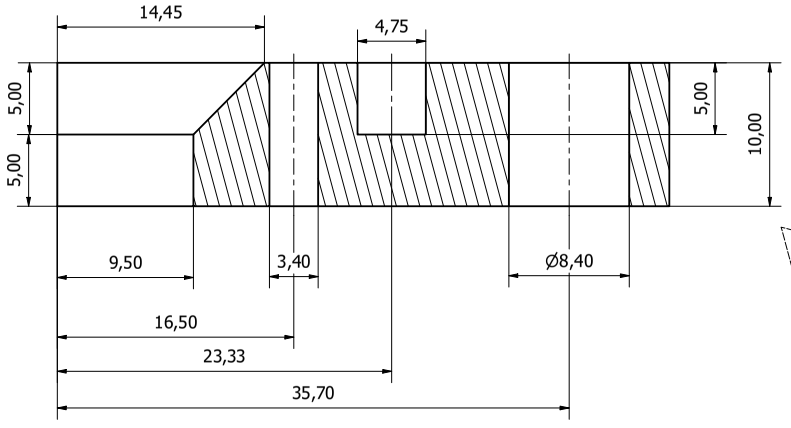

A-A (4 : 1)

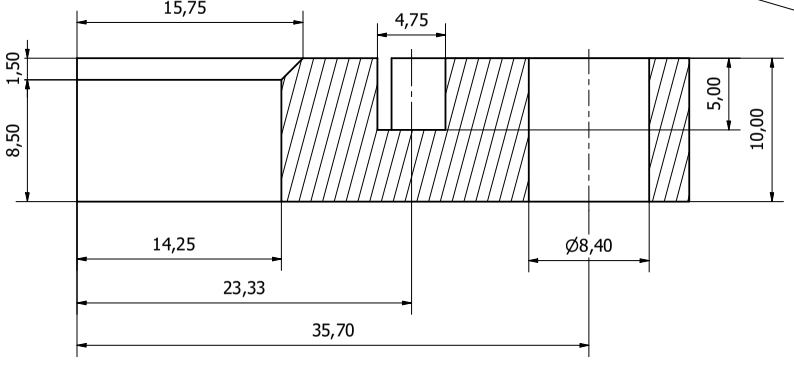

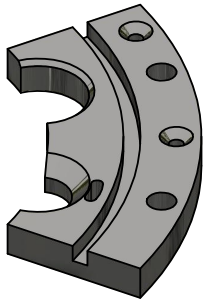

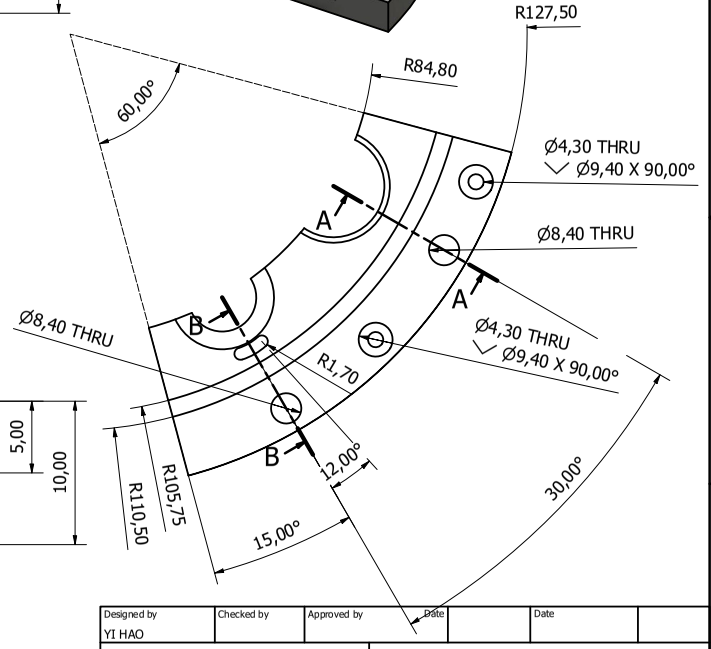

Designed by	Checked by	Approved by	Date		Date	
YI HAO						

	Edition	Sheet

Combustor: SAFRAN SCT V1
Item part: components of fuel and air injection system
Material: stainless steel and maraging steel
Description: assembled bend injector and cooling duct

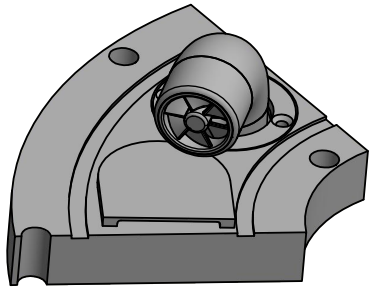

A-A (1 : 1)
fuel jet

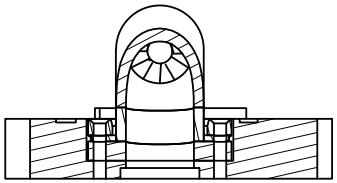

B-B (1 : 1)
cooling jet

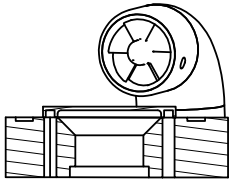

F (2 : 1)

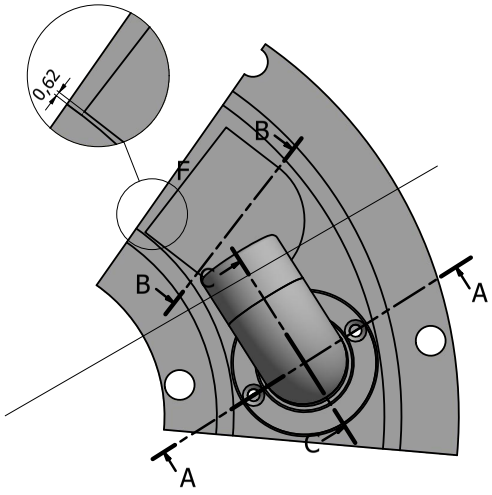

C-C (1 : 1)

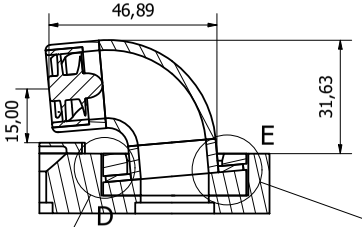

E (2 : 1)

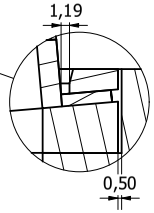

D (2 : 1)

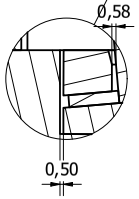

Designed by	Checked by	Approved by	Date		Date	
YI HAO						
					Edition	Sheet

Combustor: SAFRAN SCT V1
Item part: components of bend fuel injector
Material: stainless steel and maraging steel
Description: assembled bend injector and wedge

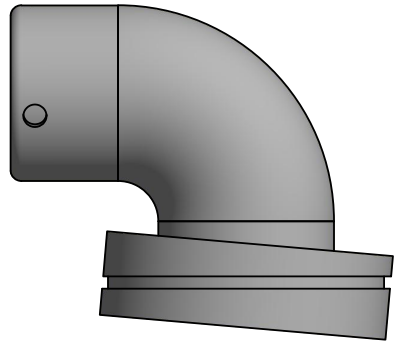

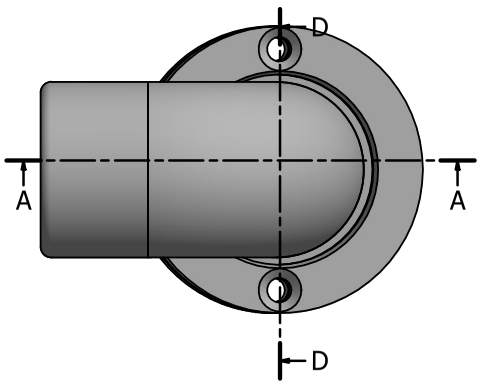

C (4 : 1)

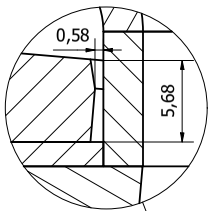

B (4 : 1)

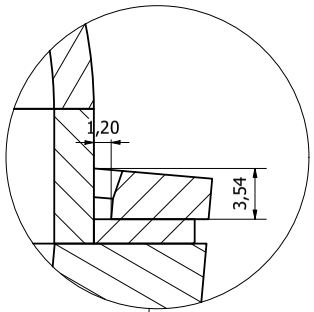

D-D (2 : 1)

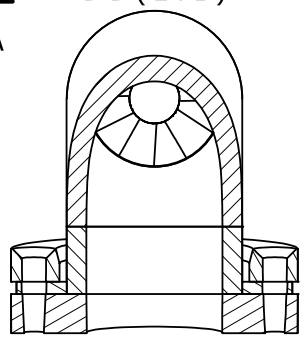

A-A (2 : 1)

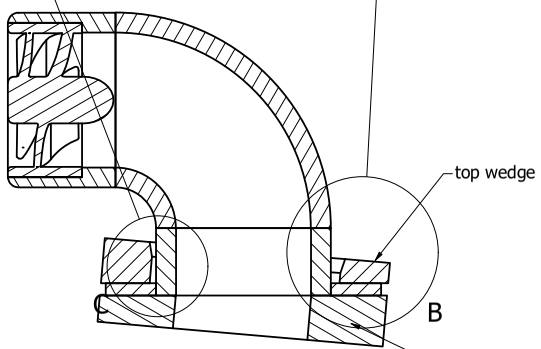

Designed by	Checked by	Approved by	Date	Date	
YI HAO					

	Edition	Sheet

Combustor: SAFRAN SCT V1
Item part: bottom wedge
Material: stainless steel

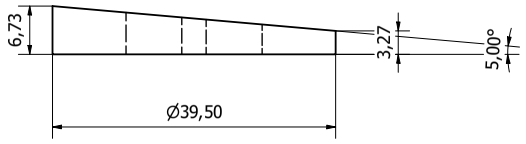

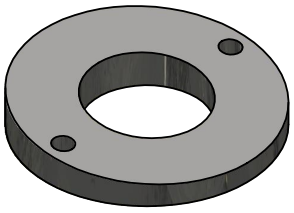

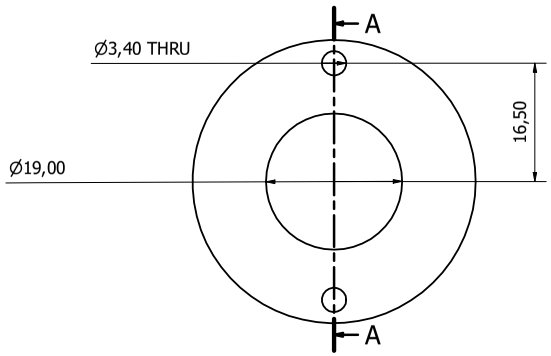

A-A (4 : 1)

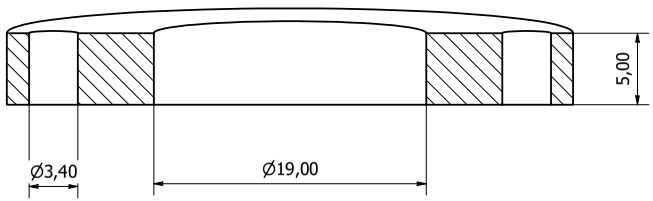

Designed by	Checked by	Approved by	Date		Date	
YI HAO						

	Edition	Sheet

Combustor: SAFRAN SCT V1
Item part: top wedge
Material: stainless steel

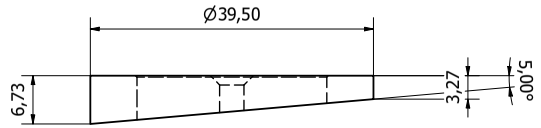

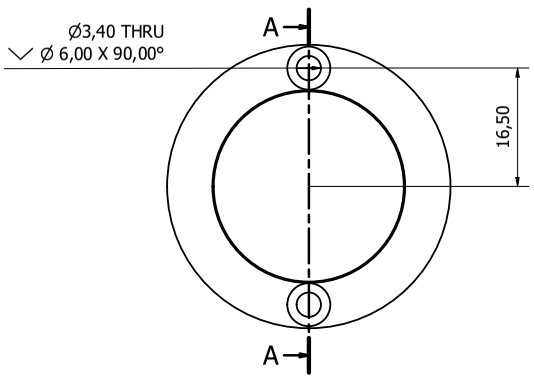

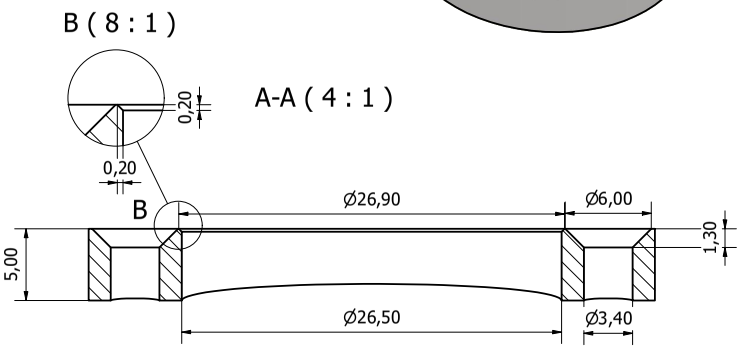

Designed by	Checked by	Approved by	Date		Date	
YI HAO						

	Edition	Sheet

Combustor: SAFRAN SCT V1
Item part: swirler (3D printed)
Material: maraging steel

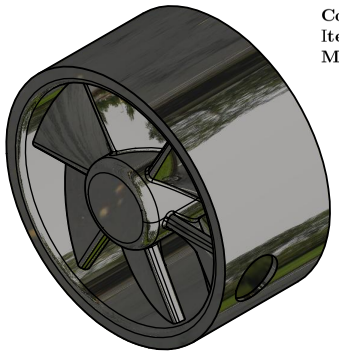

A-A (4 : 1)

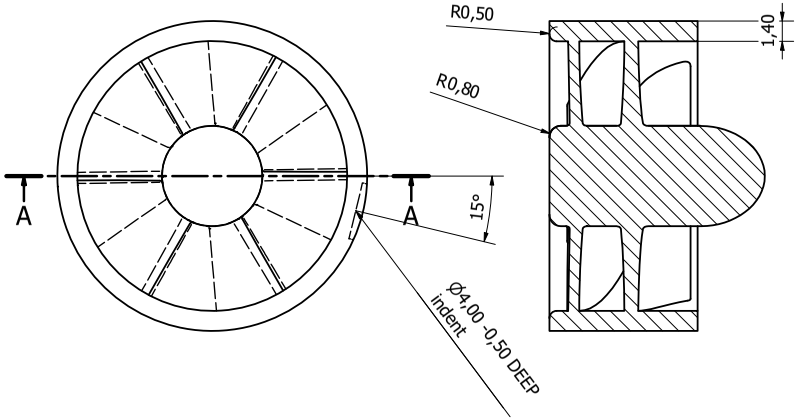

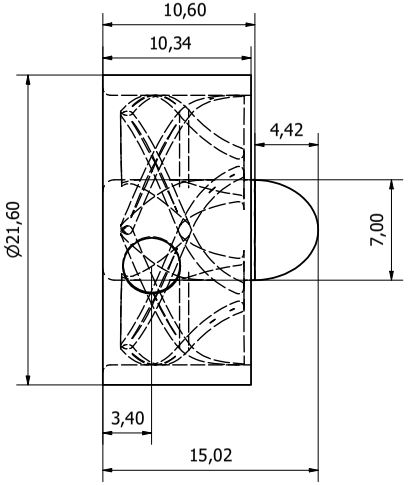

Designed by	Checked by	Approved by	Date		Date	
YI HAO						

		Edition	Sheet

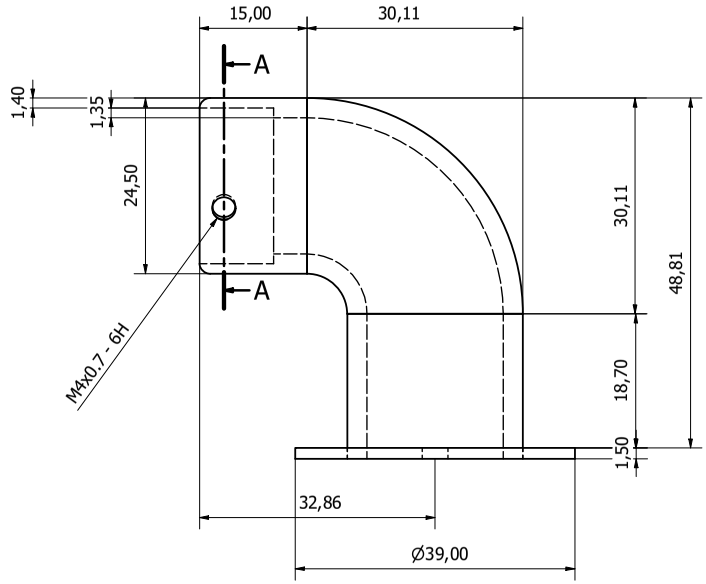

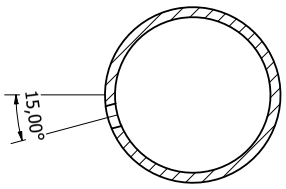

A-A (2 : 1)

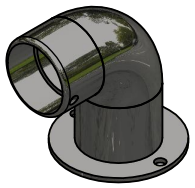

Combustor: SAFRAN SCT V1
Item part: (fuel) bend injector pipe (3D printed)
Material: maraging steel

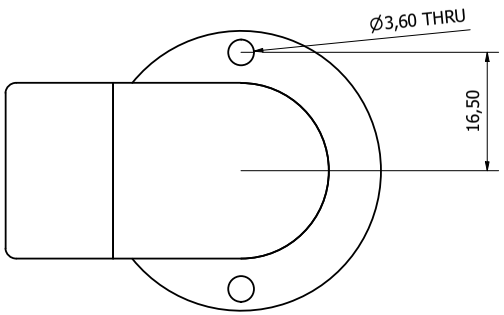

Designed by	Checked by	Approved by	Date		Date	
YI HAO						

	Edition	Sheet

Combustor: SAFRAN SCT V1
Item part: cooling duct (3D printed)
Material: maraging steel

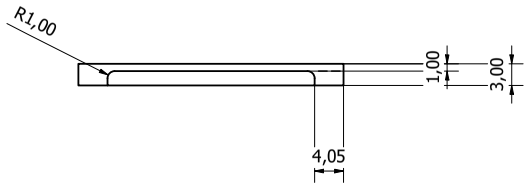

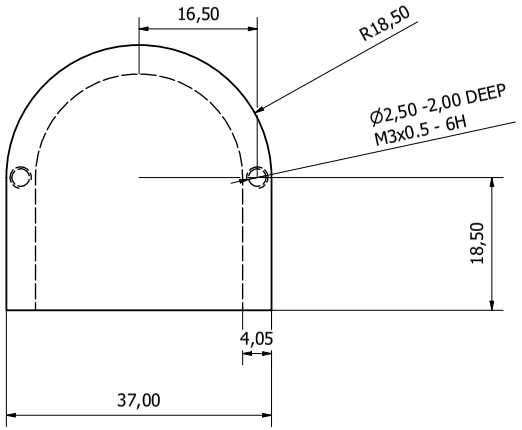

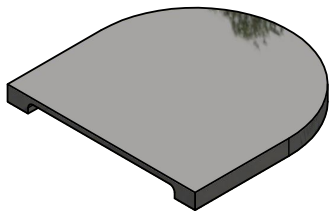

Designed by	Checked by	Approved by	Date		Date	
YI HAO						

	Edition	Sheet

Computer-aided Design (CAD) Drawings

Drawings for SAFRAN SCT V2

Combustor: SAFRAN SCT V2
Item part: angled injector (3-D printed)
Material: maraging steel

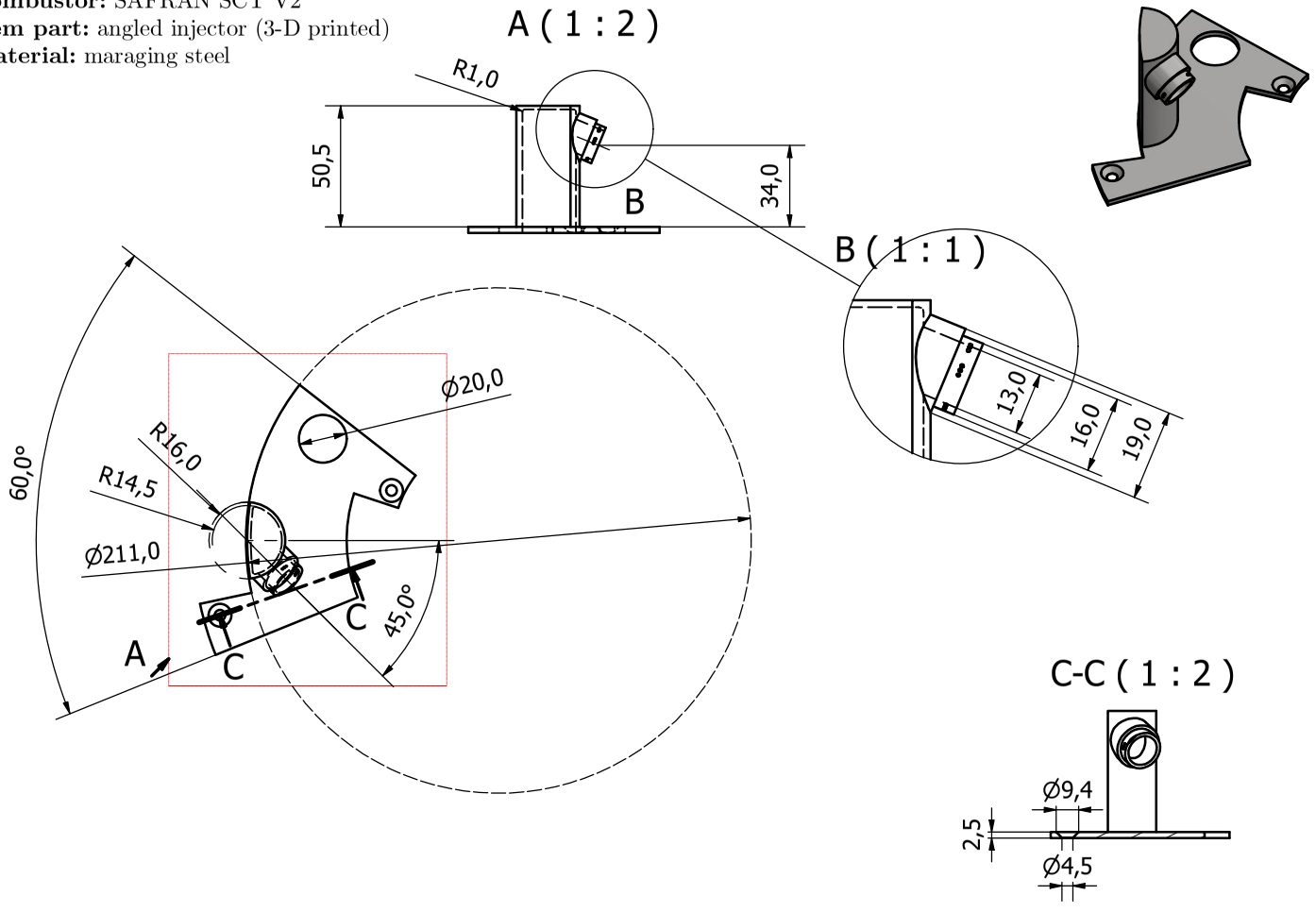

Combustor: SAFRAN SCT V2
Item part: swirler (3-D printed)
Material: maraging steel

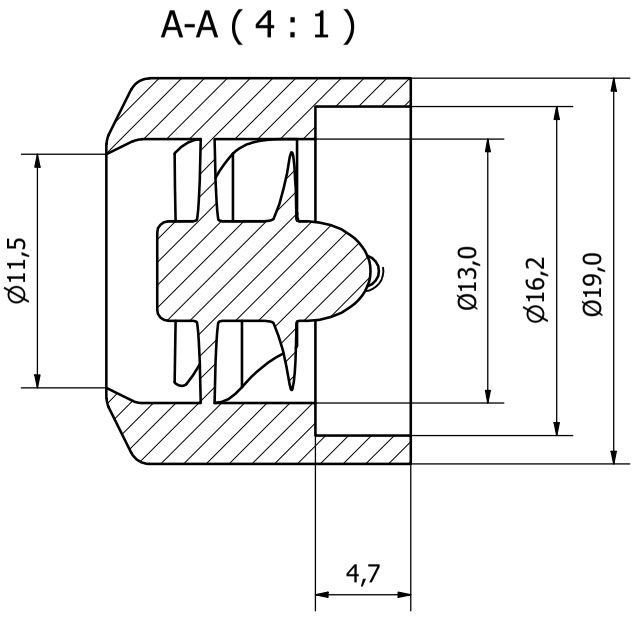

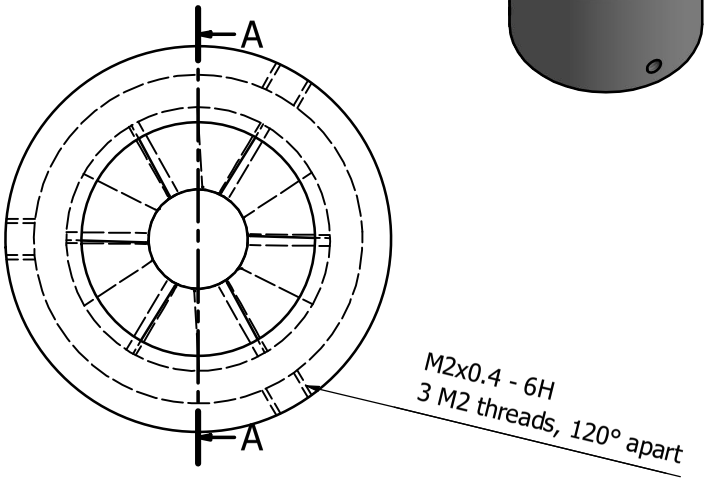

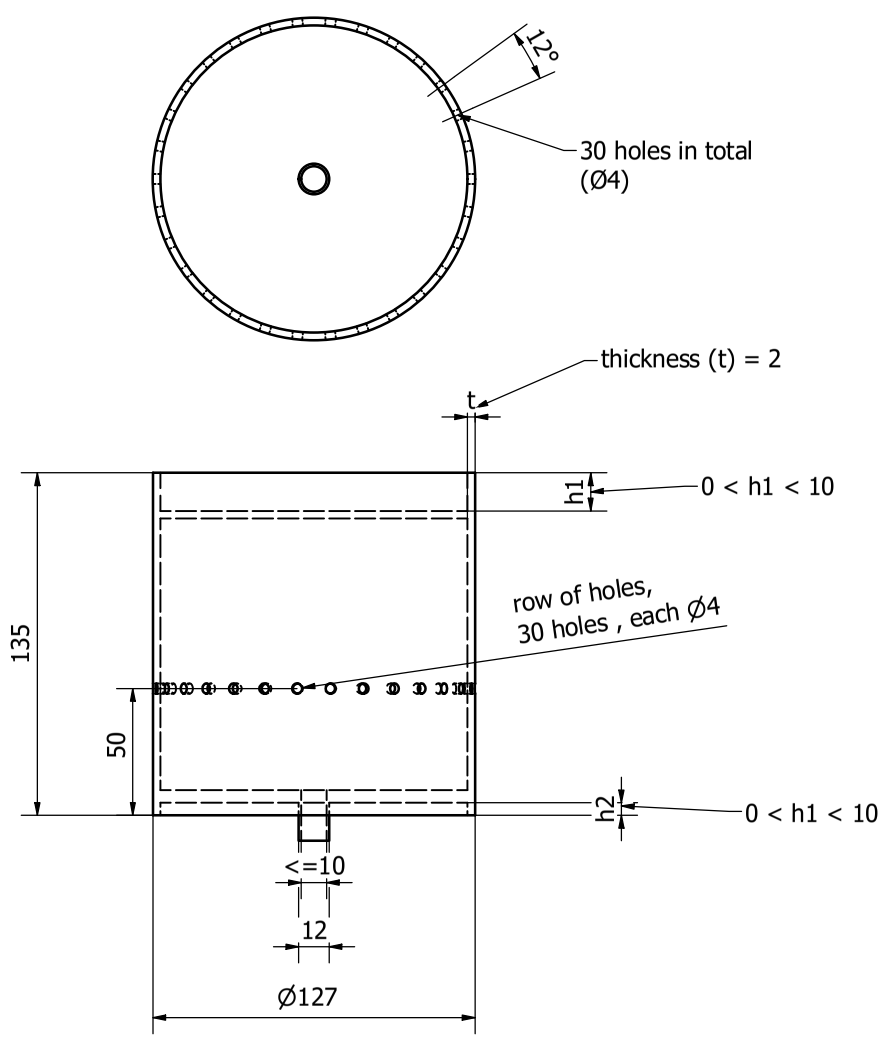

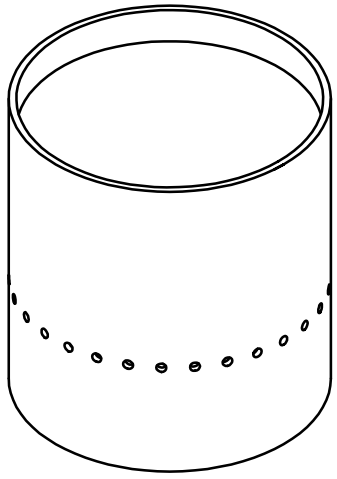

Combustor: SAFRAN SCT V2
Item part: inner wall with dilution holes
Material: stainless steel

Combustor: SAFRAN SCT V2
Item part: perforated back plate for effusion cooling (3-D printed)
Material: inconel 625